DEPARTMENT OF TRANSPORTATION

Improving and Developing Pavement Design Inputs and Performance Functions for Cold Recycled Pavement Layers in Minnesota

Eshan Dave, Principal Investigator
Department of Civil and Environmental Engineering
University of New Hampshire

January 2026

Research Report
Final Report 2026-12

LOCAL ROAD RESEARCH BOARD

To get this document in an alternative format or language, please call 651-366-4720 (711 or 1-800-627-3529 for MN Relay). You can also email your request to ADArequest.dot@state.mn.us. Please make your request at least two weeks before you need the document.

1. Report No. MN 2026-12	2.	3. Recipients Accession No.	
4. Title and Subtitle Improving and Developing Pavement Design Inputs and Performance Functions for Cold Recycled Pavement Layers in Minnesota		5. Report Date January 2026 6.	
7. Author(s) Eshan V. Dave, Jo E. Sias, Ebubechukwu Al-Ihekwaba, Gabriele Tebaldi		8. Performing Organization Report No.	
9. Performing Organization Name and Address Department of Civil and Environmental Engineering University of New Hampshire 33 Academic Way, Durham, New Hampshire 03824-2619		10. Project/Task/Work Unit No. 11. Contract (C) or Grant (G) No. (c) 1036343	
12. Sponsoring Organization Name and Address Minnesota Department of Transportation Research Services & Library 395 John Ireland Boulevard, MS 330 St. Paul, Minnesota 55155-1899		13. Type of Report and Period Covered Final Report 14. Sponsoring Agency Code	
15. Supplementary Notes http://mdl.mndot.gov/			
16. Abstract (Limit: 250 words) Existing specifications in Minnesota and many other states fail to adequately characterize the properties of cold recycled pavement materials necessary for pavement design procedures. Current assumptions for these materials are not entirely accurate as these materials often possess complex, non-linear, stress and rate dependent behavior. This can lead to under/overdesigned pavement structures that are not economically and environmentally viable. Adequately characterizing the recycled material layer will ensure that the appropriate thickness of wear course is determined through pavement design with no negative impact on structural capacity or serviceability. This research, through a series of laboratory and field investigations, develops a user-friendly, Excel-based material property prediction tool to estimate necessary material properties to be used in quality assurance evaluation and/or performance modelling efforts within mechanistic-empirical design of cold recycled pavement structures. In addition, a rutting performance function and early life rutting failure threshold is developed to assist in minimizing the risk of premature rutting failure of the recycled layer. From these, longer pavement lives can be achieved, leading to a decrease in the frequency of repair and maintenance as well as the costs associated with them.			
17. Document Analysis/Descriptors Cold in-place recycling, Full-depth reclamation, Emulsions, Predictive models, Performance based specifications		18. Availability Statement No restrictions. Document available from: National Technical Information Services, Alexandria, Virginia 22312	
19. Security Class (this report) Unclassified	20. Security Class (this page) Unclassified	21. No. of Pages 187	22. Price

Improving and Developing Pavement Design Inputs and Performance Functions for Cold Recycled Pavement Layers in Minnesota

FINAL REPORT

Prepared by:

Eshan V. Dave, PhD
Jo E. Sias, PhD, PE
Ebubechukwu Al-Ihekwaba
Gabriele Tebaldi, PhD, PE
Department of Civil and Environmental Engineering
University of New Hampshire

January 2026

Published by:
Minnesota Department of Transportation
Research Services & Library
395 John Ireland Boulevard, MS 330
St. Paul, Minnesota 55155-1899

ACKNOWLEDGMENTS

This research study was performed by the University of New Hampshire (UNH), with the Minnesota Department of Transportation (MnDOT) Office of Materials and Road Research (OMRR) and the MnDOT Pavement Design Unit serving as subcontractors. We sincerely acknowledge Eyoab Zegeye-Teshale and Thomas Calhoon from OMRR for their significant efforts in coordinating the in-situ distress survey testing. We would also like to thank Tim Andersen as well as Gregory Larson at MnDOT for their efforts in the Falling Weight Deflectometer testing and stiffness backcalculation processes. The field projects included in this study were realized based on the cooperation of the oversight engineers in MnDOT and the local agencies; we sincerely appreciate their efforts. The participation of the paving contractors and quality-control personnel is recognized and greatly appreciated. We would also like to acknowledge the project coordinator, Marcus Bekele, and the technical liaison, Tim Andersen, for their help in the smooth administration of this project. Special thanks also go to the rest of Technical Advisory panel (Timothy Andersen, Raul Valasquez, Dan Schellhammer, Charles Kremer, Ceren Aydin, and David Van Deusen) for their feedback throughout the course of this research.

TABLE OF CONTENTS

LIST OF FIGURES

LIST OF TABLES

LIST OF ABBREVIATIONS

AASHTO – American Association of State Highway and Transportation Officials

AASHTOWare – AASHTO design software suite

AICc – Akaike's Information Criteria

ATAF – Asphalt temperature adjustment factor

CALME – California Mechanistic-Empirical Pavement Design Program

CCPR – Cold Central Plant Recycling

CIR – Cold In-Place Recycling

CR – Cold Recycled

CSAH – County State Aid Highway

D_0 – Peak surface deflection (FWD metric)

DevSR – Deviator Stress Ratio

DOT – Department of Transportation

E* – Complex modulus

EE – Engineered Emulsion

ERM – Empirical Risk Minimization

FDR – Full-Depth Reclamation

FHWA – Federal Highway Administration

FPR – False Positive Rate

FWD – Falling Weight Deflectometer

HMA – Hot Mix Asphalt

HPMS – Highway Performance Monitoring System

HVS – Heavy Vehicle Simulator

ITS – Indirect Tensile Strength

ITSM – Indirect Tensile Stiffness Modulus

IRI – International Roughness Index

ISAP – International Society for Asphalt Pavements

kPa – Kilopascal

LASSO – Least Absolute Shrinkage and Selection Operator

LKD – Lime Kiln Dust

LWD – Light Weight Deflectometer

M-E – Mechanistic-Empirical

MAE – Mean Absolute Error

MDD – Maximum Dry Density

ML – Machine Learning

MnDOT – Minnesota Department of Transportation

MnROAD – Minnesota Road Research Facility

MPa – Megapascal

M_R – Resilient modulus

N/A – Not Applicable

OFC – Optimum Fluids Content

OMRR – Office of Materials and Road Research

PN – Pavement Number

PCC – Portland Cement Concrete

PPRA – Pavement Preservation & Recycling Alliance

PSI – Pavement Serviceability Index

QC – Quality Control

RASE – Root Average Square Error

RAP – Reclaimed Asphalt Pavement

RDSV – Road Doctor Survey Vehicle

RLPD – Repeated Load Permanent Deformation

ROC – Receiver Operating Characteristic

SCI – Surface Curvature Index

SFDR – Stabilized Full Depth Reclamation

SRM – Structural Risk Minimization

STT – Simple Triaxial Test

SVEM – Self-Validating Ensemble Model

SVR – Support Vector Regression

E_{tan} – Tangent Modulus

T_{MC} – Total Moisture Content

TH – Trunk Highway

TPR – True Positive Rate

TM_r – Triaxial Resilient Modulus

TSR – Tensile Strength Ratio

UCS – Unconfined Compressive Strength

UNH – University of New Hampshire

UTM -Universal Testing Machine

EXECUTIVE SUMMARY

The transportation sector is confronted with the necessity of sustainability, and the use of recycling techniques in the construction and rehabilitation of asphalt pavements has emerged as a viable strategy for preserving pavement infrastructure. Among the various recycling methods, cold recycling is distinguished by its efficient reuse of existing materials, ease of mix preparation and construction, and reduced dependence on virgin materials and fossil fuels, thereby contributing to lower emissions. The three primary cold recycling techniques used in Minnesota, cold in-place recycling (CIR), cold central plant recycling (CCPR), and full-depth reclamation (FDR), differ in their construction methodologies, material processing approaches, and extent of recycling depth. However, they share a common material composition, primarily consisting of reclaimed asphalt pavement (RAP), stabilizing agents such as asphalt emulsion or foamed asphalt, and, in some cases, chemical additives and virgin aggregates. Currently, this material behavior is not adequately characterized, resulting in under/overdesigned pavement structures. A comprehensive characterization of the recycled layer is essential to accurately determine the appropriate thickness of the wear course during pavement design, thereby preventing unnecessary under and/or overdesign while ensuring structural integrity and long-term serviceability.

The overall goal of this research is to develop pavement design inputs and performance functions for cold recycled layers used in Minnesota. The study was further divided into three (3) principal objectives, which are to:

- Use case-study approach to quantify pavement structural contributions of cold recycled asphalt layers
- Build database of cold recycled asphalt material properties for use in pavement design method
- Correlate mechanistic measures and pavement performance to develop performance functions

As a starting point, a comprehensive literature review involving cold recycling techniques, material characterization methods, factors affecting mechanical properties, cold recycled layer pavement design procedures, and methodologies for developing pavement performance transfer functions, as well as a review of the current state of practice for Cold Recycled (CR) layer pavement design and analysis were performed to inform the methodologies necessary to fulfill the objectives, facilitating the efficient design of cold recycled pavements. A total of 13 projects were incorporated, identified through a survey of Local Road Research Board (LRRB) and Minnesota Department of Transportation (MnDOT) district agencies for candidate projects planned for the 2023 construction season, along with projects drawn from the *Evaluation of Curing Effects on Cold In-Place Recycled* (CIR) research study (Dave et al., 2022). Of these 13 projects, consisting of County State Aid Highways (CSAH) and Trunk Highways (TH), 11 were CIR while two were Stabilized FDR (SFDR). These field projects were limited to engineered emulsion stabilization and in-place cold recycling technology (CIR and SFDR) and hence, all developments and results presented are based on these only.

Field assessments, conducted by a team from MnDOT and the Office of Materials and Road Research (OMRR), included Falling Weight Deflectometer (FWD) tests and measurements of roughness and rutting using MnDOT's Road Doctor equipment, primarily conducted to determine the early life performance of the pavement structure and the CR layers within the pavement structure. Findings from

these in-situ evaluations indicate that the pavement structures were generally in good condition, with moisture accumulation from freeze-thaw events potentially also influencing the pavement's structural performance.

Laboratory assessments involved resilient modulus, tensile strength and shear strength tests on mixtures produced with as-built properties and variations from the as-built conditions to explore the effect of mix and non-mix attributes on the mechanical properties. Initial results from the resilient modulus tests suggest that mixtures may become less dependent on confining pressure after full curing. More so, it was observed that the material density, temperature, and emulsion content significantly influenced the stiffness. On the other hand, the tensile strength was observed to be significantly influenced by the emulsion content, mixture density, and gradation characteristics. Findings from the shear strength evaluations highlighted the importance of mix density, gradation, and stabilizer content while carefully managing emulsion levels and chemical additive use to achieve balanced internal bonding and shear resistance in CR mixtures.

Leveraging the extensive dataset generated during the laboratory assessments, material property prediction models were developed with the aim of estimating the material properties necessary for performance modelling efforts within mechanistic-empirical design of cold recycled pavement structures. Several statistical analyses were conducted to process and refine the dataset to ensure accurate delivery of predictive models. The factors incorporated include stabilizer (engineered emulsion) amount, presence of chemical additive, compacted density, gradation characteristics, and temperature, and are all selected based on their routine availability in cold recycling mix design and construction practices. An advanced machine learning (ML) approach called Self-Validating Ensemble Model (SVEM), which integrates principles of bootstrapping and ensemble modeling, and the Support Vector Regression (SVR) technique were employed for model developments. The best model was identified through model performance evaluations and the final disposition for implementation was provided as a Microsoft Excel-based tool for predicting material properties.

Finally, a CR layer rutting performance function was developed, leveraging key material properties, critical pavement responses, and a mechanistic parameter known as the Deviator Stress Ratio (DevSR). The final calibrated rutting performance function relates the allowable number of load repetitions to rutting failure (defined as 0.5 inches of rut depth) to three relevant variables: DevSR, vertical compressive strain at the top of the CR layer, and CR material/layer density. Among these, DevSR and density were found to be statistically significant, with DevSR exerting the greatest negative influence on rutting life, while density was positively associated with rutting resistance. The DevSR parameter was further employed to establish a threshold to limit early life rutting of cold recycled layers. A rut depth of 0.125 inches (3 mm) was set as the limiting rut depth value to indicate early-life performance of the CR layer. A DevSR value of 0.31, which yielded a true positive rate (TPR) of 0.75, a false positive rate (FPR) of 0.25, and an accuracy of 75% based on a Receiver Operator Characteristics (ROC) verification analysis, suggesting good practical performance in identifying poor-performing sections, was proposed as the early-life rut threshold for these CR materials. The developed performance function, supported by both mechanistic analysis and statistical threshold validation, stands as a viable tool for evaluating rutting

behavior of these cold recycled pavement layers and facilitates more efficient and reliable pavement designs.

Chapter 1: Introduction

1.1 Background and Motivation

The transportation sector is confronted with the necessity of sustainability, and the use of recycling techniques in the construction and rehabilitation of asphalt pavements has emerged as a viable strategy for preserving pavement infrastructure. Among the various recycling methods, cold recycling is distinguished by its efficient reuse of existing materials, ease of mix preparation and construction, and reduced dependence on virgin materials and fossil fuels, thereby contributing to lower emissions. The three primary cold recycling techniques used in Minnesota, cold in-place recycling (CIR), cold central plant recycling (CCPR), and full-depth reclamation (FDR), differ in their construction methodologies, material processing approaches, and extent of recycling depth. However, they share a common material composition, primarily consisting of reclaimed asphalt pavement (RAP), stabilizing agents such as asphalt emulsion or foamed asphalt, and, in some cases, chemical additives and virgin aggregates. Currently, this material behavior is not adequately characterized, resulting in overdesigned pavement structures. A comprehensive characterization of the recycled layer is essential to accurately determine the appropriate thickness of the wear course during pavement design, thereby preventing unnecessary under/overdesign while ensuring structural integrity and long-term serviceability. By enhancing material characterization and incorporating performance-based design approaches, this study aims to improve the current pavement analysis and design methodologies to appropriately characterize and evaluate cold recycled (CR) pavement layers.

1.2 Objectives

The overall goal of this research was to develop pavement design inputs and performance functions for cold recycled layers used in Minnesota. The study was further divided into three (3) principal objectives, which were to:

- Use case-study approach to quantify pavement structural contributions of cold recycled asphalt layers.
- Build database of cold recycled asphalt material properties for use in pavement design method.
- Correlate mechanistic measures and pavement performance to develop performance functions.

1.3 Research Methodology

This research integrates both field and laboratory data to develop mechanical property prediction models as well as rutting performance functions, facilitating the efficient design of cold recycled pavement layers. The developed mechanical property prediction models utilize readily available mix design (stabilizer content, presence of chemical additive, RAP gradation characteristics, density), and climatic information (temperature) to estimate property inputs for pavement analysis and design processes. Specifically, the mechanical property prediction models include resilient modulus, indirect tensile strength, and shear strength parameters, developed using machine learning algorithms and then programmed into a user-friendly computer tool. In addition, a rutting performance function was developed, leveraging key material properties, critical pavement responses, and a mechanistic

parameter known as the Deviator Stress Ratio (DevSR). The DevSR parameter was further employed to establish a threshold to limit early life rutting of cold recycled layers. It is important to note that model and performance function developments were only peculiar to engineered emulsion stabilized CIR and SFDR cold recycled pavement sections due to the limited available data during this study. The project was divided into 9 tasks, and a flowchart (Figure 1-1) schematically shows project activities and information.

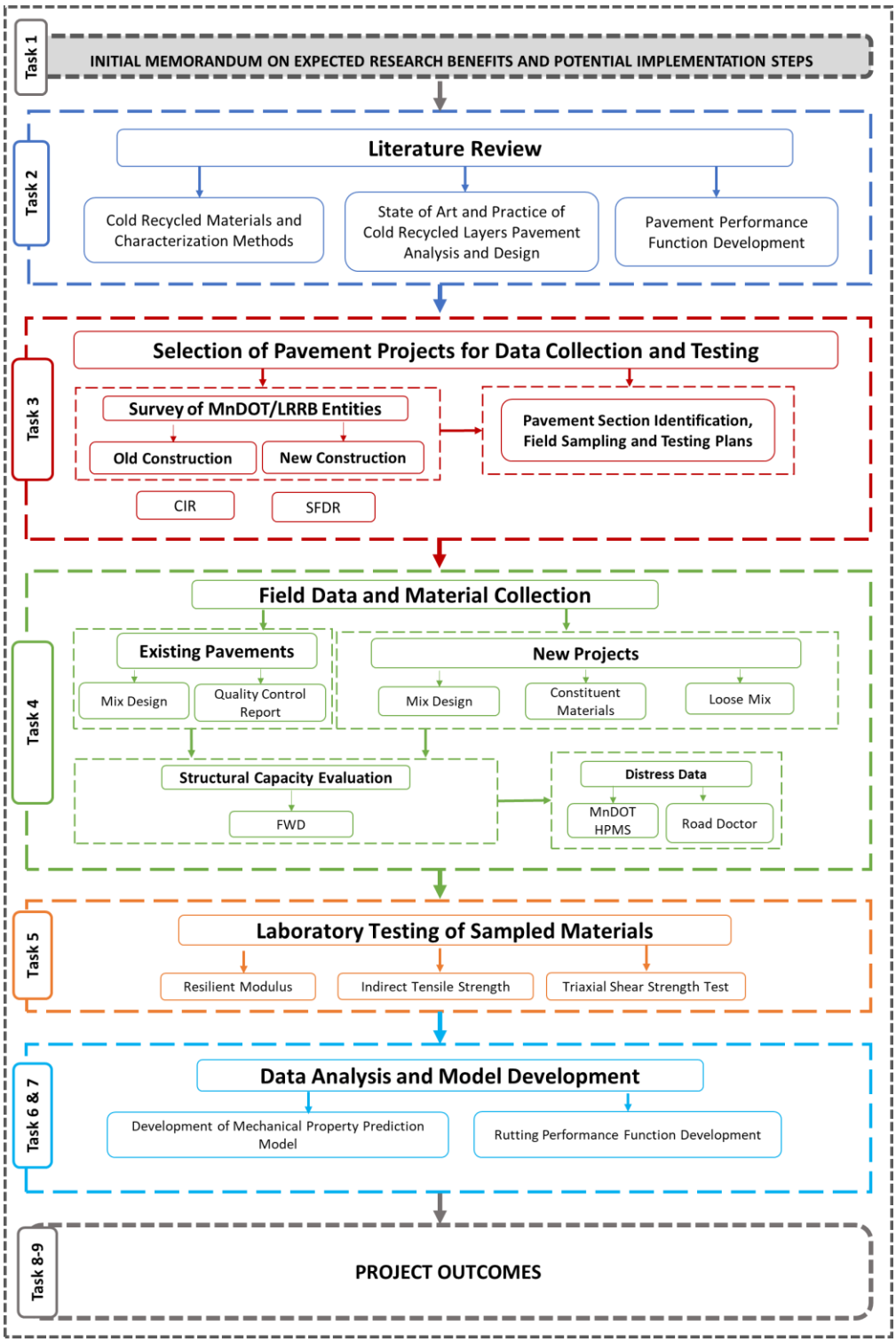

Figure 1-1: Project Methodology Flowchart

1.4 Organization of this Report

This report is organized into seven chapters with appendices. Chapter 1 covers the introduction and motivation for this research, as well as the study objectives and research approach. Chapter 2 contains a

detailed literature review of the current state of practice and state of the art for cold recycled layer pavement design and analysis. Chapter 3 provides details of the cold recycling projects selected for this study, together with the field and laboratory assessment methodologies. Chapter 4 presents results and discussions on the field and laboratory assessments conducted. Chapter 5 provides comprehensive details of the approach undertaken and analyses conducted to develop the mechanical property prediction models as well as the final prediction tool for utilization. Chapter 6 provides details of the performance function development, facilitating the efficient design of cold recycled pavement layers. Key conclusions and recommendations of the outcomes of this study are presented in Chapter 7, where limitations and considerations for future extension are also discussed.

Chapter 2: Literature Review

This chapter provides detailed review of the current state of practice and state of the art for cold recycled (CR) layer pavement design and analysis. This includes an overview of the cold recycling techniques, material characterization methods, factors affecting mechanical properties, pavement design procedures, and methodologies for developing pavement performance transfer functions. Existing literature and current methods were used as a starting point to identify the various factors affecting mechanical properties which would be further integrated into developing mechanical property prediction models and performance functions. Details on the current practices employed by Minnesota Department of Transportation (MnDOT) and Minnesota's counties, cities and townships for CR layer pavement design and analysis were collected via a survey and are incorporated in this chapter along with the challenges faced in employing these design methodologies.

2.1 Cold Recycling Technology

In recent years, because of the evident benefits of rehabilitating existing pavements, recycling technology has received considerable focus. Although cold recycling is becoming increasingly prevalent in a number of U.S. states, it is neither widespread nor uniform throughout the nation. Several reasons exist for this, such as the lack of defined material property inputs for engineered structural design, the absence of rapidly applied quality control and/or assurance procedures, and the distinct lack of long-term performance data in the literature that documents the structural performance of existing sections (Timm et al., 2018). In general, cold recycling technology provides the benefits of minimizing use of virgin materials and fossil fuel, lowering emissions, and improving the performance of pavements (Xiao et al., 2018). The three cold recycling techniques utilized are:

- Cold In-place recycling (CIR)
- Cold Central Plant recycling (CCPR)
- Stabilized Full depth reclamation (SFDR)

These techniques have distinctive methodologies with respect to construction technology, material processing, and depth of recycling. These techniques are discussed in detail in the following sub-sections.

2.1.1 Cold In-Place Recycling (CIR)

CIR occurs in-place and uses 100% of the reclaimed asphalt pavement (RAP) (PPRA, 2022). Typically, cold recycled asphalt consists of RAP, stabilizing agents (asphalt emulsion and foamed) and optional virgin aggregates, and chemical additives (active filler). Water is required when mixing in order to distribute the emulsion or foamed asphalt throughout the mixture. In addition, water aids in asphalt mixture compaction, improving its workability (Tebaldi et al., 2014; Dave et al., 2022).

The typical recycling depth for CIR is 2 to 4-inches. With adequate underlying support, 2-inch thickness is sufficient. Multiple passes and the use of chemical additives like cement, lime, kiln dust, or fly ash to increase the layer's resistance to moisture damage may allow for thicker layers. Lime or Portland cement may be applied as slurry or dry. The slurry approach removes dust issues so does dry additive

systems currently used in the market today which loads lime or Portland cement into the recycling mixing chamber. The dry application approach does help eliminate the need for costly slurry equipment and the energy needed to operate the slurry equipment. (Stroup-Gardiner, 2011; Asphalt Recycling and Reclaiming Association, 2015).

CIR can address most pavement defects, improve ride quality, and be used to widen the roadway (Kandhal & Mallick, 1998). CIR is utilized when the number and severity of non-load-related distresses are high and/or extend beyond the pavement surface and can be integrated with asphalt overlay to treat distresses caused by traffic (Stroup-Gardiner, 2011). Usually, 70% of the existing asphalt layer thickness can be treated to prevent reflective cracking. A minimum of 1-inch and preferably 2-inches of asphalt or 6-inches of aggregate base should remain to sustain the weight of the recycling equipment. Reflective cracking will reappear more frequently if the treatment depth is shallow. CIR is an effective remedy for wear rutting (caused by progressive loss of material from the asphalt surface due to actions like raveling, which is usually due to poor durability of HMA). By using the proper stabilizing agents, modifiers, and/or granular materials, minor instability rutting can also be treated (Asphalt Recycling and Reclaiming Association, 2015). CIR is used in all temperature zones, without any climate restrictions although it is more preferred in hot, dry climates (not appreciable in extreme conditions, 48-52°C) since wet weather lengthens the curing time in emulsion treated CIR (Stroup-Gardiner, 2011; Dave et al., 2022).

2.1.2 Cold Central Plant Recycling (CCPR)

CCPR incorporates RAP with foamed asphalt or emulsion, additives, and/or recycling agents in a central recycling facility to generate a base pavement material that can be placed using conventional asphalt paving equipment. (Timm et al., 2018). CCPR is suitable for circumstances where in-place recycling is not feasible due to logistical constraints, large quantities/production rates are desired, and precise mix design control is required (Kandhal & Mallick, 1998; PPRA, 2022).

The conventional layer thickness for CCPR is between 2- and 6-inches. Multiple lifts can be used to increase the total thickness of the recycled layer. CCPR can serve as a base course for reconstruction or new construction projects. Significant structural improvements can be performed without altering the vertical or horizontal geometry of the roadway, which is one of the benefits of CCPR (Timm et al., 2018). With the exception of fatigue cracking and base problems, CCPR can repair almost all forms of flexible pavement distress. To resolve fatigue cracking and base-related failures, underlying materials must be corrected. The two most significant distresses that can be addressed using CCPR are ride quality and reflection cracking (Kandhal & Mallick, 1998).

2.1.3 Stabilized Full Depth Reclamation (SFDR)

This recycling technique is similar to CIR and is executed in-situ (Hill & Braham, 2016; Romanoschi et al., 2004). SFDR is the rehabilitation method in which the complete thickness of the asphalt pavement and a predefined portion of the underlying components (aggregate base, subbase, and/or subgrade) are uniformly pulverized and blended with emulsion or foamed asphalt and optional chemical additve (Portland cement or lime) to produce an upgraded, homogenous base material (Jones et al., 2009). This mixture is also adequate to serve as the base for a new surface course without the addition of stabilizing

agent. Typically, the SFDR treatment depth ranges from 4- to 12-inches (Asphalt Recycling and Reclaiming Association, 2015).

Pavements with substantial deformation or deterioration owing to subgrade or drainage issues are only eligible for SFDR if further work is performed to rectify the subgrade and drainage problems. To address subgrade issues, the reclaimed material is moved to the side, the subgrade is then reworked or stabilized with an additive, and then the reclaimed material is placed back on the prepared subgrade. Pavement distresses treated by SFDR include fatigue cracking, rutting, reduced ride quality due to heaves, loss of bonding between pavement layers, raveling, potholes amongst others (Asphalt Recycling and Reclaiming Association, 2015). SFDR is a viable alternative to conventional rehabilitation and reconstruction considering that it is quick, affordable, and offers a life span of up to 25 years. Typically, the service life of an SFDR rehabilitated pavement is limited by the service life of the wearing course rather than the SFDR layer itself. SFDR is also advantageous since it can improve pavement structure without altering the geometry of the pavement or shoulder reconstruction, it can be used to widen pavement, and it is environmentally desirable (Kandhal & Mallick, 1998; Lewis et al., 2006; PPRA, 2022).

2.2 Cold Recycled Mixtures

There is not a nationally established approach for the design of CR mixtures, and most public transportation agencies that use cold recycling have their own mix design procedures (Asphalt Recycling and Reclaiming Association, 2015). For reliable performance, CR mixtures must be optimally designed and to accomplish this, a mix design technique is required to assess the mixture's components, namely, reclaimed asphalt pavement (RAP), water, asphalt binder, and chemical additive. The mix design technique generally involves evaluating both the individual components and the composite material (Asphalt Academy., 2020).

2.2.1 Constituent Materials of Cold Recycled Mixtures

To provide context for the findings of the literature review on the factors affecting the performance of CR materials, a brief overview of the constituent materials in the mix design procedures is presented:

Reclaimed Asphalt Pavement (RAP): The influence of the RAP composition must be carefully considered in the mix design (Asphalt Academy., 2020). Moisture content, source of aggregate, asphalt binder content and condition, and RAP grading are typical variables that affect the quality of RAP to be used in the CR mixture. Since the temperature production for CR mixtures is low, there is no significant reactivation of the asphalt binder in RAP. For this reason, RAP gradation should be carefully considered when evaluating RAP materials for CR applications (Lee et al., 2007; Kim et al., 2012; Tebaldi et al., 2014).

Asphalt stabilizers: Asphalt binder's use as a stabilizing agent has increased in popularity as a result of technological advancements (design procedures and construction methods) and the economic and environmental benefits that result. Asphalt binders are employed as stabilizing agents in two forms (Wirtgen GmbH, 2012).

- **Emulsion:** This binder consists of asphalt binder that emulsifies in water. In the form of an oil-in-water asphalt emulsion, the asphalt binder is distributed in water. The charge of the asphalt

emulsion is determined by the emulsifying agent that maintains the asphalt in suspension. When emulsion and aggregate are combined, the charged asphalt binder droplets are attracted to the oppositely charged aggregate particles, concentrating on the smaller fractions due to their larger surface area and higher charge concentration characteristics. Moisture and aggregate type play a significant effect in dispersing emulsion and separating asphalt binder from water during mixing. Asphalt emulsion is produced at a specialized plant and, if maintained properly, has a shelf life of several months in storage.

- **Foamed Asphalt:** Water is injected into heated asphalt binder, resulting in spontaneous foaming of the asphalt. The viscosity of the asphalt is greatly reduced when the injected water comes into touch with the hot asphalt and is exploded into hundreds of bubbles of vapor. The foaming process takes place in an expansion chamber into which asphalt, water, and sometimes air is introduced under high pressure. In its unstable stage, foamed asphalt is created and mixed with the aggregate. The higher the volume of the foam, the more evenly the asphalt is distributed throughout the aggregate.

Chemical Additives (Active filler): Chemical additives for CR mixtures include cement (different types, excluding rapid-hardening cements), lime (hydrated lime), fly ash, and slag. Multiple types of chemical additives can be employed individually or in combination. The application of a particular chemical additive depends on its availability, cost, and effectiveness with the material being treated. Without trial tests during mix design, it is difficult to forecast which chemical additive will prove to be the most successful, according to research and experience. Indirect Tensile Strength on moisture conditioned samples (ITS_{WET}) can be utilized as guidance for the selection of chemical additives. The optimum chemical additive content is often determined by adjusting the chemical additive content while keeping the water content constant. The optimum chemical additive content is determined by analyzing the content at which different property parameters, such as Marshall stability, unconfined compressive strength (UCS), and indirect tensile strength (ITS), are satisfied. Chemical additive is added to CR mixtures in order to improve the adherence of the asphalt binder to the aggregate, enhance the dispersion of asphalt binder in the mixture, alter the elasticity of natural materials (reduce plasticity index), increase the rate of stiffness and strength gain of the mixture (curing) (Asphalt Academy., 2020; Wirtgen GmbH, 2012).

Water: Moisture has a comparable role in the aggregate for emulsion treated CR mixtures and foamed asphalt treated mixtures, although there are some distinctions. The total fluid content of the mixture, including moisture and asphalt binder, must be considered. The fluids in CR mixtures are the sum of the moisture in the aggregates before mixing, the water in the asphalt emulsion, the amount of asphalt in the emulsion or residual asphalt in case of foamed asphalt stabilization, and any additional water injected to the mixture. Water also aids in dust suppression and cooling of mill head teeth when a multi-unit cycle train is utilized. The amount of fluid influences the packing of aggregate particles. The optimum fluids content idea is frequently applied to CR mixtures in an effort to maximize the packing of solid particles. The optimum fluids content (OFC) is defined as the fluid content at the closest packing of aggregate particles or the maximum dry density (MDD). Since asphalt binder permits more dense packing of aggregate particles than water, the OFC of a given mixture may be less than the optimum

water content (OMC). Typically, for foamed asphalt treated mixes, the OFC is believed to be equal to the OMC (Asphalt Academy., 2020; Dave et al., 2022).

2.3 Distress Mechanisms for Cold Recycled Pavements

The flexibility and durability of CR mixtures enables the design of a base layer that meets the specific requirements of a project. The requirements of the mixture are determined by a combination of material properties, traffic carrying capacity, and environmental effects. By adjusting the proportions of aggregate, asphalt binder, and chemical additive in the mixture, it is possible to construct a layer with the required balance of stiffness (load spreading ability), rut resistance (shear strength), flexibility, and durability (moisture resistance) (Asphalt Academy, 2020).

The two fundamental distresses of CR pavements that need to be considered in the mix design are rutting (permanent deformation) and moisture susceptibility. Thermal cracking resistance through the use of low temperature indirect tensile creep and strength tests (AASHTO T322-07) has also been considered during the design of the mix (MnDOT- *Grading and Base Manual*, 2022).

Permanent Deformation: This is the cumulative deformation brought on by repeated load applications, and it depends on the material's shear properties and degree of densification. Similar to granular materials, the failure of CR materials is attributed to permanent deformation, which makes it the crucial parameter in the design of CR layers, rather than fatigue cracking (Bierman, 2018). The improvement of resistance to long-term deformation (rutting) is achieved by:

- An Increased maximum particle size
- Improved compaction
- Improved aggregate grading, shape, hardness and roughness.
- Curing (reduced moisture content)

Moisture Susceptibility: When CR mixtures are exposed to high moisture contents and pore-pressures brought on by traffic, the damage that results are measured by moisture susceptibility. Due to the partially coated nature of the RAP aggregate and the presence of water in CR mixtures (both for compaction and any moisture intrusion), moisture susceptibility is a significant factor to take into account when evaluating the performance of a material. Decrease of adhesion between the asphalt binder and aggregate, which results in a loss of shear strength, is the main cause of damage in CR materials. Moisture resistance can be improved by:

- Addition of chemical additives
- Continuous grading
- Increased asphalt binder
- Improved compaction

Thermal Cracking: This is brought on by the CR material’s tendency to contract because of exposure to low (cold) temperatures or high cooling rates, and is influenced by the material’s tensile stress capacity, fracture characteristics and the coefficient of thermal expansion/contraction. The following factors typically increase resistance to thermal cracking:

- Improved compaction
- Adequate asphalt binder application
- Improved aggregate grading
- Curing (reduced moisture content)
- Limited chemical additive application (less than 1.5%)
- Decreased maximum particle size.

2.4 Cold Recycled Material Characterization

There has been a lack of consensus regarding the fundamental, engineering, or empirical features used to characterize CR materials for pavement design and performance evaluation (Dave et al., 2022). This section provides a summary of tests from existing literature utilized to evaluate CR mixtures.

2.4.1 Stiffness Measures

The majority of evaluations of CR material properties have centered on determining the structural capacity through the assessment of stiffness and load resistance capabilities. This is particularly relevant during pavement design and measurement of rutting resistance. Preliminary findings from previous research show promising results in CR materials using the resilient modulus test alongside Falling Weight Deflectometer (FWD) and Light Weight Deflectometer (LWD) field investigations. These tests are described in detail in the following sub-sections.

2.4.1.1 Complex Modulus (E*) test

Numerous studies have examined the stiffness characteristics of CR materials using the complex modulus (E*) test, in accordance with the AASHTO T 342 specification. The NCHRP 09-51 project (Schwartz et al., 2017) provided major advancements in establishing design inputs by developing E* and repeated load permanent deformation (RLPD) models from field core samples. The application of E* testing in CR materials has also been demonstrated in several investigations. For instance, Kim et al. (2011) evaluated the effects of curing time and moisture content on the stiffness of CIR mixtures, while Godenzoni et al. (2015) investigated how RAP content influences the stiffness of cement–bitumen treated materials. Similarly, Kim et al. (2009) used E* testing to compare the viscoelastic behavior of CIR materials against conventional hot mix asphalt (HMA). More recently, Gatiganti et al. (2023) explored the influence of specimen size on E* characterization of FDR mixtures, reporting less than 15% variation in measured modulus values between large- and small-scale specimens across all test temperatures and loading frequencies.

2.4.1.2 Triaxial Resilient Modulus (TM_r) test

Resilient modulus determines a layer's ability to distribute stress and is therefore a crucial property to consider, particularly in the elastic design of pavement structures (Bierman, 2018). This test is typically conducted in accordance with the AASHTO T 307-99 (1999) at room temperature and involves the application of cyclic haversine loading at a frequency of 1Hz, with a loading period of 0.1s and rest period of 0.9s. Different combinations of confining and deviator pressures are used to simulate various stress-state conditions. Fedrigo et al., (2018) examined a CR mixture consisting of 50% RAP, 50% graded crush stone and 2% cement by conducting the TM_r test and comparing the results with Indirect tensile

resilient modulus. The results from this study established that confining and deviator stresses increased the TM_r. This behavior was comparable to that of granular materials, probably owing to the low cement content. TM_r increased with increasing confining stress, possibly because the mixture's density increased. It was also indicated that due to strain hardening, the moduli increased with the deviator stress. Similar to the Indirect tensile resilient modulus results, TM_r increased linearly with curing time.

2.4.1.3 Falling Weight Deflectometer (FWD) and Light Weight Deflectometer (LWD)

The assessment of the performance of existing road pavements has become a priority in current practice. Engineers must have a reliable approach to evaluate the structural state of pavements in order to make suitable rehabilitation and management recommendations (Tebaldi et al., 2014). Falling weight deflectometer (FWD) testing is a widespread monitoring and testing method in the field and is usually conducted in accordance with the ASTM D4694-09 (2020). FWD may be utilized to assess structure conditions, construct performance models, and select the optimal CR technique. FWD data metrics available include deflection, stiffness, structural bearing capacity, and structural number (Xiao et al., 2018).

Using FWD, Guatimosim et al., (2018) evaluated the structural performance of an experimental section of CIR with foamed asphalt. The experiments were conducted one day after construction and 3, 13, 22, and 33 months afterwards. Back calculation of the FWD data was performed to analyze the evolution of the resilient modulus of the layers, and several deflection basin characteristics were compared to estimate the structural performance of the pavement. The FWD measurements were adjusted for temperature. Observations revealed that the resilient modulus increased significantly as the curing period progressed, leading to a dramatic reduction of pavement deflections. Diefenderfer et al., (2015) also utilized FWD to gather information on structural capacity of CR layers.

Typically, FWD is used to evaluate the properties of the newly constructed pavement or to evaluate the remaining life of the old pavement. Light weight deflectometer (LWD) tests can also be performed with the objective of calculating the surface modulus (also reported as composite modulus) of the tested surface in order to evaluate the structural contribution of the CR layer to the bearing capacity of the pavement or the short-term bearing capacity of cement/bituminous bound CR materials. The LWD is a portable device that delivers the same type of stress pulse as the FWD; however, the maximum stress is often less (normally not more than 200-kPa (29-psi) with a 300-mm (12-inches) diameter standard loading plate) and the center deflection is often the sole parameter evaluated. The LWD is usually conducted in accordance with the ASTM E2583-07(2020).

2.4.2 Strength Measures

Lab measured strength parameters are the most commonly used parameters in designing CR asphalt mixtures (Ma et al., 2015). One of the limitations of CR mixes is the low early strength. This is, however, better enhanced with the optimal use of stabilizers. There exist numerous test procedures to assess the strength of CR mixtures. The most commonly used tests are described in the following sub-sections.

2.4.2.1 Indirect Tensile Strength test (ITS)

The ITS test is utilized as an indirect assessment of the tensile strength and flexibility of CR mixtures (Asphalt Academy., 2020). It gives an index for evaluating engineering properties and is also used to measure the layer's sensitivity to moisture using the tensile strength ratio. In conjunction with laboratory mix design testing, ITS strength measurements may be used to evaluate the relative quality of CR mixtures and to estimate the likelihood of rutting or cracking. As a result, several studies have employed the ITS test to evaluate the performance features of CR materials (Cross, 2000; Kim et al., 2011; Diefenderfer et al., 2012; Dave et al., 2022). This test is typically conducted in accordance with the ASTM D6931-17 (2017) specifications and involves loading minimum three cylindrical specimen (Laboratory prepared specimens, Core specimens) at a defined rate of deformation (50 ± 5mm/min) and test temperature of 25°C (77°F) over its vertical diametral plane. The peak load upon failure is recorded and utilized to determine the specimen's ITS strength.

2.4.2.2 Triaxial Shear Strength test

For the last 50 years, the triaxial shear strength test has been considered as the standard test for measuring the shear strength of materials (Kaloush et al., 2010). The shear behavior of a CR material is comparable to that of the granular material, with a few notable exceptions. Binder stabilization modifies shear properties by substantially increasing cohesion (c) and causing a slight decrease in friction angle (ϕ) (Bierman, 2018). CR materials are intended to be more similar to traditional unbound granular materials with increased cohesion in the early phases following construction (Collings and Jenkins, 2011). It may be appropriate to test shear strength rather than tensile strength during this early period (Dave et al., 2022). Further, shear strength is a fundamental property of CR materials that is tied to rutting in these layers caused due to plastic deformations. Čížková et al., (2016) proposed that CR materials may benefit greatly from the triaxial test, which may be best appropriate to materials with low binder levels whose material behavior may be better represented by the cohesion and shear characteristics. Other researchers (Jenkins et al., 2007; Fu et al., 2009; Jenkins et al., 2012; Dal Ben & Jenkins, 2014; Guatimosim et al., 2018) have determined the triaxial test's appropriateness for describing the shear and shear characteristics of typical CR materials.

The development of the Simple Triaxial Test (STT) (Mulusa, 2009) has facilitated triaxial testing in laboratories. While the STT apparatus can primarily be used for monotonic triaxial testing in order to determine cohesion and friction angle values, the material's monotonic stiffness, tangent modulus (E_{tan}) can be measured. This parameter provides an indication of the material's resilient behavior and can be used to follow trends in the stiffness of different mix compositions (Asphalt Academy., 2020). Typically, the CR specimens used for this type of characterization are 300-mm (12-inches) in height and are compacted using five layers of equal thickness. The simplified technique for testing comprises of placing the material into a mold fitted with an inflating plastic membrane. The specimen is then topped with a metal disk, and a monotonic vertical displacement is applied until shear failure of the material. The heavy-duty rubberized plastic membrane permits various confining pressures up to 200-kPa (29-psi) to be applied to the test specimen.

Triaxial testing can be used to determine and convey the moisture susceptibility of CR materials as the retained cohesion. CR materials are considerably less susceptible to water than granular materials and

have a greater cohesion retention. Using monotonic triaxial experiments at a confining pressure of 100 kPa, the retained cohesion is calculated as a ratio of soaked (submerged in water for 24 hours at 25°C) to unsoaked principal stress. Equation 2-4 depicts the determination of retained cohesion.

$$Retained\ Cohesion = \frac{\sigma_{1,100,S} - 100}{\sigma_{1,100,U/S} - 100} * 100$$

Equation 2-1

In which.

$\sigma_{1,100,S}$: Applied principal stress at failure for the soaked specimen at σ_3= 100-kPa (14.5-psi)

$\sigma_{1,100,U/S}$: Applied principal stress at failure for unsoaked specimen at σ_3= 100-kPa (14.5-psi)

2.5 Factors Affecting Mechanical Properties of Cold Recycled Mixtures

This section summarizes the review of literature on various factors that have been identified to affect the mechanical properties of CR mixtures. These are described in the following subsections.

2.5.1 Curing

Ogbo et al. (2022) conducted a study involving field and laboratory investigations, which revealed that the mechanical properties exhibit a more rapid change in the field compared to controlled laboratory environmental conditions, specifically in relation to the evolution of moisture content. Furthermore, it was reported that the mechanical properties of the CR material may undergo further alterations even after attaining moisture equilibrium conditions. Yang et al. (2021) conducted a study to compare the effects of mixed curing conditions (3 days @ 20°C followed by 2 days curing at 60°C) and single curing conditions (2 days curing at 60°C) on the indirect tensile strength and critical strain energy density (CSED) of an emulsion treated CR mixture under different compaction levels. The results indicated that the mixed curing condition was more effective in enhancing these properties when the cement content was high (2%), whereas the single curing condition was more effective when the cement content was low (0-1%). The recommendation is to utilize single curing conditions for low cement content (0-1%) and mixed curing conditions for high cement content (above 2%). Graziani et al. (2016) conducted a study on two mixtures containing 1% and 2.5% chemical additive (Portland cement). The results showed that the indirect tensile strength (ITS) increased with an increase in curing time for both mixtures, irrespective of the curing temperature. Additionally, a constant ITS was obtained at longer curing periods.

2.5.2 Chemical Additive (Active Filler)

Researchers have shown that chemical additive in CR mixtures influence the mechanical properties. Halles & Thenoux, (2009) identified the level of influence of the various chemical additives on the mechanical properties of CR materials. The utilization of Portland cement and kiln dust was observed to yield better results in the performance (lab measured) of CR mixes, as compared to the use of fly ash and lime, as evidenced by improvements in both the Indirect Tensile Strength (ITS) and resilient modulus. Furthermore, it was observed that the curing process of foamed asphalt is time-consuming.

Therefore, the incorporation of chemical additives, primarily cement, was found to significantly enhance the initial strength of CR mixes. It was recommended in this study that chemical additives should be considered in foamed asphalt treated SFDR as it aids in early strength gain and medium to long term mechanical properties. Yang et al., (2021) explored the influence of cement content in CR mixes with respect to curing. For various curing conditions, it was shown that ITS and critical strain energy density increased with both low (0-1%) and high cement contents (2%) as evaluated in the study. Li et al., (2016) in their study revealed that cement played a crucial role on the early strength during the early curing stages (0-3 days of curing). The NCHRP 09-51 study (Schwartz et al., 2017) studied the role of chemical additives in CR mixtures based on a repeated load permanent deformation analysis and it was discovered that cement significantly reduced the amount of permanent deformation.

It is also noteworthy that the chemical additive content impacts the mechanical property of CR materials. Ma et al., (2015) varied the cement content in CR mixtures and subsequently subjected each mixture to both dry and immersion splitting tests. The experimental results indicate a positive correlation between the tensile strength and the cement content. The observed relationship between the tensile strength and cement content was found to be non-linear, whereby the rate of increase in tensile strength decreases upon exceeding a cement content of 1%. The study revealed that the tensile strength exhibited minimal variation at cement contents above 2%.

2.5.3 RAP Gradation

The significance of RAP gradation on CR mixture mechanical properties has been explored in different studies. Zhu et al., (2019) investigated three gradations by varying the passing rate of 4.75mm critical sieve size. Of the 3 gradations, regardless of the aging conditions, the CR mixture with finer gradation appeared to have better mechanical properties which can be attributed to its dense skeletal structure, high optimum water content, and asphalt emulsion content in comparison with other gradations. It was also observed that after long-term ageing, the effect of gradation on the mechanical properties becomes increasingly significant. Another study by Raschia et al., (2019) provided that the indirect tensile stiffness modulus (ITSM) of the finer RAP gradation was higher compared to other gradations investigated in the study.

2.5.4 Amount of RAP

The amount of RAP in a CR mixture plays an important role in its mechanical performance. Ma et al. (2015) observed that the incorporation of varying amounts of RAP into a cement treated CR mixture resulted in a reduction in tensile strength with an increase in RAP content. Xie et al. (2021) discovered that the incorporation of RAP in emulsion treated CR mixture resulted in an increase in both tensile strength and fracture energy. Valdés et al. (2011) noted a similar trend in their study, whereby an increase in the content of RAP resulted in an increase in both tensile strength and stiffness.

2.5.5 Temperature

Although limited studies have been conducted on this aspect, the influence of temperature by simulating geographic conditions for production and compaction is important in evaluating mechanical properties and their evolution in CR materials. A study conducted by Raschia et al. (2020) aimed to

assess the mechanical properties and compatibility of emulsion treated CR materials that were produced at low temperatures. This research conducted simulations of production, transport, and compaction temperatures at 5°C and 25°C for a CR mixture treated with two types of emulsion. The study found that the long-term strength and stiffness of the Type-1 Emulsion mix remained unaffected by the production temperatures, as indicated by the ITS and Indirect Tensile Strength modulus values. The ITS value of the type-2 emulsion mixture that was produced and compacted at a temperature of 25°C exhibited a higher value than the ITS value of the mixture that was produced at a temperature of 5°C. While acknowledging the influence of the emulsion source on the mechanical characteristics of the end product, it was recommended that further investigation and analysis be undertaken across a broader range of temperatures and temperature combinations. Another study conducted by Cheng et al. (2020) investigated the impact of mixing temperature on foamed asphalt treated mixture within the temperature range of 17°C to 30°C. The findings revealed that an increase in mixing temperature resulted in a moderate improvement of the CR mixture strength. The study revealed that an increase in mixing temperature resulted in a corresponding increase in the Tensile Strength Ratio (TSR), indicating a heightened ability to withstand moisture-induced damage at elevated mixing temperatures.

2.5.6 Stabilizer Type

Iwański & Chomicz-Kowalska (2013) investigated the effect of foamed asphalt on the mechanical performance of CR mixes containing Portland cement as chemical additive through resilient modulus and indirect tensile strength. Results from this study highlighted that both the indirect tensile strength (soaked and unsoaked) increased with an increase in the foamed asphalt content. Also, increase in foamed asphalt and cement content led to a higher retained tensile strength. Another study by Valentin et al., (2016) varied cement content between 0% and 5% and foamed asphalt between 2% and 4.5%. Results from this study show differing effects of both foamed asphalt and cement where the optimal foamed asphalt level appears to be between 2.0% and 2.5% and higher foamed asphalt content results in a decrease in stiffness modulus and ITS. In comparing foamed asphalt to emulsion, Iwański & Chomicz-Kowalska, (2016) conducted a comparative study between foamed asphalt and emulsion and found that the foamed asphalt exhibited higher dry and wet indirect tensile strength. It was also indicated that foamed asphalt exhibited higher resistance to moisture damaging effects.

By evaluating the impacts of emulsion contents without cement addition in a CR mixture, Valentin et al., (2016) observed that the optimal range of emulsion content was around 2.5 - 3% of the mixture. Further addition of emulsion led to a reduction of the stiffness modulus and indirect tensile strength evaluated properties. Flores et al., (2020) explored the influence of emulsion on the fatigue resistance of cement-asphalt binder treated CR mixes. CR mix containing 4% emulsion provided better resistance than the CR mix containing 3% emulsion as evaluated in the study. Chen et al., (2020) in their study observed an increasing Indirect tensile strength with an increasing emulsion content. It was also suggested that cement and asphalt emulsion in a cement-emulsion treated CR mixture should be thoroughly blended prior to contact with aggregate/RAP to achieve best performance of the mixture and prevent the creation of an unfavorable interface. Also noteworthy is the emulsion source as studied by Raschia et al., (2020). It was discovered that performance of the two emulsion mixtures at production temperatures of 5°C and 25°C were different in that the ITS and Indirect Tensile Stiffness Modulus (ITSM) of one

emulsion treated mixture showed generally low values. In addition, according to the NCHRP 09-51 study (Schwartz et al., 2017) on the dynamic modulus analysis, CR mixtures treated with emulsion was found to be stiffer at lower temperatures.

2.5.7 Compaction (Density)

Method of compaction and energy used to determine density and optimal performance of CR mixtures have gained attention recently. Filho et al. (2020) conducted a study to compare the effects of three compaction methods on the bulk density and performance of CR materials. The methods evaluated were the modified proctor, Marshall with 50 and 75 blows on both sides, and gyratory compactor with 40, 75, and 100 gyrations. The results indicate that the mixtures that underwent modified proctor compaction exhibited a reduced bulk density and consequently, a higher air void in comparison to alternative compaction techniques. The results indicate that the gyratory compactor exhibited better results in terms of bulk density, air void content, indirect tensile strength, and resilient modulus. Yang et al. (2021) conducted a study to evaluate compaction techniques, which were classified as single compaction with 50 blows per side, single compaction with 75 blows per side using the Marshall hammer, and double compaction (50 blows per side followed by 25 blows per side after curing with the Marshall hammer). As per the findings of this study, an increase in the number of compaction blows results in a reduction in voids. Furthermore, the utilization of the double compaction technique resulted in the reduction of voids generated by the process of water evaporation throughout the curing phase, leading to a substantial decrease in void content and a corresponding increase in the ITS.

2.6 Pavement Design Procedures, Modeling, and Performance of Cold Recycled Pavements

2.6.1 Empirical Pavement Design Procedures

CR pavement structural design relies on the evaluation of the remaining pavement life and the required structural adjustments for future traffic. The Asphalt Academy Technical Guide 2 (Asphalt Academy, 2020) which is based on the South African system recommends two methods for CR pavement design. The pavement number (PN) method, which is a knowledge-based approach and an improvement on the structural number as originally used in the AASHTO empirical design guide, and the Mechanistic-Empirical (M-E) method. Wirtgen Group (2012) offers the structural number (SN) method and the deviator stress ratio (DSR) design method developed for higher traffic levels (more than 30 million ESALs). The DSR method is founded on the premise that the rate of permanent deformation in a CR layer is proportional to the applied deviator stress relative to the deviator stress at material failure (Bierman, 2018).

The predominant approach employed is the structural number (SN) design method which bases the design of a pavement structure on empirical correlations between pavement thicknesses and traffic loads and is further determined by multiplying the individual thicknesses of each layer by two empirical coefficients, layer coefficient (a_i) and drainage coefficient (m_i), which account for the layer-specific structural contribution and drainage capacities, respectively (Diaz-Sanchez et al., 2017). Wirtgen Group (2012) suggests a structural layer coefficient between 0.20-0.38 for CR layers. Nemati et al., (2021)

proposed structural coefficient values for CCPR of 0.40 at 50% reliability and 0.28 at 95% reliability from a laboratory and field investigation study on pavement structures in New Hampshire. Diefenderfer and Apeagyei (2014) estimated layer coefficient ranging from 0.36 to 0.48 based on deflection tests and laboratory measurements of the resilient modulus and indirect tensile strength of foamed asphalt treated CCPR field cores. However, the deflection measurements were also impacted by an FDR layer beneath the surface. Diaz-Sanchez et al., (2017) also estimated a_i values for foamed asphalt treated CCPR from an empirical relationship between layer coefficient and back-calculated modulus data and obtained values ranging from 0.36-0.39 at a reference temperature of 20°C and indicated that a service life of 10 million ESALs can be achieved without any major reduction in the structural capacity. Several other studies have proposed layer coefficients for CR layers (Tia and Wood, 1983; Van Wijk and Wood, 1983; Van Wyk et al., 1983; Marquis et al., 2003; Sebaaly et al., 2004; Loizos and Papavasiliou, 2006; Carvajal et al., 2021).

2.6.2 Mechanistic-Empirical Pavement Design Approaches

The M-E design approach presents a departure from the empirical pavement design methodologies. This approach is currently gaining attention and studies have utilized these approaches to further assess and design CR pavements. M-E methods are much more comprehensive than empirical pavement design approaches and include numerous variables and parameters to characterize materials and predict pavement performance. Elements of mechanical modeling and performance observations are combined in determining the required pavement thickness for a set of design conditions. Along with inputs for traffic, climate, and materials, inputs for the geometry of a pavement structure are required in this approach. M-E computes pavement responses to load (stresses and strains) that are used to calculate damage (distresses and loss of rideability) over time (Baus & Stires, 2010). The approach employed for M-E design is outlined in Figure 2-1.

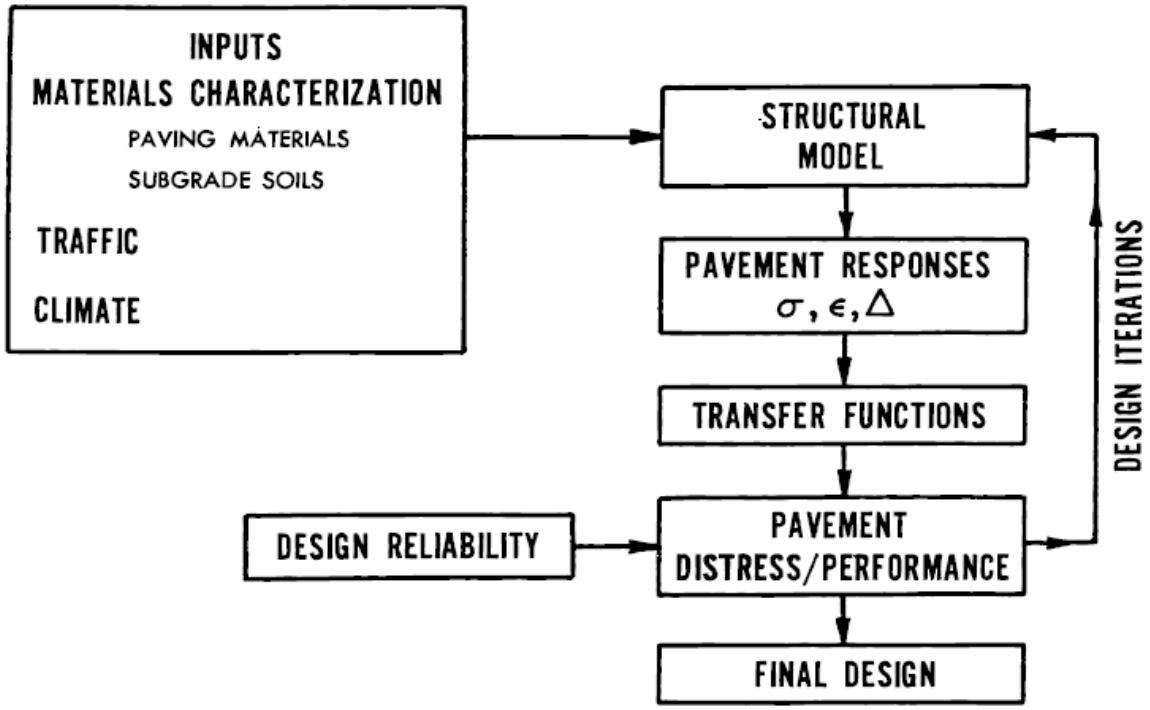

Figure 2-1: Mechanistic Empirical Design Approach (Thompson, 1996)

When the design approach is selected and all the relevant information for a pavement structure is supplied, the M-E computational program assesses the performance of the pavement throughout its design life. The program's structural response model and transfer functions compute the performance indicators, which represent significant pavement distresses. The structural response model computes the critical pavement responses (Figure 2-2) by including mechanistic models into the program. These important pavement responses are converted by empirical transfer functions into performance indicators that are examined throughout the design life (Baus & Stires, 2010).

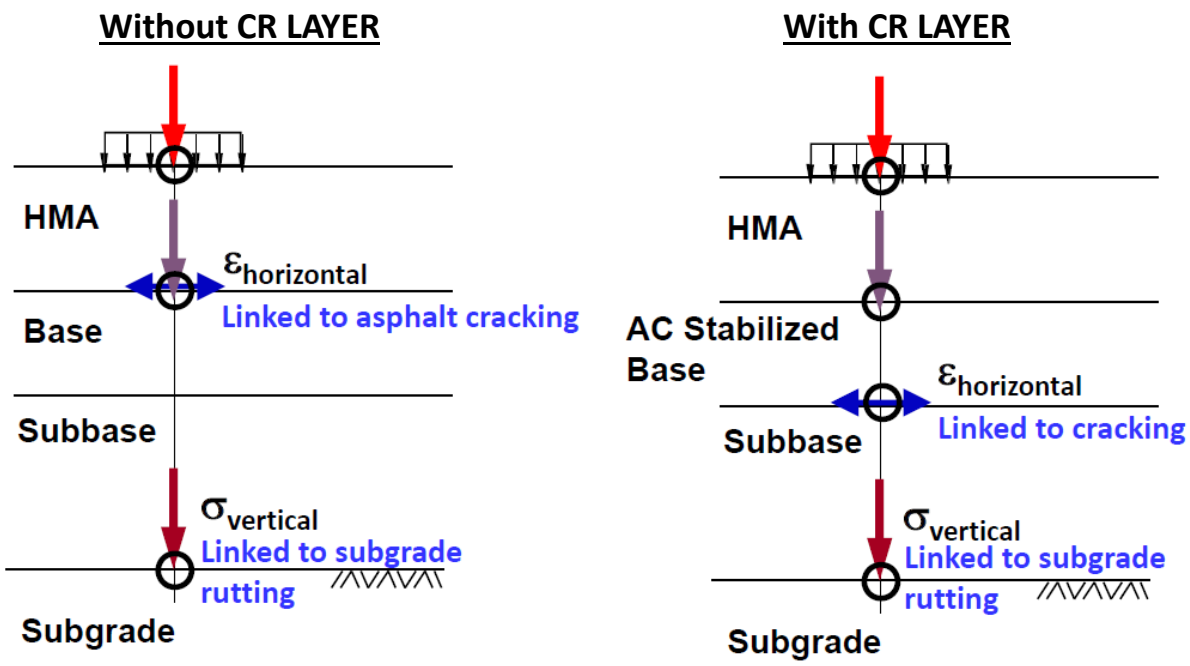

Figure 2-2: Critical responses used in M-E design (ISAP Cold Recycling of Asphalt Pavement Short Course, 2022)

2.6.2.1 Minnesota Flexible Pavement Design: MnPAVE

The MnPAVE flexible version 6.5 software (MnPAVE) integrates empirical relationships (also known as transfer functions) with mechanical structural response parameters (such as, critical strains in asphalt and subgrade layers) responsible for flexible pavement structural life. The utilization of MnPAVE for structural analysis and design is gradually replacing the usage of the Hveem R-value and soil factor in Minnesota's flexible pavement design procedures (MnDOT Design Guide, 2024). The mechanistic components of the program rely on determining the tensile strain at the base of the asphalt layer, the compressive strain at the top of the subgrade, and the maximum principal stress in the center of the aggregate base layer. This approach contains a layer-elastic analysis (LEA) software tool for pavement structures with up to five layers that is compatible with Microsoft Windows. The software's LEA component has evolved from the WESLEA framework.

MnPAVE consists of three information modules and three design levels: Traffic, Climate, and Structure. The level is determined by the quantity and quality of information regarding the material's characteristics and traffic statistics. Material information comprises of layer thickness, Poisson's ratio, dynamic modulus, and an index showing the degree of layer slippage. MnPAVE assumes a zero-slip condition at all layer contacts. Other variables include load and evaluation locations. To calculate stresses and strains in the structure, it is necessary to know the elastic modulus and thickness of each layer. Resilient modulus (M_r), which is the ratio of deviator stress to recoverable strain under specific conditions, is used to define the elastic modulus. Direct laboratory measurements utilizing a repeated load triaxial test, an estimate of M_r using a standard lab test such as the R-Value, or an estimate of M_r from the AASHTO or unified soil classification can be used to determine the resilient modulus. Using either the FWD or the dynamic cone penetrometer (DCP), resilient moduli can also be calculated from field observations. Other devices have been designed for this purpose as well. For a specific pavement design, there are three design levels (basic, middle, and advanced) based on the quality of information

on the material qualities and traffic data. For basic level, only a general knowledge of the materials and traffic data are required. The intermediate level corresponds to the quantity of data necessary for MnDOT projects at present. The advanced level requires that moduli be measured for a specific project.

MnPAVE considers the seasonal variation in M_r of the pavement layers. The years are divided into five seasons, the lengths of which can be altered dependent on geography or exceptional circumstances. Modulus values used in the current edition of MnPAVE are based on in-situ measurements at MnROAD and statewide testing.

The LEA model calculates stresses and strains at critical locations in the pavement structure for damage and reliability determinations. MnPAVE can conduct Monte Carlo simulations to determine design reliability. Transfer functions, given by Equation 2-1 and Equation 2-2, and Miner's hypothesis are then used to compute the damage factor and expected life of the pavement. The fatigue transfer function was derived from the Fred Finn–Asphalt Institute model, whereas the rutting transfer function was calibrated using existing R-value designs (Xiao et al., 2011). Additional performance transfer functions are also present in MnPAVE that a user can access in the advanced mode of the software.

Fatigue Transfer function:

$$N_f = C * S * (4.32 * 10^{-3}) \in_k^{-3.291} * E^{-0.854}$$

Equation 2-2

Rutting:

$$N_r = (6.18 * 10^{-3}) \in_v^{-2.5592}$$

Equation 2-3

In which,

N_f, N_r = allowed load repetitions for fatigue and rutting, respectively.

C = correction factor based on air voids and binder content,

S = shift factor (preliminary MnPAVE shift factor 92.6 is based on calibration with existing R-value designs), and

$\in_k, \in_v$ = tensile strain at bottom of HMA and vertical strain at top of subgrade respectively,

MnPAVE provides guidelines for designing pavement thicknesses of FDR, CCPR and CIR. For base layer on the input interface of the program, the aggregate base (AggBase), subbase, rubblized portland cement concrete pavement (RPCC), SFDR, and CIR can be selected. FDR is also provided as a subtype of aggregate base. There may only be two aggregate/granular layers in the pavement structure. Among these are the AggBase, Subbase, RPCC, SFDR, and CIR layers. If the pavement structure consists of more than two aggregate/granular layers, "Multi-Layer" may be used as a subtype for the aggregate base or subbase layer. Within the "Multiple Aggregate Layers" form, the layer can be specified by up to three layers of distinct aggregate/granular materials, with MnPAVE-Flexible combining their properties into a single composite layer using the equivalent layer concept.

One of the parameters used for the design of CR layers is the M_r, which is determined through field and laboratory investigations. The M_r is used to calculate the thickness required to meet the design criteria, which can include both structural and functional requirements. The thickness design of the CR layer considers the traffic loading, subgrade strength, and the desired performance of the pavement. MnPAVE also requires CIR design to include thickness of any residual existing HMA with the thickness of the CIR layer as the 5-layer limit of WESLEA prevents the use of a separate existing HMA layer beneath the CIR layer. That is, as an example, the top 4-inches of 6 inches of existing HMA will be recycled as CIR, while 2-inches of existing HMA will remain. This should be defined as a 6-inch layer of CIR. Further, it is specified that minimum 4-inches HMA overlay be used on FDR sections and minimum 2-inches HMA overlay on SFDR, CIR and CCPR sections.

2.6.3 Performance (Transfer) Function Development for Cold Recycled Materials

The bulk of pavement ME design approaches now in use lack a dedicated transfer function exclusively for CR pavements. AASHTOWare Pavement ME design guide (AASHTO MEPDG) (AASHTO, 2008) treats CR layers (CIR/CCPR) as asphalt layers. The California ME Pavement design program (CalME) (Ullidtz et al., 2010) on the other hand uses the same transfer function for asphalt layers for rutting in CR layers. The NCHRP 09-51 study (Schwartz et al., 2017) has made major contributions towards the development of design inputs by developing necessary E* and repeated load deformation (RLPD) model based on field cores. More research is still ongoing to build a database for CR materials as there is still no dedicated transfer function for CR layers at this time.

The initial point for the development and advancement of a mechanistic-empirical design function for CR materials was based on the transfer function of waterbound macadam as presented by Theyse et al., 2000. The Stellenbosch transfer function was developed in an effort to address the limitations of the waterbound macadam design function and the Loudon Transfer function. Details on the development of these transfer functions are discussed in the following subsections.

2.6.3.1 WaterBound Macadam Transfer Function

The failure mechanism of CR, which is permanent deformation or rutting, is comparable to that of granular materials. The transfer function pertaining to CR was first obtained from the design function for waterbound macadam, as presented in Equation 2-3 (Theyse et al., 2000). This model was developed using triaxial and heavy vehicle simulator (HVS) test data for waterbound macadam material with crusher sand and natural sand filler. The waterbound macadam transfer function computes the bearing capacity in terms of the number of standard axle load repetitions (N) that can be maintained prior to inducing a specific level of plastic strain in the layer.

$$\log N = 1.891 + 0.075(RD) - 0.0009(S) + 0.028(PS) - 1.643(SR)$$

Equation 2-4

In which,

N = number of standard axles the layer can sustain before reaching the deformation limit,

RD = relative density (%)

S = saturation (%)

PS = plastic strain limit as a percentage of the layer thickness (%), and

SR = stress ratio (-)

As shown in Equation 2-3, the stress ratio (SR) is a function of the load intensity, the shear characteristics of the materials, and the overall pavement structure. The relative density (RD) represents the percent of the material's maximum dry density derived from the Proctor test while the Plastic strain limit (PS) on the other hand can be tied to the rutting depth when multiplied to the layer thickness. According to Equation 2-4, the stress ratio for waterbound macadam can be calculated. Theyse et al., (2000) developed a model for the angle of friction of water-bound macadam material (Equation 2-5). This model defines the angle of friction in terms of the material's relative density and saturation (Relative density expressed as a percentage of apparent density and saturation expressed as a percentage of interparticle voids).

$$SR = \frac{(\sigma_1^a - \sigma_3)}{\sigma_3\left[\left(tan^2\left(45 + \frac{\emptyset}{2}\right) - 1\right)\right] + 2C\tan\left(45 + \frac{\emptyset}{2}\right)}$$

Equation 2-5

$$\emptyset = -26.38 + 1.021RD - 0.171S$$

Equation 2-6

In which,

σ_1^a: Applied major principal stress (kPa)

σ_3: Minor principal stress acting in the middle of the granular layer (kPa)

C: Cohesion (kPa)

Ø: Angle of internal friction (radian), calculated using Equation 2-5

2.6.3.2 Loudon Transfer Function

The transfer function for waterbound macadam was modified by Loudon International to more accurately characterize the performance of CR materials. The 'Loudon Transfer Function' was developed as a heuristic design tool based on the performance of pavement structures incorporating CR materials in five continents. Before a function based on in-service performance was developed, numerous CR pavements were considered. Equation 2-6 illustrates the Loudon Transfer Function. This function has not been published, and there is limited information regarding its calibration and verification (Bierman, 2018).

$$\log N = 1.55 + 0.1(RD) - 0.05(RetC) + 0.1(PS) - 22.333(SR)$$

Equation 2-7

In which,

N = number of axle repetitions to reach a rut depth of PS*CR layer thickness,

RD = relative density (%)

RetC = Retained cohesion (%)

PS = plastic strain limit as a percentage of the layer thickness (%), and

SR = stress ratio

2.6.3.3 Stellenbosch Transfer Function

The approach for granular type behavior was utilized to construct the Stellenbosch transfer function following the waterbound and Loudon transfer functions. This transfer function was based on 14 distinct roadways and 22 distinct analysis sections. The model equation is represented in Equation 2-7 (Bierman, 2018; Jenkins et al., 2020):

$$\log N = A - B(DevSR)^3 + C(P_{mod}.RetC) + D$$

Equation 2-8

In which,

DevSR = deviator stress ratio as a fraction,

P_{mod} = maximum dry density as a percentage of modified AASHTO density (%),

RetC = retained cohesion (%),

A = constant based on design reliability, and

B, C, and D = constants from data correlation as indicated in Table 2-1

The relative density (RD), as depicted in the waterbound macadam equation, was replaced in the developed equation with P_{mod} (percentage of Modified AASHTO density) because compaction obtained during construction plays a significant role in the behavior of the material. Likewise, saturation (S) was replaced by retained cohesion. This was done due to the superior moisture resistance and cohesion retention of CR material compared to granular materials.

Table 2-1: Reliability coefficients and limits (Jenkins et al., 2020)

Reliability	A	Rut limit (mm)
95	0.8436	10
90	0.9312	15
80	1.0198	20
50	1.1369	25

The DevSR term characterizing the effect of deviator stress on pavement performance gave a power three function, highlighting its significance and sensitivity. The DSR is measured at a depth equal to 25% of the thickness of the CR materials layer and is represented in Equation 2-8.

$$DevSR = \frac{\sigma_1 - \sigma_3}{\sigma_{1,f} - \sigma_3}$$

$$\sigma_{1,f} = \frac{(1 + sin\varphi)\sigma_3 + 2C.cos\varphi}{(1 - sin\varphi)}$$

Equation 2-9

In which,

σ_1 = major principal stress (kPa),

σ_3 = minor principal stress, i.e., confining pressure (kPa),

$\sigma_{1,f}$ = major principal stress at failure (kPa),

C = cohesion of the CR materials default value (kPa),

φ = frictional angle of the CR materials default value (°)

Calibration of the design function was performed in order to best represent the relative influence of each input variable on CR materials and to determine values for the constants in Equation 2-7. The transfer function connects the number of standard axles the pavement can support to the amount of permanent strain left in the CR materials layer, i.e., a design-specified limit value. This allows the designer to determine the amount of permanent deformation that can occur before the CR materials is regarded to have failed, which is related to the design reliability.

Long-term pavement performance data, permanent strain development with reported loading and safety adjustments for design where all explored in the development of the transfer functions and are discussed in detail by Jenkins et al., (2020). The new CR materials design function that has been calibrated is depicted in Equation 2-9. For design purposes, the design function can be used to estimate the CR materials lifespan. However, the deployment of this function must adhere to the requirements given in the Asphalt Academy Technical Guide 2 (Asphalt Academy., 2020), where the stiffness of allotted materials and analysis positions in the CR materials layer are described.

$$\log N = A - 57.286(DevSR)^3 + 0.0009159(P_{mod}.RetC) + 0.86753$$

Equation 2-10

The resistance of unbound granular materials to permanent deformation under repetitive loads can be enhanced by increasing the material's density (van Nierkerk, 2002). The performance and longevity of a CR mixture are dependent on its level of compaction (Jenkins, 2000). Significantly contributing to the deterioration of pavement materials, particularly CR materials, is moisture damage. A decrease in shear strength due to moisture intrusion, i.e., a higher degree of saturation (S), accelerates the rate of permanent deformation (Lekarp et al., 2000). The rate of permanent deformation increases as the deviator stress and confining pressure decrease. This, together with the relative density, greatly depends on the grading of the material. (Werkmeister, 2003).

2.6.4 Modeling of Cold Recycled Pavements

Gu et al., (2018) studied the structural performance of four CR pavements (CCPR and CIR), oth treated with emulsion and foamed asphalt through laboratory and field investigations. The results of the laboratory investigation were used to define the inputs for the AASHTOWare Pavement M-E program to estimate the pavement performance, and the results from the field sections were utilized to validate the laboratory study's performance prediction. Based on the results of the dynamic modulus, it was suggested that CR mixtures be considered thermo-viscoelastic materials. This study also revealed that CCPR mixtures were less susceptible to rutting than CIR mixtures, and that CCPR foamed treated mixture exhibited rutting resistance comparable to that of HMA. Similar trends were seen for the first two years of service when comparing the predicted and monitored performance of field sections, but the Pavement M-E program over predicted the rutting depth of these sections relative to field measurements. This study further confirmed that bottom-up fatigue cracking was not a significant mode of pavement distress for CR pavements. Arimilli et al. (2017) compared the mechanical performance of conventional asphalt pavement with HMA surfacing with CR emulsion and foamed treated base layers with overlay using finite element simulations. The results indicated that CR layers treated with emulsion and foamed asphalt can be utilized as effective base layers in flexible pavements. Based on the multilayered elastic analysis, the strain at the base of the HMA layer is lower in the emulsion- and foam-treated layers than in the unbound granular base. In addition, the deflection and vertical compressive strain are maximum when conventional layers and emulsion-treated bases are employed, whereas they are less when foamed-treated layers are used. Furthermore, it was revealed that due to the lower binder contents in optimization for foamed asphalt treated mixtures, the calculated allowable fatigue life is less, resulting in a thicker pavement layer compared to the emulsion treated layer. The emulsion treated layer was discovered to be thinner than the other three designed pavement sections.

Preti et al. (2021) modeled a pavement structure composed of a CR mixture treated with cement and foamed asphalt to better understand the effect of CR layers on the overall pavement response to traffic loading in terms of buildup of pavement deformation at the surface. By utilizing the Mohr-Coulomb failure criterion and the perfectly plastic flow rule, this study recommended the use of elastic-perfectly plastic models for subsurface materials in the design and analysis of flexible pavement systems. In addition, the effect of temperature on the mechanical response of CR mixtures was demonstrated, with the multilayer pavement model incorporating a realistic temperature distribution with depth. It was determined that this influence could not be disregarded while evaluating the pavement properly. This study compared the rutting performance of CR treated base layer to that of typical granular base layers, concluding that the cold treated layer placed above crushed aggregate granular material in the pavement construction produces highly beneficial results.

Kuchiishi et al., (2021) additionally investigated the impact of non-linear elastic behavior of foamed asphalt treated mixes on pavement structural performance. In this study, a pavement structure with a base layer composed of RAP with 2% foamed asphalt and 1% hydrated lime demonstrated that considering CR mixtures as non-linear elastic material reduces the horizontal strains within the recycled layer and the vertical stresses on top of the underlying layer in comparison to the linear elastic scenario, which can lead to an increase in pavement structural capacity. Also, in this study, the effect of different

resilient modulus models on the CR mixture mechanical response was evaluated. The triaxial resilient modulus test data were fitted with three distinct stress-dependent constitutive models, including the confining pressure, K-θ, and Pezo's model. By employing a pavement analysis program (AEMC), the fitted coefficients were used as input to account for the nonlinear elastic behavior. Figure 2-3 represents pavement structure as well as the strains and stresses for each of the three models considering fully bonded conditions between layers.

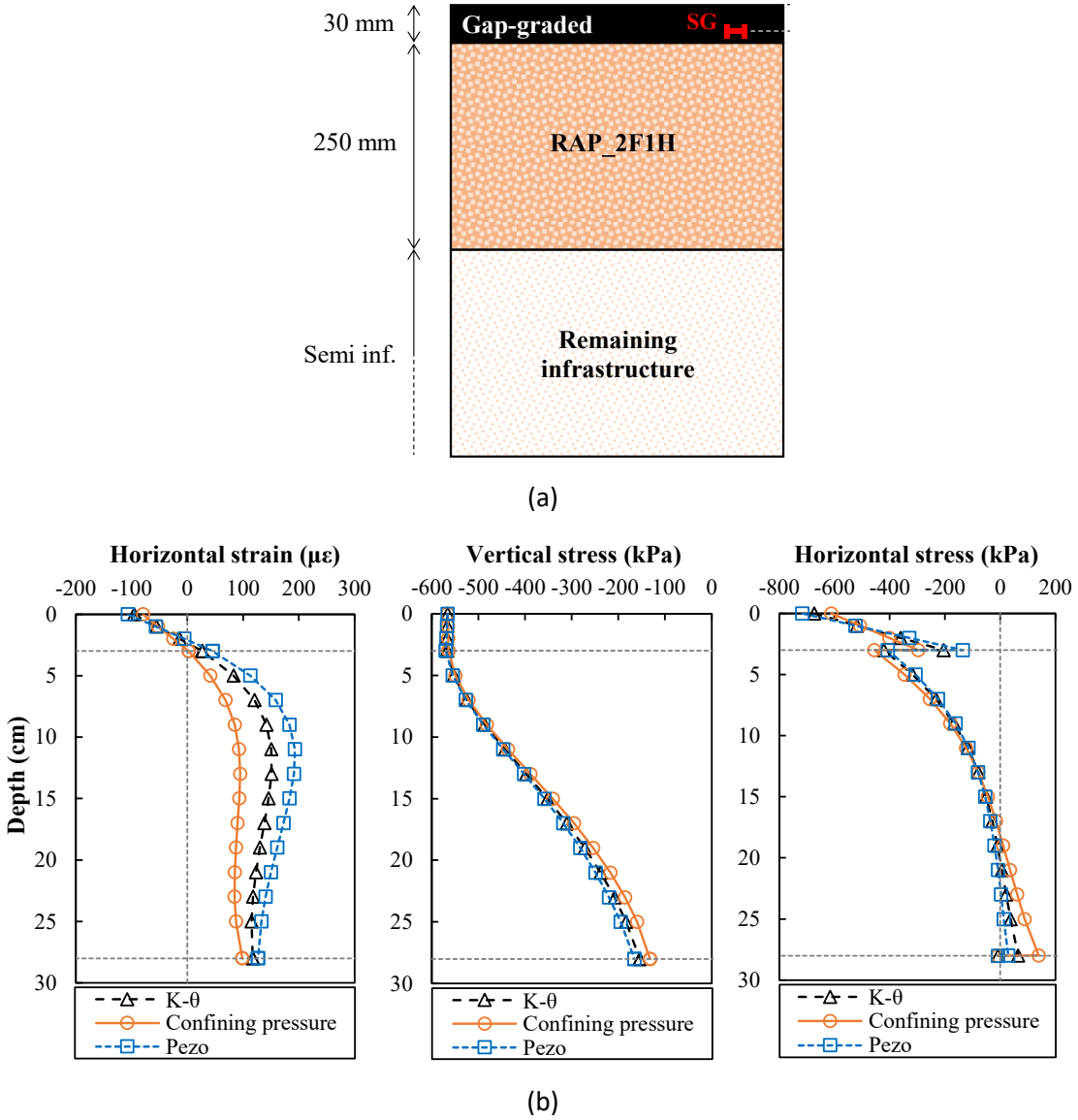

Figure 2-3: (a) Pavement structure (b) Stresses and strains using the stress-dependent resilient modulus from the three models (Images from Kuchiishi et al., 2021).

Materials characterization and pavement design can benefit from taking CR material's non-linear elastic behavior into account; however, the pavement response is highly sensitive to the type of resilient modulus model used. Horizontal strains in the CR material layer are shown to be lowest for the confining pressure and largest for Pezo's model, with the K-θ model providing intermediate findings. The authors

therefore suggested using Pezo's model to characterize materials in simulations of pavement analysis to account for CR material's non-linear elastic behavior.

2.6.5 Field Performance of Cold Recycled Pavements

2.6.5.1 CIR Performance

According to an assessment conducted on the performance of CIR projects in the northwest region of Pennsylvania (Morian et al., 2004), CIR provided service lives up to 160% of the 10-year design life provided by conventional mill and overlay projects in the same area and performed two to three times better than conventional overlay in resistance to reflection cracking. CIR materials can achieve stiffness values comparable to those of HMA if proper construction control procedures are followed. These CIR materials appeared to be stress-sensitive, meaning that their stiffness increased as traffic load increases. This quality may have a significant role in the observed equivalent performance and reflection cracking control. However, back-calculated modulus data indicated a progressive loss in material stiffness over time, which becomes substantial ten years after construction. The treatment depth, type, and depth of asphalt overlay have a significant impact on the expected service life and performance of CIR pavements. In comparison to the service life of thick lift HMA, the projected service life of CIR with surface treatment (chip seals) is 6 to 8 years, and approximately 7 to 15 years with an HMA overlay (Asphalt Recycling and Reclaiming Association, 2015). Long-term field performance of CIR projects in Nevada demonstrated that CIR is an effective and recommended approach for low- and medium-traffic roads (30-300 ESALs per day), since it generates a more resilient and flexible base, hence reducing reflecting cracking, thermal cracking, and rutting. In addition, it was determined that the CIR technique produces a better and more stable Pavement Serviceability Index (PSI) (Sebaaly et al., 2004). Figure 2-4 displays the relationship between the predicted performance of a composite pavement (asphalt overlay on PCC) and the US24 CIR pavement in terms of Illinois DOT's Condition Rating Survey measure and the result shows a better performance of CIR over the years in comparison to the composite pavement.

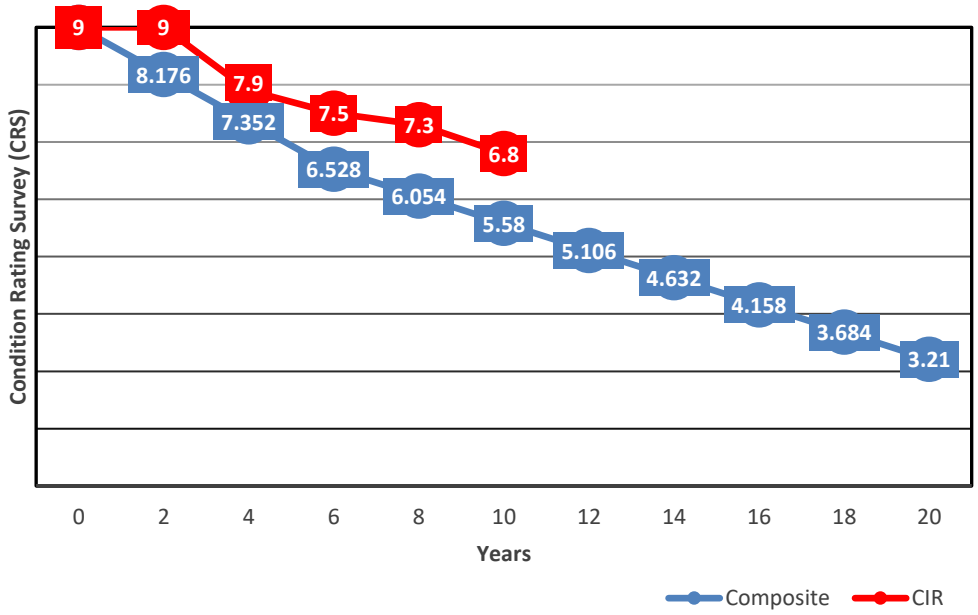

Figure 2-4: US 24 CIR Performance as Compared to Asphalt Overlay Alternative (Data provided by Illinois DOT)

2.6.6 CCPR Performance

Evaluation of the performance of CCPR sections on I-80 and I-64 in Virginia revealed that when designed and constructed appropriately, CCPR performs similarly to conventional asphalt pavements and may be used on high-volume roadways (50,000 AADT) (Al-Qadi & Ozer, 2020). Rahman and Vargas-Nordcbeck (2019) studied the influence of thin overlays on the structural performance of CR base layer for high-traffic roads (1.77 Million ESALs) in Alabama. CCPR sections resulted in more rutting than CIR sections, while sections stabilized with foamed asphalt resulted in more rutting than emulsion stabilized sections, based on three years of rutting and IRI data. IRI of untreated base sections was less than IRI of CR base sections. It was determined that the thin overlay surface of CR bases is more sensitive to ride quality deterioration under heavy usage. Except for minor cracking on the foamed CCPR section, no substantial cracking was noticed in the test sections after one year of service.

2.6.7 SFDR Performance

The performance of SFDR projects in Nevada over a 10-year period demonstrated that SFDR projects were performing well. These SFDR projects were constructed with 2% or 3% cement as a stabilizing agent (if soft subgrade was detected). Non-wheel path longitudinal cracking on one project was ascribed to the asphalt surface and not the SFDR treatment. The performance over 10 to 15 years demonstrated that the majority of projects functioned well, with the exception of a few projects that exhibited transverse or fatigue cracking. SFDR pavements older than 15 years were either rehabilitated or suffered from reflective cracking. (Bemanian et al., 2006). Johanneck and Dai (2013) analyzed three engineered emulsion (EE) SFDR sections (Cells 2, 3, and 4) constructed on I-94 in 2008 at the Minnesota Road Research Facility (MnROAD). Each test section was designed for 3.5 million ESALs for a period of five years. As of 30 June 2012, the sections had experienced approximately 2.2 million ESALs, which exceeds 60% of the design life. For the SFDR layers, various emulsion contents were investigated. The SFDR

layers of Cells 2, 3, and 4 were stabilized with 4%, 3%, and 0.75 % Engineered Emulsion (EE), respectively. Strain sensors were used to measure the strain responses of the HMA and SFDR layers at their base. The measured data revealed that the bottom of both the HMA and SFDR layers were subject to tensile strain, with the tensile strains under the SFDR layers being significantly greater than those under the HMA layers, indicating that the stabilized layer transferred strain deeply into the pavement structure. successfully. According to BISAR simulations, the horizontal strains beneath the HMA layer were reduced by approximately fifty percent when compared to an HMA over a granular base pavement structure. This reduction in tensile strain may improve efficiency and extend service life. Measurements of cracking, IRI, and rutting in the field indicated that test sections performed satisfactorily. In Cells 2 and 4, no cracking was observed. Only a single crack was observed in Cell 3, which is thought to have originated at the shoulder. There was no thermal cracking observed. After approximately 60% of the design life, rutting measurements for Cells 2 and 3 was 0.27 inches and 0.3 inches for Cell 4. Using project-specific inputs, DARWin-M-E rutting and IRI predictions were close to field measurements. Overall, it is concluded that SFDR is advantageous in minimizing the HMA tensile strains and leads to superior pavement performance compared to a conventional structure of HMA over a granular base (Vrtis, 2023). As of February 2019, the sections had experienced more than 8.5 MESALs, exceeding their design ESALs by a significant margin. After seven years of service, all cells had a Pavement Condition Index of "Good" (above 85).

2.7 State of Practice for Cold Recycled Layers Pavement Design and Analysis in Minnesota

A survey was conducted to identify cold recycling approaches currently used, pavement design methodologies, and associated challenges in their implementation by the Minnesota Department of Transportation (MnDOT) and local agencies in Minnesota pertaining to the design and analysis of CR pavements. The survey reviewed treatment approaches, observed pavement distresses resulting from cold recycling treatments, and procedures for tracking the performance of CR pavements. The survey also sought to identify agency preferences for rehabilitating or reconstructing CR pavement structures. The survey is included in Appendix A of this report with more details provided in the following subsections.

2.7.1 Cold Recycling Techniques

According to the survey results, almost 50% of the agencies utilize cold recycling technology (Figure 2-5) for rehabilitation projects. Cold recycling techniques used most commonly are CIR and SFDR (Figure 2-6).

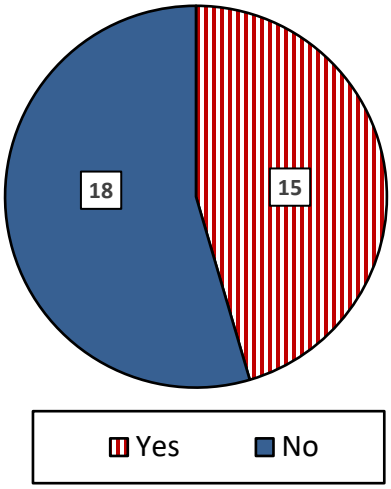

Figure 2-5: Cold recycling utilization

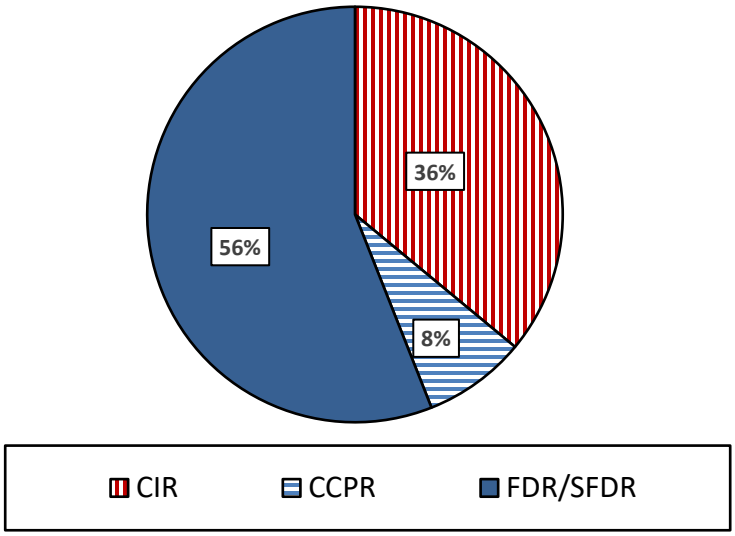

Figure 2-6: Cold recycling techniques employed by agencies

Processes for selecting these recycling techniques for specific rehabilitation projects vary amongst local agencies. Table 2-2 provides summary of typical processes and/or criterion for the deployment of each technique.

Table 2-2: Cold recycling selection criterion as reported by agencies

City/County/District	CIR	CCPR	FDR/SFDR
Beltrami County	*Not used*	*Not used*	Alligator cracking, Numerous severe cracks

Brown County	Poor pavement with numerous cracks	*Not used*	Poor pavement with numerous cracks and paving fabric in-place.
City of St. Michael	*Not used*	*Not used*	Bad pavement section but decent granular/aggregate base layer
Minnesota DOT-District 1	*Not used*	*Not used*	Distresses in the current pavement - amount of cracking
Minnesota DOT-Office of Materials & Road Research	Decision tree from pavement management. Best approach is then decided	Decision tree from pavement management. Best approach is then decided	Decision tree from pavement management. Best approach is then decided
Mower County	In-place pavement cross-section and strength	*Not used*	In-place pavement cross-section and strength
Norman County	Agency decision to extend life and minimize reflective cracking	*Not used*	Developed decision trees derived from the agency's pavement management data
St. Louis County	Pavement distress level along with in-place bituminous thickness	Pavement distress level along with in-place bituminous thickness	Pavement distress along with in-place base material
Wabasha County	*Not used*	*Not used*	Cracks/failing pavement with poor ride quality on roads with acceptable geometrics and underlying road structure.
Washington County	History of roadway and geotechnical cores	*Not used*	History of roadway and geotechnical cores

2.7.2 Treatments

Agencies indicated that various treatments are used for recycled sections, depending on the needs of a particular project. As presented in Figure 2-7, CIR layers are most commonly stabilized with emulsion while in other cases, both emulsion and foamed asphalt are employed. As for CCPR, both agencies that utilize this technique employ emulsion as stabilizing agent. SFDR (Figure 2-8) on the other hand is most often stabilized with emulsion while in other cases, both emulsion and foamed asphalt are employed.

The use of proprietary materials (recycling agent) was indicated by two agencies for FDR/SFDR treated layers, primarily to stiffen the FDR layer.

Some agencies also pointed out that roads treated with FDR are just reclamation without any added materials or stabilizing agent. One agency indicated that 100% of FDR treated roads are purely FDR as no SFDR roads have been constructed. Two other local agencies mentioned that 90% of recycled roads are just reclamation as well. In addition, three agencies indicated that 75% of CR treated roads are just reclamation.

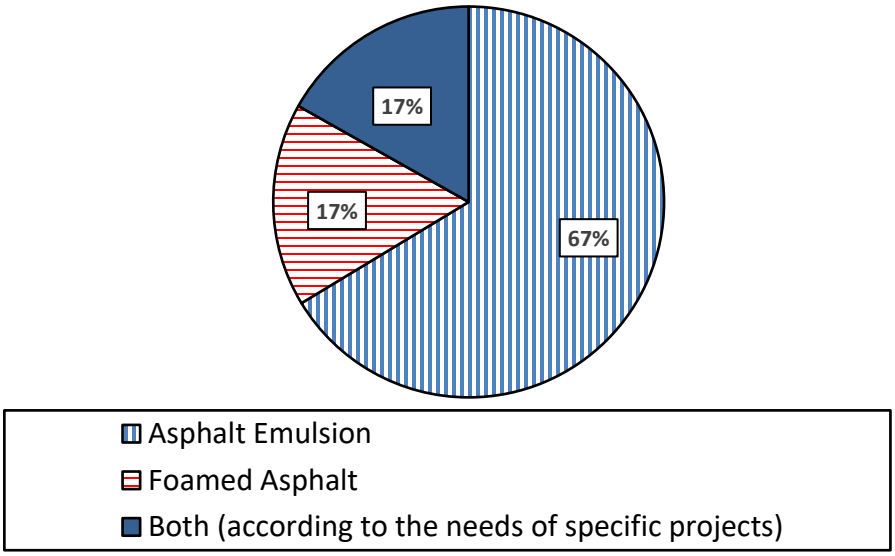

Figure 2-7: CIR treatments used

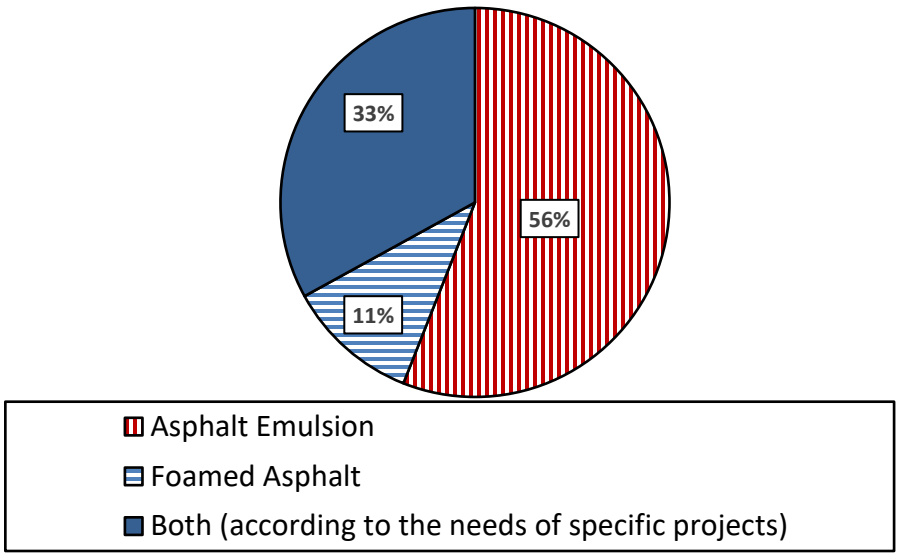

Figure 2-8: FDR/SFDR treatments used

Chemical additives utilized on the various CR sections were also specified by the agencies. As presented in Figure 2-9, most CIR treated sections utilize Portland cement as chemical additive while in other cases, no chemical additive is used. CCPR, as indicated by both agencies utilizing this technique, employ Portland cement as chemical additive. As for SFDR treated sections (Figure 2-10), a large proportion of agencies don't use chemical additives as previously indicated while 44% employ Portland cement as treatments.

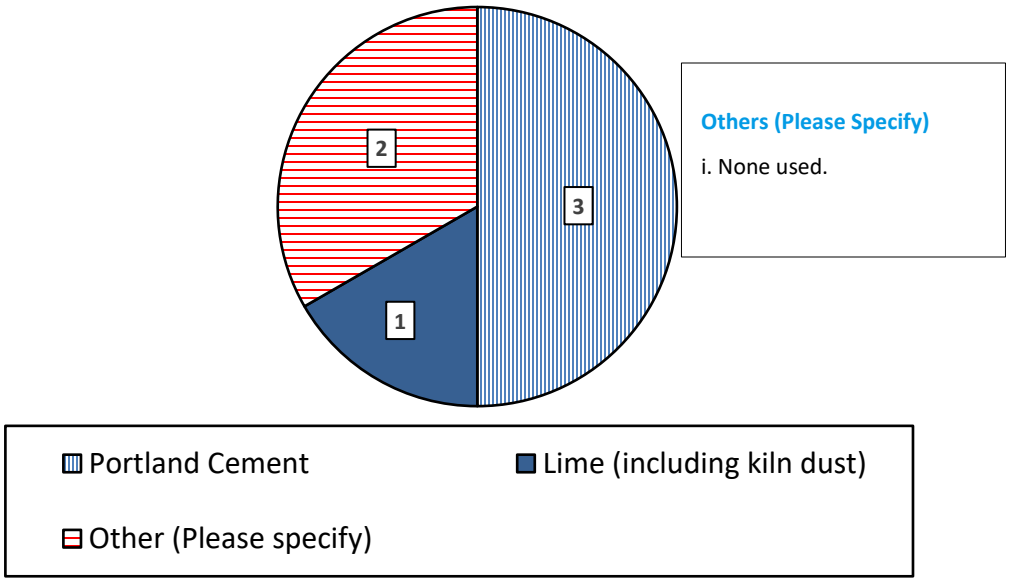

Figure 2-9: CIR chemical additive treatment

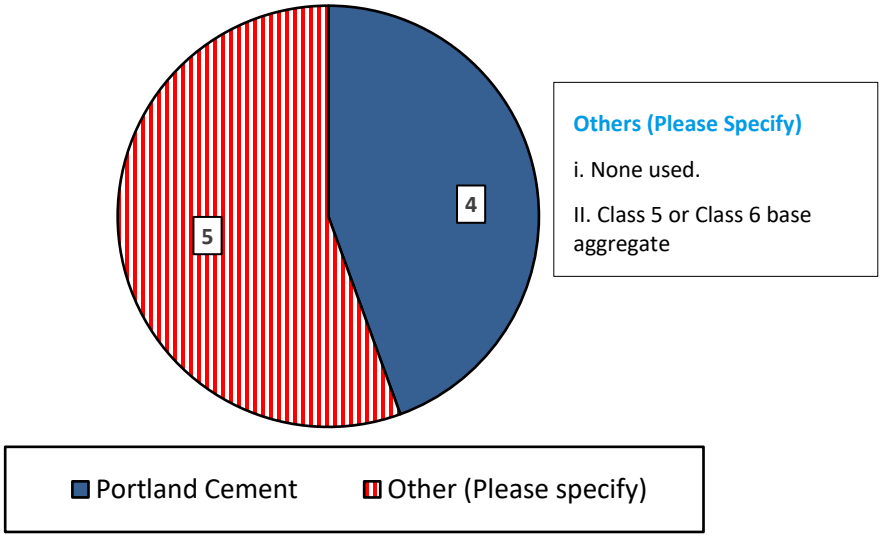

Figure 2-10: FDR/SFDR chemical additive treatment

2.7.3 Cold Recycled Pavement Design

In designing thicknesses of CR layers (CIR, CCPR, SFDR) and wearing course/overlays, several approaches are employed by the agencies. About 80% of the agencies indicate that there are no challenges in employing their specified design methodology for designing thicknesses of CR layers and wearing course/overlay whereas a few outlined specific challenges. Table 2-3 presents the approaches employed by all agency survey responders and corresponding challenges. The provided pavement design manual/methods is included in Appendix A.

Table 2-3: Cold recycled layer and overlay thickness design approach

City/County/District	CIR	CCPR	FDR/SFDR
Beltrami County	*See Note a*	*See Note a*	In-house design
Brown County	In-house design. *See Note b & h*	*See Note a*	In-house design (R-value based design). *See Note i*
City of St. Michael	*See Note a*	*See Note a*	In-house design *See Note c*
Minnesota DOT-District 1	*See Note a*	*See Note a*	In-house design (MnPAVE) *See Note j*
Minnesota DOT-Office of Materials & Road Research	In-house design (MnPAVE)	In-house design (MnPAVE)	In-house design (MnPAVE)
Mower County	In-house design (MnDOT FLEXPAVE). *See note d*	*See Note a*	In-house design (MnDOT FLEXPAVE)
Norman County	In-house design. *See Note e*	*See Note a*	*See Note a*
Sibley County	2019 MnDOT grading & base manual	*See Note a*	In-house design (Base 1 material)
St. Louis County	In-house design *See Note f*	In-house design *See Note f & g*	In-house design *See Note f & k*
Wabasha County	*See Note a*	*See Note a*	In-house design, MnPAVE *See Note f*
Washington County	In-house design *See Note f & e*	*See Note a*	In-house design *See Note f & e*

Notes:

a. Agency does not use this technique.
b. Depends on thickness of existing pavement.
c. Improve granular/gravel layer and introduce overlay.
d. CIR upper 4 inch of existing pavement
e. Geotechnical consultant recommendations.
f. Granular Equivalence (GE) calculator
g. Bituminous pavement design spreadsheet
h. Design challenge- Typically use 1.5 GE for Design for CIR
i. Design challenge- Typically use 1.0 GE for Design for FDR
j. Design challenge- GE equivalences
k. Design challenge- Variable base layers

2.7.4 Performance & Tracking of Cold Recycled Pavements

Information gathered from the survey indicates that efforts are in place to track performance of CR treated pavements (Figure 2-11). The anticipated lifespan of these recycled pavements varies from 20 to 25 years across agencies for CIR treated pavements. After 19 years of service, one agency mentioned that an overlay was introduced on one of the recycled pavements. As indicated by another agency, the section of the CIR with the longest service is currently at 10 years and in excellent condition. As for CCPR, anticipated life is set between 20 & 25 years. Agencies also estimate a 20–30-year lifespan for FDR/SFDR-treated pavements.

The recycled pavements have been identified by some agencies to have structural distresses. One agency mentioned that wheel ruts become prevalent on CIR constructed pavements. Another agency that uses all three recycling techniques indicated that distress only occurs when more extensive treatment is required on the subgrade but not implemented.

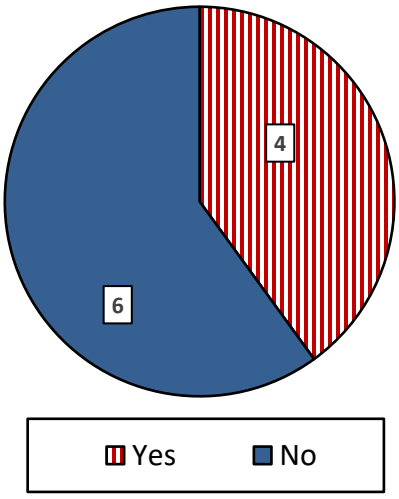

Figure 2-11: Performance tracking of cold recycled pavements

2.7.5 Post-Cold Recycling Rehabilitation Considerations

Agencies have identified the most preferred and/or best approach for rehabilitating or reconstructing CR treated pavements when they reach end of life. Details are summarized in Table 2-4.

Table 2-4: post-Cold recycling rehabilitation considerations

City/County/District	CIR	CCPR	FDR/SFDR
Brown county	Overlay or CIR & Overlay	*See Note a*	Overlay or CIR & Overlay
City of St. Michael	*See Note a*	*See Note a*	Pavement rejuvenators and mill/overlay
Minnesota DOT-Office of Materials & Road Research	Mill and fill	Mill and fill	Mill and fill
Minnesota DOT-District 1	*See Note b*	*See Note c*	FDR *See Note b*
Mower County	CIR	*See Note a*	CIR
St. Louis County	FDR	FDR	FDR/SFDR
Wabasha County	*See Note a*	*See Note a*	*See Note c*
Washington County	Mill and Overlay, Overlay	*See Note a*	Mill and Overlay, Overlay

Notes:

a. Agency does not use this technique.
b. If no subgrade improvements were warranted, then repeat the FDR process adjusting for grade control as needed.
c. Depends on the condition and severity of cracking.

2.8 Literature Review Summary

A comprehensive literature review involving cold recycling techniques, material characterization methods, factors affecting mechanical properties, CR layer pavement design procedures, methodologies for developing pavement performance transfer functions, and a review of the current state of practice for CR layer pavement design and analysis was performed. This section presents the summary of findings, organized in tables by the various topics covered. The most relevant findings and conclusions of the review to the research study are discussed.

2.8.1 Summary of the State-of-the-Art Review

Through a comprehensive review, the research team has been able to identify critical factors that would have an influence on the mechanical properties of CR layers in flexible pavement. These factors should, in turn, impact the pavement structural designs. Table 2-5 list critical factors impacting mechanical properties of CR and corresponding literature sources that have discussed these effects and Table 2-6 presents a summary of various laboratory and field characterization methods that can provide the two main types of material inputs that are necessary in conducting pavement analysis and design while considering CR layers.

Table 2-5: Summary of factors affecting mechanical properties of Cold recycled materials.

Factors	References
Curing	Tia & Wood, (1983); Serfass et al., (2004); Lee & Im, (2008); Zulakmal et al., (2009); Fu et al., (2010); Kim et al., (2011); Hainin et al., (2014); Godenzoni et al., (2016); Graziani et al., (2016); Li et al., (2016); Du, (2018); Yang et al., (2021); Ogbo et al., (2022)
Chemical Additive	Hodgkinson & Visser, (2004); Kekwick, (2005); Twagira et al., (2006); Halles et al., (2009); Zulakmal et al., (2009); Xu et al., (2011); Du, (2014); Ma et., (2015); Valentin et al., (2016); Schwartz et al., (2017); Flores et al., (2020); Ren et al., (2020); Kuchiishi, Vasconcelos, & Bernucci, (2021)
RAP Gradation	Ma et al., (2015); Yan et al., (2015); Ghavibazoo et al., (2017); Moghadam & Mollashahi, (2017); Xu et al., (2017); Raschia et al., (2019); Kuchiishi, Vasconcelos, & Bernucci, (2021)
Amount of RAP	Valdés et al., (2011); Ma et al., (2015); Ojum and Thom, (2017); Ren et al., (2020); Xie et al., (2021); Zhang et al., (2021)
Temperature	Bozyurt et al. (2013); Konieczna et al., (2020); Raschia et al., (2020); Cheng et al., (2022)
Stabilizer Type	Roberts et al., (1984); Nataatmadja, (2001); Loizos & Papavasiliou, (2006); Du, (2012); Lin et al., (2015); Bessa, (2016); Iwański & Chomicz-Kowalska, (2013), (2014), (2016); Valentin et al., (2016); Namutebi et al., (2017); Schwartz et al., (2017); Asphalt Academy, (2020); Chen et al., (2020); Flores et al., (2020); Raschia et al., (2020); Mugume, (2021); Kuchiishi, Vasconcelos, & Bernucci, (2021)
Compaction (Density)	Miljkovic & Radenberg (2016); Polaczyk et al., (2018); Filho et al., (2020); Flores et al., (2020); Raschia et al., (2020) Yang et al., (2021)

Table 2-6: Design input properties and performance measures of CR Materials

Design Input Properties	Performance Tests	References
Stiffness	Triaxial Resilient Modulus	Fu et al., (2009); Halles & Thenoux, (2009); Santagata et al., (2010); Bessa et al., (2016); Guatimosim et al., (2016); Fedrigo et al., (2018); Kuchiishi et al., (2019); Meneses et al., (2022); Orosa et al., (2023)
	Falling Weight Deflectometer (FWD) & Light Weight Deflectometer (LWD)	Tebaldi et al., (2014); Diefenderfer et al., (2015); Schwartz et al., (2017); Guatimosim et al., (2018); Xiao et al., (2018)
Strength	Indirect Tensile Strength	Cross, (2000); Kim et al., (2011); Diefenderfer et al. (2012); Asphalt Academy (2020); Dave et al., (2022)
	Triaxial Shear Strength	Jenkins et al., (2007); Fu et al., (2009); Mulusa, (2009); Kaloush et al., (2010); Collings and Jenkins, (2011); Jenkins et al., (2012); Dal Ben & Jenkins, (2014); Čížková et al., (2016); Bierman, (2018); Guatimosim et al., (2018); Asphalt Academy (2020); Dave et al., (2022)

Review of pavement design and structural assessments identified that both empirical and M-E approaches are used for designing CR pavements. Using the empirical method, several researchers developed layer coefficients for CR layers to determine structural capacity, and the M-E method was used to predict and determine the structural contributions of CR layers. Methodologies for developing fatigue and rutting transfer functions for CR layer were reviewed by examining the Mechanistic-Empirical design approach. A summary of the different design methods from existing literature is presented in Table 2-7.

Table 2-7: Design Methods for Cold Recycled Pavements

Design Method	References
Empirical (Pavement Number, Structural Number)	Tia and Wood, (1983); Van Wijk and Wood, (1983); Van Wyk et al., (1983); Marquis et al., (2003); Sebaaly et al., (2004); Loizos and Papavasiliou, (2006); Wirtgen Group (2012); Diefenderfer and Apeagyei (2014); Diaz-Sanchez et al., (2017); Asphalt Academy, (2020); Carvajal et al., (2021); Nemati et al., (2021)
Mechanistic-Empirical (Performance functions)	Theyse et al., (2000); AASHTO, (2008); Ullidtz et al., (2010); Arimilli et al. (2017); Schwartz et al., (2017); Bierman, 2018; Gu et al., (2018); Smith & Braham, (2018); MnDOT, (2019); Caltrans, (2022); Jenkins et al., (2020); Beesam & Torres-Machi, (2021); Kuchiishi et al., (2021); Preti et al. (2021)

2.8.2 Summary of the State-of-the-Practice Review

The aim of the state of practice review was to identify the pavement design methodologies currently used by agencies in MN as well as problems associated with employing these methodologies. It is essential to recognize these existing design methodologies, as they tend to influence the factors for improving and developing the design inputs for CR layer. In addition, identifying major distresses observed on CR pavements is essential in order to establish critical performance measures of CR materials and develop or repurpose existing methods that can be used to measure and remedy these identified distresses. The following preliminary conclusions were drawn from the review.

- Currently, most agencies employ In-house designs for CR pavements, varying from the use of mechanistic-empirical approach, GE and R-value based calculations. Challenges identified in employing the various design methodologies range from variable base layers in-situ and GE equivalences.
- Performance of CR materials is typically evaluated in terms of two primary distresses: permanent deformation and moisture susceptibility. However, cracking may be an issue when considerable amounts of chemical additives are used as stabilizers.

Chapter 3: Field Projects, Materials and Test Methods

This chapter presents details of the CR projects selected for this study, together with the field and laboratory assessment methodologies. Specifically, details regarding the procedures for field data collection, test methods, and analytical approaches employed for both field and laboratory evaluations are presented.

3.1 Field Projects and Material Sampling

A total of 13 projects were incorporated, identified through a survey of LRRB and MnDOT district agencies for candidate projects planned for the 2023 construction season, along with projects drawn from the Evaluation of Curing Effects on Cold In-Place Recycled (CIR) research study (Dave et al., 2022). Of these 13 projects, consisting of County State Aid Highways (CSAH) and Trunk Highways (TH), 11 were CIR while two were SFDR. Figure 3-1 shows the location of the field projects relative to the state counties, cities, and districts. Due to circumstances relating to construction schedule and logistics, materials for laboratory investigations were not sampled from all projects listed. Specific details relating to extent of data collection for all field projects are provided in Table 3-1. Further details on the construction and material sampling processes for field projects where material sampling was feasible are presented in Appendix B of this report. In addition, Quality Control reports for all projects are provided in Appendix C.

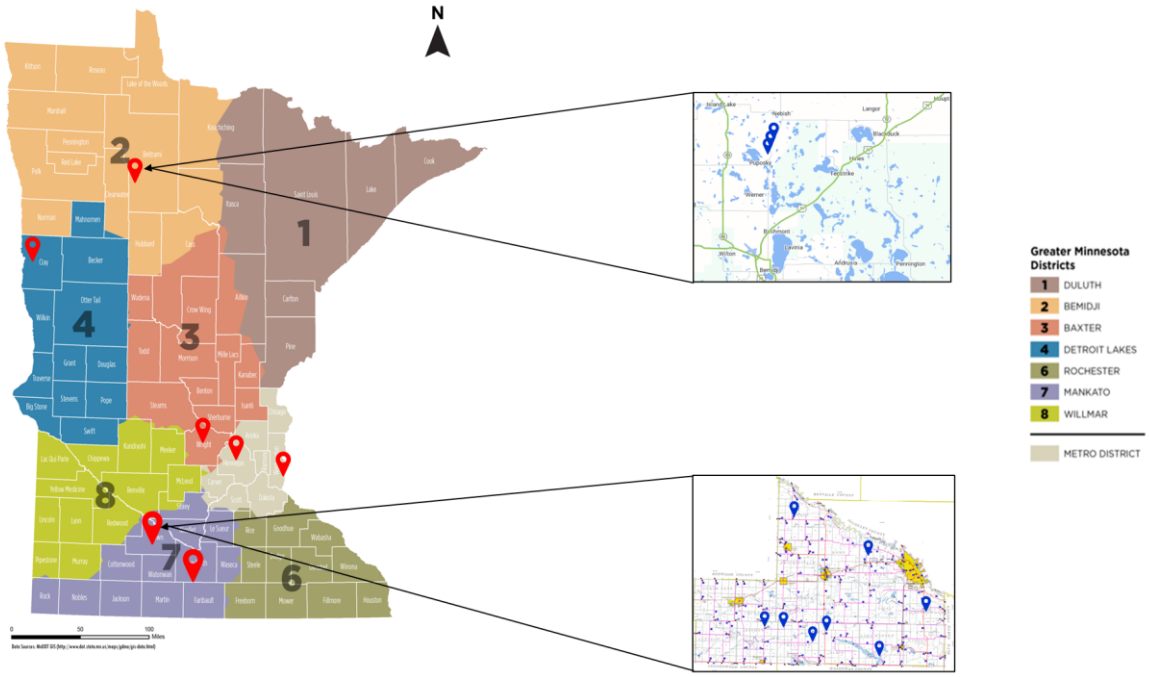

Figure 3-1: Geographical location of field study projects (Magnified map shows series of field projects and pavement sections within the districts)

Table 3-1: Details of field study projects

Agency	MnDOT District (County)	Location	CR Application	As-built Job Mix Formula	20-year Design Traffic (ESALs)	Pavement Structure
Beltrami County Highway Department	2 (Beltrami)	CSAH 15 (From CSAH 26 to CSAH 32)**	**SFDR**	Stabilizer type: Engineered Emulsion Stabilizer Content: T1- 4.5%, T2- 5%, T3- 5.5% Chemical Additive: N/A Density: 2098-kg/m^3	195,477	***Section 1-3*** 3.5" HMA 6" FDR 6" Variable Base
Brown County Highway Department	7 (Brown)	CSAH 8 (Between CSAH 30 and 10)*	**CIR**	Stabilizer type: Engineered Emulsion Stabilizer Content: 1.5% Chemical Additive: N/A Density: 1922-kg/m^3	32,000	3" HMA 3" CIR 10" Variable Base
	7 (Brown)	CSAH 21 (From 490th AVE to CSAH 3)*	**CIR**	Stabilizer type: Engineered Emulsion Stabilizer Content: 1.9% Chemical Additive: N/A Density: 1922-kg/m^3	60,000	3" HMA 6" CIR 10" Variable Base
	7 (Brown)	CSAH 9 (Between south county line and CSAH 18)***	**CIR**	Stabilizer type: Engineered Emulsion Stabilizer Content: 2% Chemical Additive: N/A Density: 1972-kg/m^3	26,800	3" HMA 4" CIR 9.5" Variable Base
	7 (Brown)	CSAH 11-Essig (From TH 14 and CSAH 29)***	**CIR**	Stabilizer type: Engineered Emulsion Stabilizer Content: 2.5% Chemical Additive: N/A Density: 1970-kg/m^3	67,000	3" HMA 4" CIR 14.25" Variable Base
	7 (Brown)	CSAH 11-Hanksa (From C.S.A.H. 6 to C.S.A.H. 20)**	**CIR**	Stabilizer type: Engineered Emulsion Stabilizer Content: 3.1% Chemical Additive: N/A Density: 1986-kg/m^3	68,700	3" HMA 4" CIR 10.75" Variable Base
	7 (Brown)	CSAH 20 (From C.S.A.H. 8 to T.H. 4)**	**CIR**	Stabilizer type: Engineered Emulsion Stabilizer Content: 2.5% Chemical Additive: N/A Density: 1922-kg/m^3	50,000	***Section 1*** 3" HMA 3" CIR 16.25" Variable Base ***Section 2*** 3" HMA 3" CIR 10.25" Variable Base
	7 (Brown)	CSAH 24 (From C.S.A.H. 13 to T.H. 15)**	**CIR**	Stabilizer type: Engineered Emulsion Stabilizer Content: 2.4% Chemical Additive: N/A Density: 1890-kg/m^3	137,000	3" HMA 4" CIR 9.5" Variable Base

City of Maple Grove Public Works	Metro (Hennepin County & City of Maple Grove)	CSAH 101 (From 73rd Avenue to 500' North of 83rd Avenue)**	**SFDR**	Stabilizer type: Engineered Emulsion Stabilizer Content: 3.3% Chemical Additive: 0.5% Density: 2130-kg/m^3	2,818,000	5" HMA 6" FDR 3" Granular base	
Cottonwood Highway Department	7 (Cottonwood)	CSAH 11 (From U.S. HWY 71 to 490th AVE)*	**CIR**	Stabilizer type: Engineered Emulsion Stabilizer Content: 1.9% Chemical Additive: 0.5% Density: 1922-kg/m^3	60,000	3" HMA 3" CIR 10.25" Variable Base	
Clay County Highway Department	2 (Clay)	CSAH 18 (From CSAH 11 to intersection of CSAH 18 & TH 9)**	**CIR**	Stabilizer type: Engineered Emulsion Stabilizer Content: 3.3% Chemical Additive: N/A Density: 2066-kg/m^3	446,000/368,000	***Section 1*** 3" HMA 3" CIR 16.25" Variable Base	***Section 2*** 3" HMA 3" CIR 16.25" Variable Base
Minnesota Department of Transportation	7 (Blue Earth)	TH 30 (From 140' East of TH22 to 1200' East of CSAH)*	**CIR**	Stabilizer type: Engineered Emulsion Stabilizer Content: 2% Chemical Additive: N/A Density: 1970-kg/m^3	60,000	3" HMA 3" CIR 19" Variable Base	
	Metro (Washington)	TH 95 (From .1 Mile South of TH94 to .5 Mile North of County Road 14)*	**CIR**	Stabilizer type: Engineered Emulsion Stabilizer Content: 2% Chemical Additive: 0.5% Density: 2098-kg/m^3	2,990,000	2.6" HMA 3" CIR 19" Variable Base	

***:** Field Projects from Dave et al. (2022) which were monitored as part of this study.

**: Field projects constructed during the 2023 construction season where materials were sampled, and pavement sections were monitored.

***: Field projects constructed during the 2023 construction season which were monitored as part of this study.

CSAH: County State Aid Highway

TH: Trunk Highway

HMA: Hot Mix Asphalt

T1: Section 1; T2: Section 2; T3: Section 3

N/A: Not applicable

1-kg/m^3 = 0.062-pcf

3.2 Field (In-situ) Assessments

Field assessments, conducted by a team from the Minnesota Department of Transportation (MnDOT) and the Office of Materials and Road Research (OMRR), included Falling Weight Deflectometer (FWD) tests and measurements of roughness and rutting using MnDOT's Road Doctor equipment. For field projects where measurements of roughness and rutting were not directly conducted by the OMRR team, relevant distress data were obtained from the County Engineers through the Highway Performance Monitoring System (HPMS) database. Table 3-2 summarizes the field projects for which performance data were collected. Detailed descriptions of the test approach and analysis procedure are provided in the following subsections.

Table 3-2: Range of available data from field project performance evaluation

Agency	Project Location	Falling Weight Deflectometer Test Period		Roughness (IRI)	Rutting
		Fall 2023	Summer 2024		
Beltrami County Highway Department	CSAH 15 (T1, T2 & T3) (From CSAH 26 to CSAH 32)	*	*	*	*
Brown County Highway Department	CSAH 8 (Between CSAH 30 and 10)	*	-	*	*
	CSAH 9 (Between South County line and CSAH 18)	-	*	*	*
	CSAH 11-Essig (From TH 14 and CSAH 29)	*	-	*	*
	CSAH 11-Hanska (From C.S.A.H. 6 to C.S.A.H. 20)	*	*	*	*
	CSAH 20 (T1 & T2) (From CSAH 8 to T.H. 4)	*	*	*	*
	CSAH 21 (From 490th AVE to CSAH 3)	*	*	*	*
	CSAH 24 (From CSAH 13 to TH 15)	*	*	*	*
City of Maple Grove Public Works	CSAH 101 (From 73rd Avenue to 500' North of 83rd Avenue)	*	-	-	-
Clay County Highway Department	CSAH 18 (S1 & S2) (From CSAH 11 to intersection of CSAH 18 & TH 9)	*	*	-	-
Cottonwood Highway Department	CSAH 11 (From U.S. HWY 71 to 490th AVE)	*	*	*	*
Minnesota Department of Transportation	TH 30 (From 140' East of TH22 to 1200' East of CSAH 1)	*	-	*	*
	TH 95 (From 0.1 Mile South of TH94 to 0.5 Mile North of County Road 14)	*	*	*	*

* Test conducted
- Test not conducted
T1, T2, T3: Test sections 1, 2 and 3

3.2.1 Falling Weight Deflectometer (FWD)

Falling Weight Deflectometer tests were conducted to determine the early life performance of the pavement structure and the CR layers within the pavement structure. This was achieved by conducting FWD tests at two test periods; Fall and Summer (Table 3-2). Testing on all field projects was conducted at a defined section, spanning 1000-ft. at 250-ft. interval within the length of the roadway. These defined sections, established using GPS coordinates, were selected to have minimal variability in terms of construction features and to further support material sampling efforts for laboratory investigations. The selection criteria for the defined sections are outlined below.

1. Distant from a bridge approach or departure point. To ensure consistency in construction.
2. At a distance from, prior to, and within the vicinity of an intersection: In order to mitigate the impact of traffic patterns and speeds.
3. Avoiding irrigation channels passing under the roadway as well as sections proximal to lakes, river and ditches in order to minimize impact on moisture content variation.
4. Excluding areas where maintenance or rehabilitation activities have been recently conducted in order to reduce variability in the characteristics of current pavement and reclaimed asphalt pavement (RAP).
5. Not situated on a curved section of the roadway: Primarily a safety and traffic control convenience requirement during field testing.

Appendix B of this report provides clear illustrations of the test section definitions based on field projects where material sampling was achieved. As for other projects, the test sections were defined using the Google Maps web application, in accordance with the selection criteria outlined above.

Figure 2-2 shows the planned FWD testing map for all projects. Details regarding the test approach and analysis procedure are discussed further in subsequent subsections.

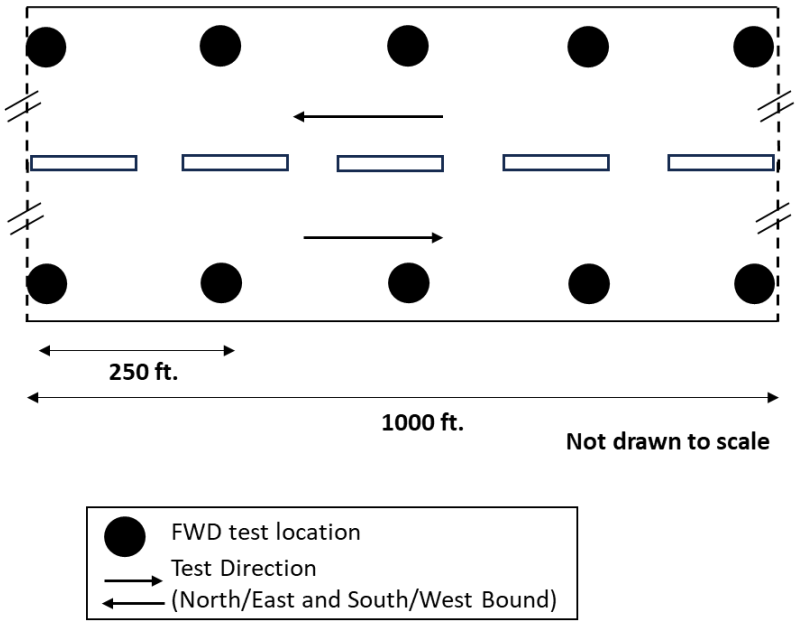

Figure 3-2: FWD Testing Map

3.2.1.1 FWD Analysis Procedure

A Dynatest 8000 series FWD setup was employed to measure the deflection of the pavement surface at the outer wheel path of the defined test section(s) within each project. Conducted at a minimum of five intervals spaced approximately 200-ft distance apart, four load drops (approximately 27-kN [6000-lb], 40kN [9000-lb], 55kN (12000-lb) and 72-kN [15000-lb]) were conducted using a 300-mm (12-inch) loading plate. Data from the 9000-lb (40-kN) FWD drop, which represents the standard half single-axle wheel load, was used for analysis. All individual basin deflections were examined to ensure validity. Statistical comparisons were conducted for each study section and each test date to identify potential outliers in the basin deflections. This process utilized the peak deflection (D_0) and employed Tukey's fences approach to detect and eliminate outlier measurements. Based on this analysis, a total of 18 outlier basins were identified and removed.

Deflection Basin parameters were employed to evaluate the overall performance of the pavement sections as well as the performance of the CR layer within the pavement structure. This was achieved using the peak deflection (D_0) and the surface curvature index (SCI), known for its depiction of the condition of base layers (Horak, 2008), CR layer in this case. Both metrics were calculated using temperature-normalized deflection indices (D_0 and D_{12}), with the expression for the temperature normalized peak deflection and SCI presented in Equation 3-1 and Equation 3-2, respectively (Kim & Park, 2002).

$$\boldsymbol{D_{0/12adj} = D_{0/12} * 10^{(-C_0+Ar)*(H_{ac})(T-T_0)}}$$

Equation 3-1

$$\boldsymbol{SCI = D_{0adj} - D_{12adj}}$$

Equation 3-2

In which:
$D_{0/12}$ = measured deflection under the center of the load and at 300mm radial distance.
C_0 = -5.47E-08
A= 4.65E-05
r = radial distance from the center of load.
H_{ac} = depth of asphalt layer (mm).
T= measured effective pavement temperature at 1/3 of the asphalt layer by BELLS3, °C (Equation 3-3)
T_0 = reference temperature (25°C).

$$T = 0.95 + 0.892 * T_{surface} + (\log_{10}\left(\frac{H_{ac}}{3}\right) - 1.25) * (-0.448 * T_{surface} + 0.621 * T_{prev.day} + 1.83 * \sin(hr_{18} - 15.5)) + 0.042 * T_{surface} * \sin(hr_{18} - 13.5)$$

Equation 3-3

In which:
$T_{surface}$= pavement surface temperature (°C)
$T_{prev.day}$ = average air temperature the day before testing (°C)
$\sin(hr_{18} - 15.5)$ = 18-hr sine function, 15.5 variation.
$\sin(hr_{18} - 13.5)$ = 18-hr sine function, 13.5 variation.

The performance of the pavement structure and CR layer are categorized using thresholds recommended by Horak (2008). These are highlighted as follows.

- Peak Deflection: < 400-µm (Sound); >600-µm (Severe)
- SCI: <200-µm (Sound); >400-µm (Severe)

3.2.2 Pavement Distress Assessment (HPMS Database and Road Doctor)

Distress measurements were conducted to evaluate the initial performance of the pavement sections. The Highway Performance Monitoring System (HPMS) database, alongside the Road Doctor Survey Van (RDSV), equipped with specialized equipment and instrumentation to access pavement condition, was utilized to gather distress data which were further applied for International Roughness Index (IRI) measurements. Evaluations were conducted over the entire roadway length, covering both North/Eastbound and South/Westbound lanes (Figure 3-3), with data for analysis primarily from the defined test section as will be described in the next subsection.

Distress data from both RDSV and HPMS included measurements taken before rehabilitation and immediately after CR pavement construction, aiming to quantify the benefits of the CR rehabilitation. It should however be noted that distress data before rehabilitation were not available for all pavement sections. The approach employed in processing the data of both pavement rutting and IRI evaluations are outlined in the following subsection.

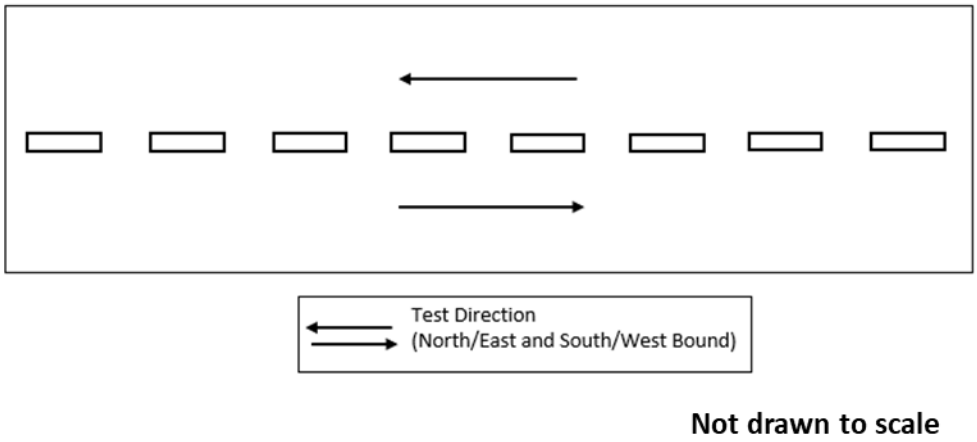

Figure 3-3: Road Doctor Survey Testing Map

3.2.2.1 Distress Measurements Analysis Procedure

The total pavement rutting, as measured through RDSV and recorded in the HPMS database, included assessments of both the left and right wheel paths of the pavement sections. For RDSV testing, which covered the entire roadway, GPS coordinates from the evaluations were matched with the GPS coordinates of the defined test section on each roadway. This ensured the results were accurately associated with the corresponding field section. Since RDSV records rut depths across the transverse profile of the roadway and at intervals throughout the length of a roadway, representative rut depth for a field section was determined using the following procedure:

1. For each survey along the transverse profile of a pavement section, the maximum rut depth across the transverse section of the roadway, which includes both left wheel and the right wheel paths, was selected as the rut depth for that specific transverse survey location.
2. For the entire pavement section of the defined test section, the representative rut depth for the field section was determined by calculating the average of the maximum rut depths from all transverse survey location within the section.

An example rut depth result obtained from the RDSV equipment is shown in Figure 3-4. The red line represents the general shape of the rut measurement across the transverse section of the roadway. For pavement sections where distress data were sourced from the HPMS database, the representative rut depth for the field section was calculated as the average of all rut depth measurements along the entire roadway section.

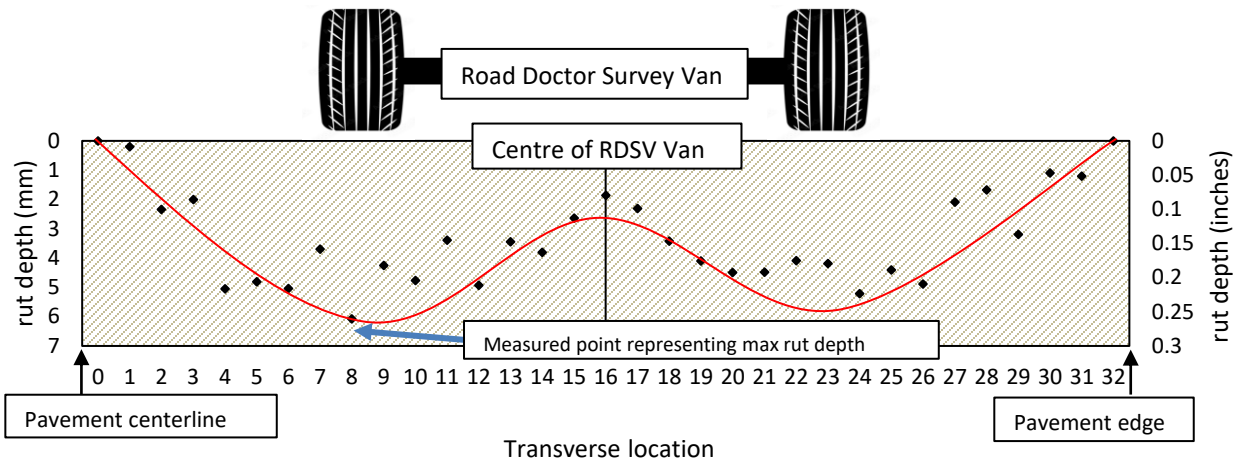

(a)

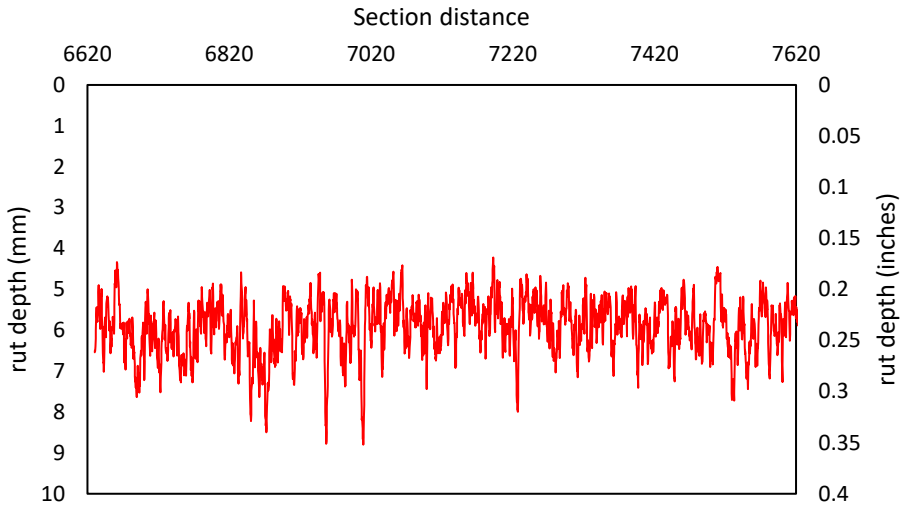

(b)

Figure 3-4: Example RDSV rut depth result (a) test location transversal rut measurements (b) pavement longitudinal section ruth depth based on maximum ruth depth at test locations

3.3 Laboratory Assessments

This section describes the laboratory experimental plan, material processing and tests employed to assess the mechanical properties of the sampled materials and subsequent processed CR mixtures.

3.3.1 Experimental Design

The as-placed job mix obtained from the CR projects and variations introduced to each as-built mix design were evaluated to explore the effect of the various mix and non-mix attributes/components influencing the properties of CR materials. Considering the nature of the identified field projects and

current practices with cold recycling in Minnesota, it was both feasible and practical to incorporate the following components into the introduced mix variations.

- **Chemical Additive (Portland cement):** Since all projects utilized Portland cement as a chemical additive, and based on the as-placed mix formula, variations to this mix attribute for all projects was achieved by specifying cement content to 0% (no cement) and 1% except for two mix variations where cement was specified at 0.5%.
- **Density:** By comparing densities across projects, high and low levels of density were specified with respect to actual density of each project. Overall, the densities specified were in the range of ±15%.
- **Emulsion content:** While only Engineered Emulsion was employed in the field projects identified, high and low levels of engineered emulsion were specified such that, in cases where a project's as-placed job mix had a lower emulsion content, a higher level was specified based on the emulsion content used in other projects with higher levels.

To further increase the database of mixtures for this study, component RAP materials from two project sources were blended at a 50% proportion rate to create a representative RAP for a mix variation. Table 3-3 provides details on both the mix variations, mix variations constituting a RAP blend and the as-placed mixture properties reproduced in the lab. This brings the total number of mixtures assessed to 32 (18 CIR and 14 SFDR mixes). It is important to note that the RAP utilized for CMG101-C (Table 3-3) was sourced from the phase two segment of the project, which comprised a combination of the asphalt layer, granular base, and portions of the subgrade. In addition, the mix components outlined in Table 3-3 for CMG101 were originally designed for the RAP from phase one of the project. However, because the RAP from phase one was not available within the required timeline, the phase two project RAP was employed. For the purposes of this study, this will be considered a mix variation.

Table 3-3: Mixture properties assessed in this study

Agency	Project	Engineered Emulsion Content- % by weight of RAP	Portland Cement- % by weight of RAP	Density (kg/m³)	RAP blend (Project from which blend was achieved)	Mix identification	CR Technique
Brown County Highway Department	CSAH 11-Hanksa	3.1	-	1974	-	BC11-X	**CIR**
		2.5	-	1730	-	BC11-A	**CIR**
		3.3	1	1974	-	BC11-B	**CIR**
		3.1	1	1974	CSAH 24	BC11-C	**CIR**
		3.1	-	2068	CSAH 18	BC11-D	**CIR**
	CSAH 20	2.5	-	1922	-	BC20-X	**CIR**
		2.5	1	1922	-	BC20-A	**CIR**
		3.1	-	2172	CSAH 24	BC20-B	**CIR**
	CSAH 24	2.4	-	1893	-	BC24-X	**CIR**
		3.3	-	2035	-	BC24-A	**CIR**
		3.0	1	2083	CSAH 20	BC24-B	**CIR**
		2.4	1	1893	CSAH 18	BC24-C	**CIR**
		3.1	1	1893	-	BC24-D	**CIR**
Clay County Highway Department	CSAH 18	3.3	-	2068	-	CC18-X	**CIR**
		3.3	1	1974	-	CC18-A	**CIR**
		2.5	1	2068	-	CC18-B	**CIR**
		3.3	1	2068	CSAH 11	CC18-C	**CIR**
		2.5	-	1965	-	CC18-D	**CIR**
Beltrami County Highway Department	CSAH 15	5	-	2098	-	BelC15-X	**SFDR**
		4.5	-	2098	-	BelC15-A	**SFDR**
		5.5	-	2098	-	BelC15-B	**SFDR**
		5.0	-	1937	CSAH 101	BelC15-C	**SFDR**
		5.0	1	2098	-	BelC15-D	**SFDR**
		4.0	-	1868	-	BelC15-E	**SFDR**
		5.5	-	1937	-	BelC15-F	**SFDR**
		4.5	1	1937	-	BelC15-G	**SFDR**
		4.5	1	2098	-	BelC15-H	**SFDR**
		3.3	0.5	2131	-	BelC15-I	**SFDR**
		5.5	1	2068	-	BelC15-J	**SFDR**
		4.5	-	1937	-	BelC15-K	**SFDR**
		3.5	1	2098	-	BelC15-L	**SFDR**
City of Maple Grove Public Works	CSAH 101	3.3	0.5	2131	-	CMG101-C	**SFDR**

X: As-built mix
A-L: Variations
1kg/m³ = 0.062pcf

3.3.2 Specimen Fabrication and Curing

3.3.2.1 Specimen Fabrication

The overall goal of the specimen fabrication process is to mimic the mixtures from the as-built constituent materials as closely as possible. In order to achieve this, the constituent materials were sampled and prepared as follows:

- **Reclaimed Asphalt Pavement (RAP)**: Material was sampled from sections defined along the length of each project for post-construction in-situ evaluations. For the CIR projects, RAP was obtained directly from the reclaiming machines (post gradation control before stabilizer

addition) while RAP was sampled after the initial reclamation phase and before stabilization for the SFDR sections. Following transportation of materials to the lab, the quartering approach as specified by AASHTO T 248 was employed prior to any mixing efforts to ensure homogeneity and/or uniform distribution of the sampled RAP. This also enabled efficient drying of the RAP to ensure it was free from any moisture. In addition, a second cycle of drying was done at 25°C (77°F), 24 hours before mix production and specimen fabrication. The gradation (black curve) of all the sampled RAP material across projects are presented in Figure 3-5.

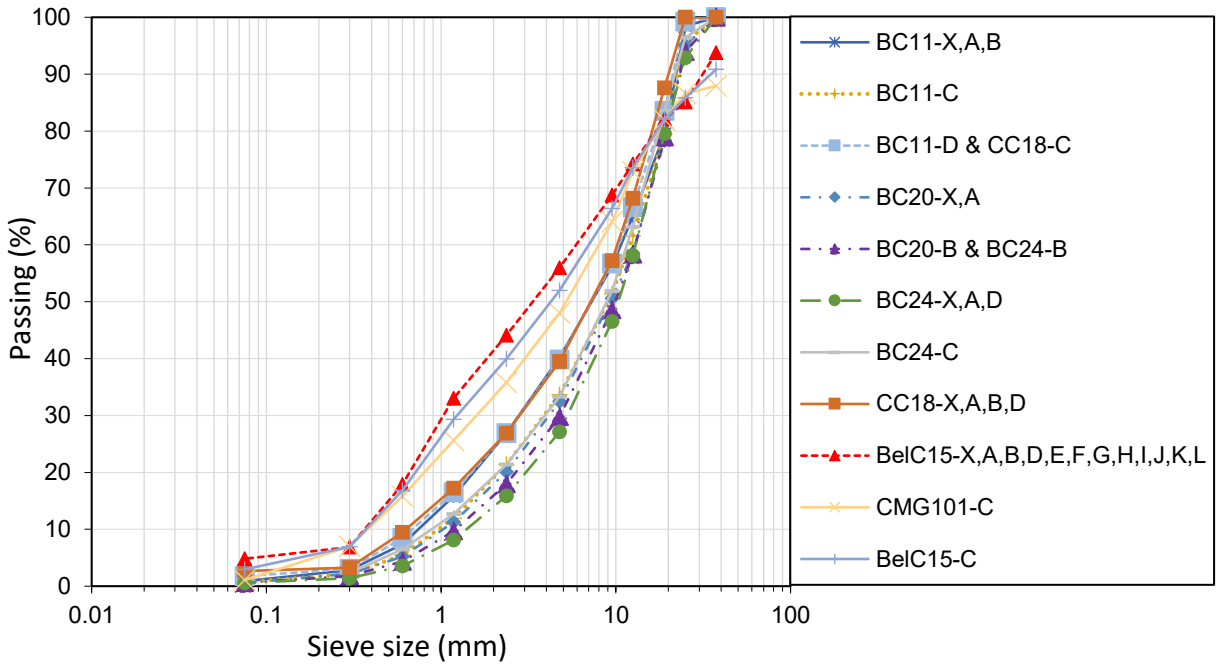

Figure 3-5: Black curve (gradation without binder extraction) for all mixtures

- **Total Moisture Content (T_{MC})**: The moisture content of loose mix obtained at the time of construction was measured to determine the amount of moisture required for fabrication purposes. Total moisture content of the sampled loose mix in this regard consists of the existing in-situ moisture prior to recycling, moisture associated with the recycling process, and water existing in the emulsion. The T_{MC} was determined following ASTM D2216.
- **Moisture content (Water added)**: The moisture content of the emulsion sampled from the projects was determined following the ASTM D7497 procedure. The moisture content to be employed in the mixing process was then determined following Equation 3-1.

$$\boldsymbol{MC = T_{MC} - MC_{emulsion}}$$

Equation 3-1

In determining the amount of moisture needed for the mix variations, a linear relationship between the as-built job mix specimen density/weight requirements and the amount of RAP was used to back-calculate both the amount of RAP and the moisture content needed for the mix variation for each project.

- **Engineered Emulsion**: Prior to mixing, the emulsion was conditioned to a temperature similar to that measured at the time of field sampling. Generally, this was at 25°C (77°F).
- **Portland Cement**: A Type I/II cement was utilized in the fabrication process for the cement stabilized sections. No special preparation was needed.

The proportions of the constituent materials including the RAP, stabilizing agent (Engineered Emulsion), water and cement were determined and batched individually. The mixtures were produced by first adding water to the RAP and mixing for 1 minute 30 seconds, then cement (for mixes with cement) for 1 minute 30 seconds, followed by the stabilizing agent (emulsion) mixed for an additional 4 minutes. Figure 3-6 shows the Wirtgen twin-shaft pugmill mixer (Model WLM30) used for mixing.

Figure 3-6 Wirtgen Pugmill Mixer (Model WLM30)

Following mixing, compaction was achieved using the Wirtgen Vibratory Hammer (Model WLV1 (see Figure 3-7) at target densities specific to each project and mix variation. With respect to the tests conducted, compaction was done at the specified number of lifts, that is, two lifts for 95mm height specimens and five lifts for 300-mm height specimens. The compaction mold has a diameter of 150-mm (6-inch).

Figure 3-7 Wirtgen Vibratory Hammer (Model WLV1)

3.3.2.2 Curing

Based on the findings of Dave et al. (2022) on a linear/equilibrium mechanical property attainment after a 14-day curing period, this study incorporated a minimum 14-day curing with the additional criterion of ensuring that each specimen reached a constant mass. To simulate curing at 25°C (77°F), a forced draft oven was used. As shown in Figure 3-8, all specimens were cured uncovered to accelerate the curing process. Metal plates were used at the base for easier handling after compaction.

Figure 3-8 Specimen Curing in Oven (at 25°C/77°F)

3.3.3 Laboratory Test Methods

3.3.3.1 Indirect Tensile Strength Test

The Indirect Tensile Strength (ITS) test is utilized as an indirect assessment of the tensile strength and flexibility of CR mixtures (Asphalt Academy, 2020). This test was conducted in accordance with the ASTM D6931 specifications at a temperature of 25°C (77°F) on a minimum of three 150-mm diameter cylindrical specimens for all mixtures. Loading was applied at a defined rate of deformation (50 ± 5mm/min) along the vertical diametral plane. The test configuration is illustrated in Figure 3-9. The peak load upon failure is recorded and utilized to determine the specimen's tensile strength. ITS calculations and variables are indicated in Equation 3-2.

$$S_t = \frac{2000 \times P}{\pi \times t \times D}$$

Equation 3-2

S_t: Tensile Strength, kPa (10^{-3} psi)
P: maximum load, N (lb)
t: Specimen's height before test, mm (in.)
D: Specimen's diameter, mm (in.)

Figure 3-9 Indirect Tensile Strength Test Setup

3.3.3.2 Resilient Modulus Test

Currently, there is no standardized method for assessing the resilient modulus of CR mixtures. Several studies have recommended evaluation using triaxial configuration as some of these materials may present stress dependency. To this end, an approach that utilizes a triaxial setup and incorporates procedural aspects of the ASTM D7369 specification was adopted. The principle governing this approach is based on the behavior of asphalt materials under repeated loading. When the applied loads are relatively small compared to the material's strength and occur over numerous cycles, the deformation experienced during each cycle is predominantly recoverable and proportional to the load, classifying it as elastic. (Huang, 1993; Kavussi and Modarres, 2010). The number of load repetitions required to achieve stable resilient deformations typically ranges from 50 to 200, influenced by factors such as

loading frequency, temperature, and mixture composition (Kavussi and Modarres, 2010). For this study, a minimum of three test specimens measuring 300-mm (12-inches) in height and 150-mm (6-inches) in diameter were used for stiffness measurements. Although the quantity of material required for this characterization is substantial, the same test specimen can be employed for shear strength evaluations, as will be described in the following sub-section. The triaxial test setup included two extensometers positioned to precisely measure the specimen deformation (Figure 3-10) with axial stresses selected to generate strain levels within the linear elastic range (50-100με). The test protocol generally involved applying 105 load cycles at a frequency of 1Hz, with each cycle consisting of 0.1 seconds of load application followed by 0.9 seconds of rest. The initial 100 cycles functioned as a conditioning period, with data from the last five cycles used for analysis. Equation 3-3 presents the expression used to calculate the resilient modulus.

$$M_R = \frac{\sigma_{d\ (average\ of\ last\ 5\ cycles)}}{\varepsilon_{recoverable\ (average\ of\ last\ 5\ cycles)}}$$

Equation 3-3

Where,

M_R= Resilient modulus

σ_d= applied axial stress (deviatoric stress) (MPa, psi)

$\varepsilon_{recoverable}$ = recoverable axial strain (mm/mm, in/in)

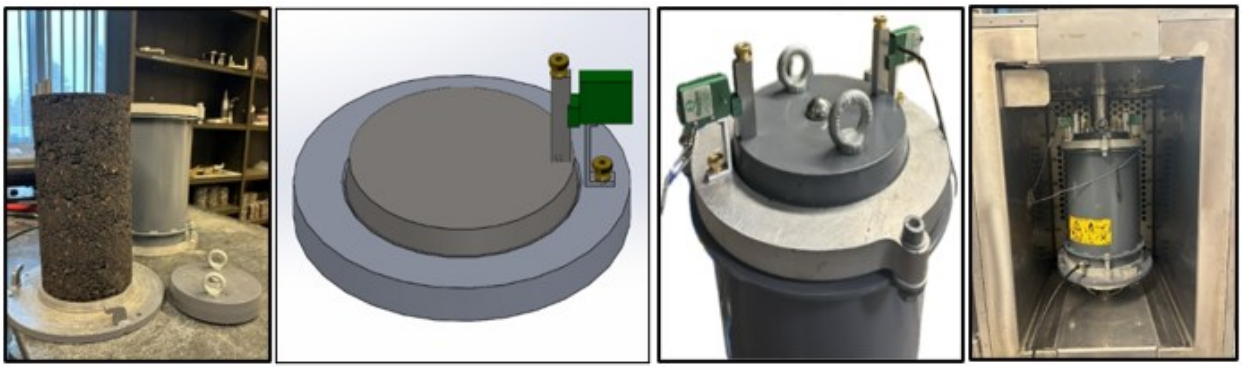

Figure 3-10 Triaxial Resilient Modulus Test Design and Setup

A subset of mixtures was tested across a wide range of temperatures and confining pressures to evaluate whether the mixtures exhibit stress-dependent stiffness and temperature sensitivity, and to determine if these findings would be applied to all mixture variations. This was conducted on the as-built mix specimens at confining pressures defined at 0, 20kPa and 40kPa. Tests were conducted at temperatures corresponding to the estimate average CR layer pavement temperatures for the fall, late spring and summer season (10°C/50°F, 15°C/59°F and 30°C/86°F, respectively), derived from the MnPAVE flexible design software using GPS coordinates of the project sites. Prior to each test, each specimen was conditioned in a separate environmental chamber for at least 24 hours to bring the specimens to the required test temperature.

Results of these investigations are shown in Figure 3-11a-c. Error bars represent ± one standard deviation, and letters within boxes indicate Tukey's Kramer groupings for statistical differences. Generally, the effect of confining pressure is observed to be non-linear across most of the evaluated mixtures at all evaluated temperatures, as also confirmed by Tukey's Kramer groupings. This suggests that the materials may have transitioned from behaving like granular materials to more asphalt-like materials following full curing. Having established the non-dependence of confining pressure on the resilient modulus, the effect of temperature on these mixtures was also examined, utilizing all stiffness metrics from all confining pressures. To ensure reliability in the conclusions drawn from the statistical analysis, the Mahalanobis distance approach was used to filter out outliers within each mixture. The results of the effect of temperature on these mixtures based on the Tukey's Kramer groupings are presented in Table 3-4. For the majority of the mixtures, a temperature-dependent stiffness response was observed between tests conducted at 10°C and 30°C, with similar stiffness behavior between tests at 10°C and 15°C. Based on these findings, subsequent testing and analysis for the mixture variations was conducted at a zero confining pressure and test temperatures of 10°C and 30°C.

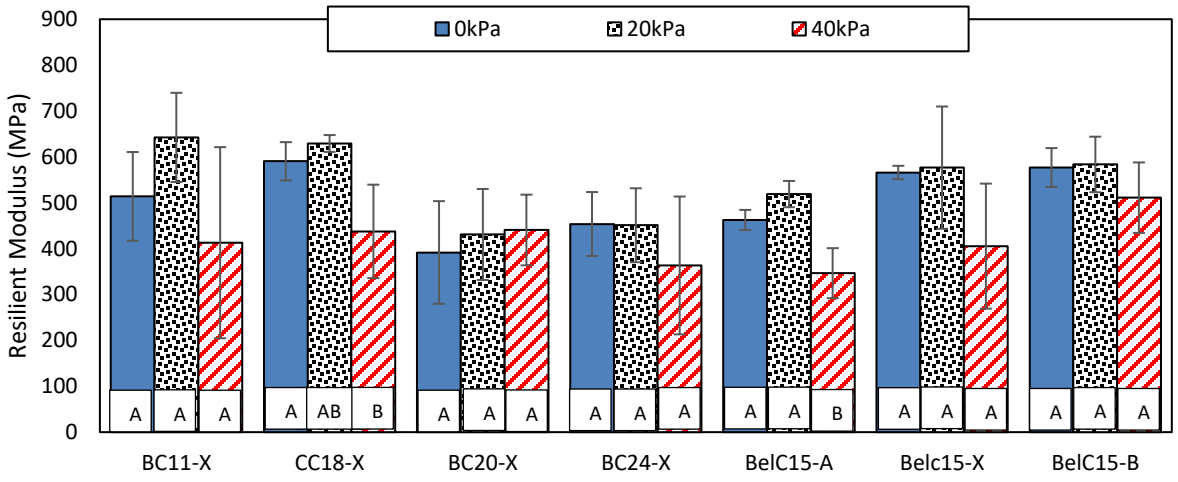

(a) 10°C (50°F)

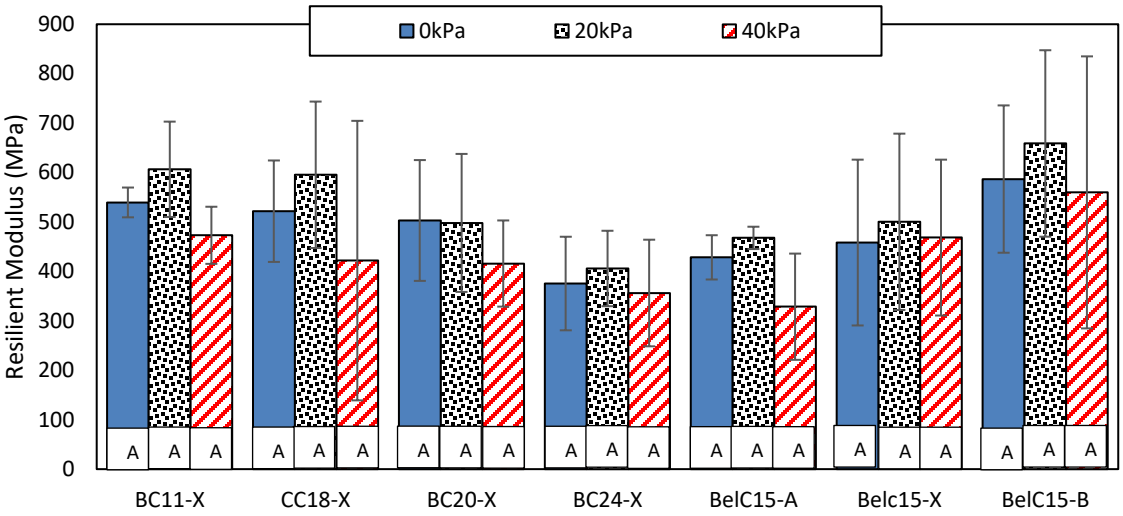

(b) 15°C (59°F)

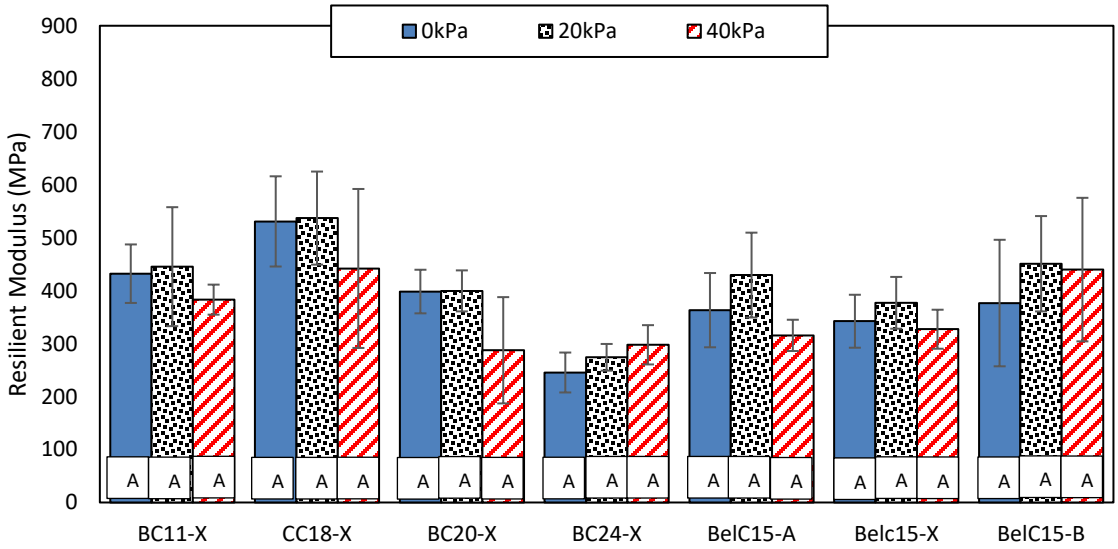

(c) 30°C (86°F)

Figure 3-11: Confining pressure effects on resilient modulus (a) 10°C (b) 15°C (c) 30°C

Table 3-4: Effect of temperature on resilient modulus (Tukey-Kramer's grouping)

Mixtures	Test Temperature		
	10°C/50°F	15°C/59°F	30°C/86°F
BC11-X	A	A	B
CC18-X	A	A	A
BC20-X	A	A	A
BC24-X	A	A	B
BelC15-A	A	A	B
BelC15-X	A	AB	B
BelC15-B	A	AB	B
Test temperature not connected by the same letters indicates statistically significant difference			

3.3.3.3 Triaxial Shear Strength Test

Shear strength is a fundamental property of CR materials that is tied to rutting in these layers from plastic deformations. The development of the Simple Triaxial Test (STT) (Mulusa, 2009) has facilitated triaxial testing in laboratories. This test is conducted by inserting the cylindrical test specimens into a mold equipped with an inflatable rubberized-plastic membrane (see Figure 3-12). The specimens are compacted to a height of 300-mm (12-inches). A circular metal plate is placed on the top of the mold for subjecting the test specimen to vertical axial compressive load until failure. This is done under displacement-controlled mode at a rate of 3mm/min. The peak load at failure is recorded to determine failure stress using Equation 3-4. The major principal stress at failure is then computed by accounting for the weight of the metal plate using Equation 3-4.

$$\boldsymbol{\sigma_f = \frac{P_f}{\pi \times \frac{D^2}{4}}}$$

Equation 3-4

Where:

σ_f = Failure Stress, kPa
P_f = Peak load, N
D = Diameter of specimen, mm

$$\boldsymbol{\sigma_1 = \sigma_f + \sigma_{dw}}$$

Equation 3-5

Where:

σ_1 = Major principal Stress at failure, kPa
σ_{dw} = Pressure resulting from weight of metal, N

A series of tests are performed on specimens subjected to increasing lateral confining pressure. A linear regression is performed to obtain the relationship between the major principal stress at failure and confining stress as described in Equation 3-6.

$$\boldsymbol{\sigma_1 = A \times \sigma_3 + B}$$

Equation 3-6

Where:

σ_3 = Confining stress, kPa

A , B = Regression constants

Through use of the Mohr-Coulomb model, the shear failure envelope in terms of internal friction angle and cohesion can be determined. These are obtained from the regression constants using Equation 3-7 and Equation 3-8, respectively.

$$\boldsymbol{A = \frac{1 + sin\varphi}{1 - sin\varphi}}$$

Equation 3-7

$$\boldsymbol{B = \frac{2 \times C \times cos\varphi}{1 - sin\varphi}}$$

Equation 3-8

Where:

φ = Frictional angle, degrees

C = Cohesion, kPa

Triaxial testing was done at room temperature with confining pressure set at 0-, 50- and 100-kPa. The typical test setup in the UTM is shown in Figure 3-5. An example result from this test is displayed in Figure 3-14.

Figure 3-12 Components of Triaxial Testing Device (Mulusa, 2009)

Figure 3-13 Triaxial Test Setup in the Universal Testing Machine

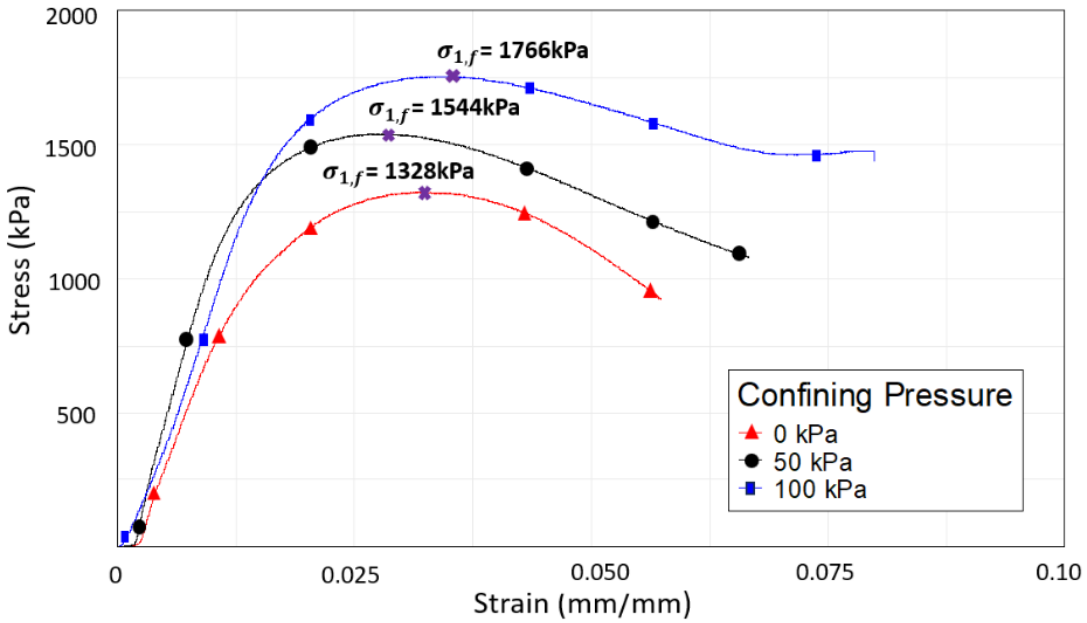

(a)

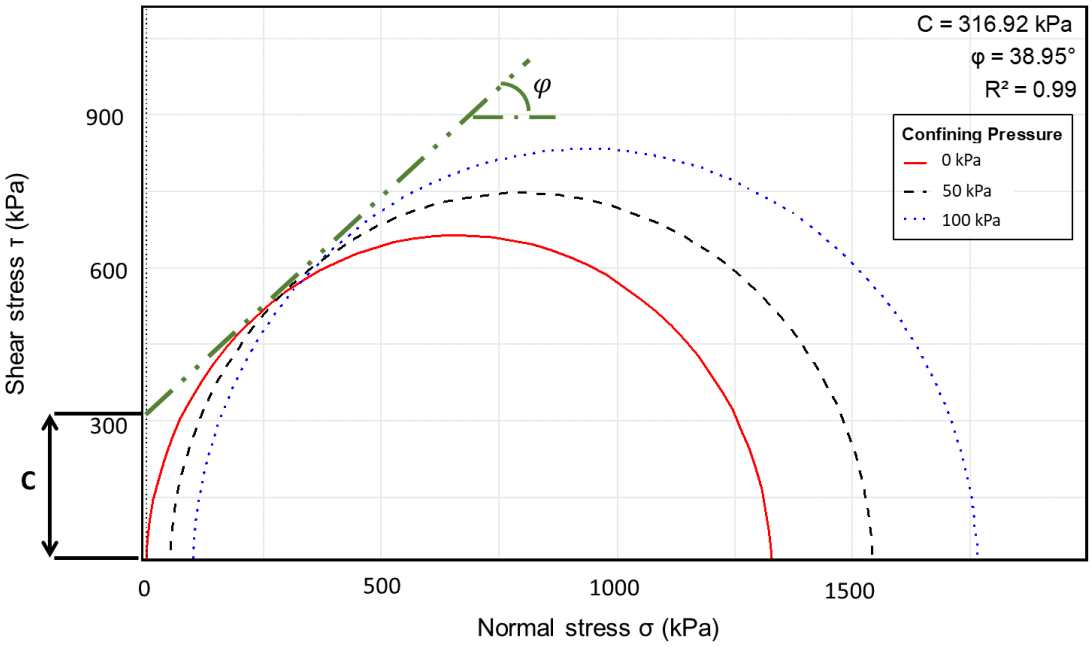

(b)

Figure 3-14: BC11-X results from the monotonic triaxial shear strength test (a) as measured stress and strain; (b) use of peak stresses and confinement to determine Mohr-Coulomb failure envelope and properties)

Chapter 4: Field and Laboratory Assessment Results

This chapter presents results and discussions on the field and laboratory assessment conducted.

4.1 Field Assessment Results

4.1.1 Falling Weight Deflectometer Results

Figure 4-1 and Figure 4-2 illustrate the structural condition of the pavement sections, represented by peak deflection, and the condition of the CR layers based on SCI, respectively. Error bars indicate one standard deviation from the mean while letters in boxes indicate statistical differences between deflection basin parameters (DBPs), D_0 and SCI in this case, at both test campaigns based on Welch's t-test conducted at a 95% confidence level assuming unequal variances. Results connected by the same letter indicate no statistical difference between DBPs at both test campaign and vice versa.

Across both test campaigns for all field sections, the pavement structure is generally in good condition, with average values falling below the severe threshold. A notable trend is the increase in average peak deflection (supported by the Welch's t-test for a number of the field sections) observed during the spring/summer test period compared to the fall season evaluations across all sections. This increase may be attributed to moisture accumulation within the pavement layers resulting from freeze-thaw events during the preceding winter, potentially affecting the pavement structure. The analysis also shows that average SCI values for all sections remain well below the threshold for sound condition. Similar to peak deflection trends, the spring/summer evaluations consistently exhibit higher average SCI values compared to the fall season evaluations, further supporting the hypothesis that moisture accumulation from the freeze-thaw events may have impacted the CR layers. Field sections CSAH 24 and TH 95, however, do not follow this trend.

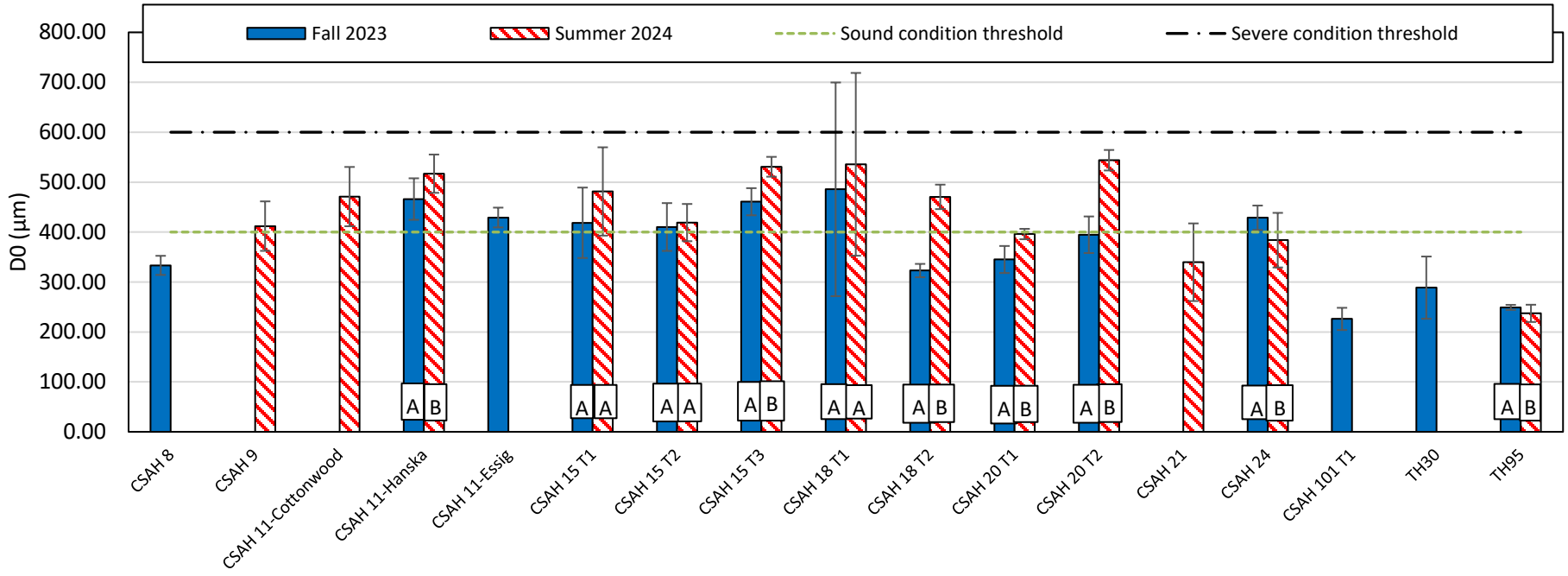

Figure 4-1: Peak deflection (D_0) metrics for all pavement sections

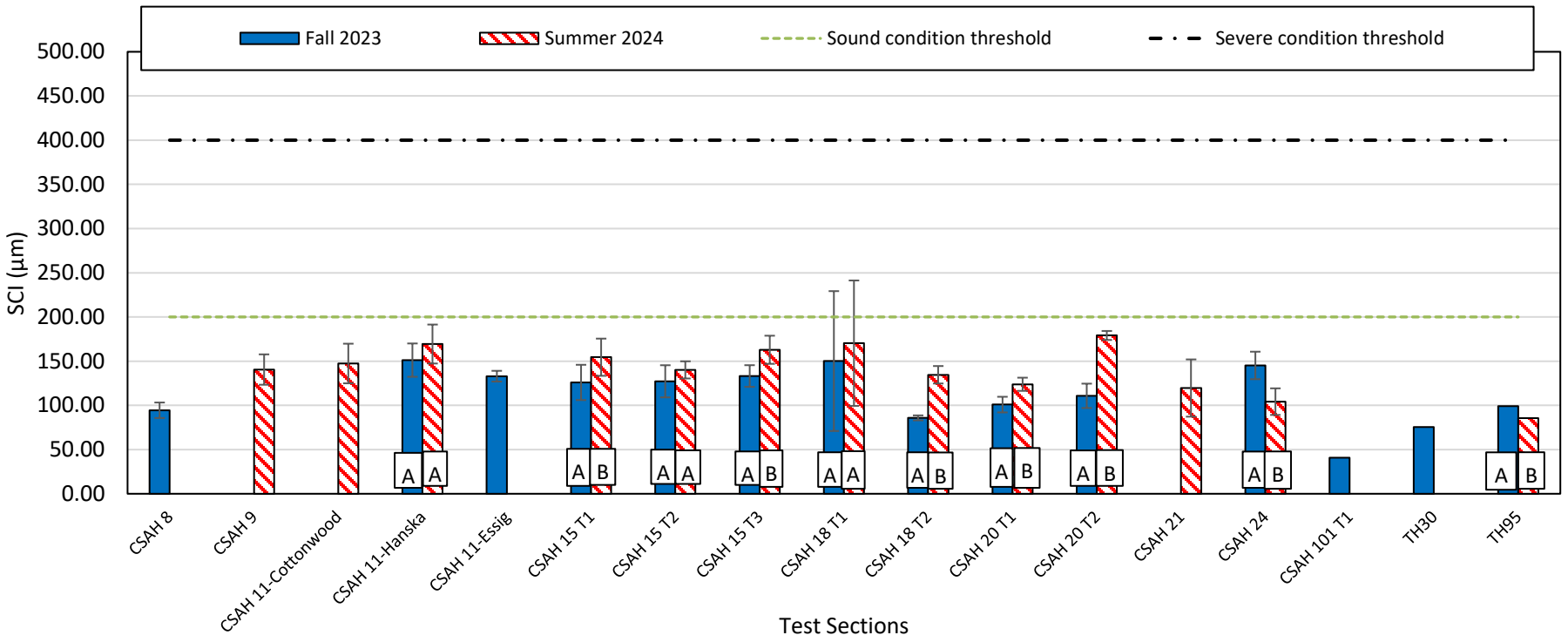

Figure 4-2: SCI metrics for all pavement sections

4.1.2 Pavement Rutting Results

Figure 4-3 presents the average rut depth measurements for the field pavement sections. Most sections demonstrate improved performance, with reductions in rut depth following rehabilitation ranging from 2% to 27%. However, field sections CSAH 15-T3 and CSAH 20-T2 deviate from this trend, exhibiting increased rut depths of approximately 3% and 2%, respectively. This increase may be attributed to additional consolidation and/or compaction of the CR layers. A detailed forensic investigation would be necessary to confirm this hypothesis. The analysis further indicates that all sections remain well within the conventional rutting acceptance threshold of 0.5-inches (12.5mm).

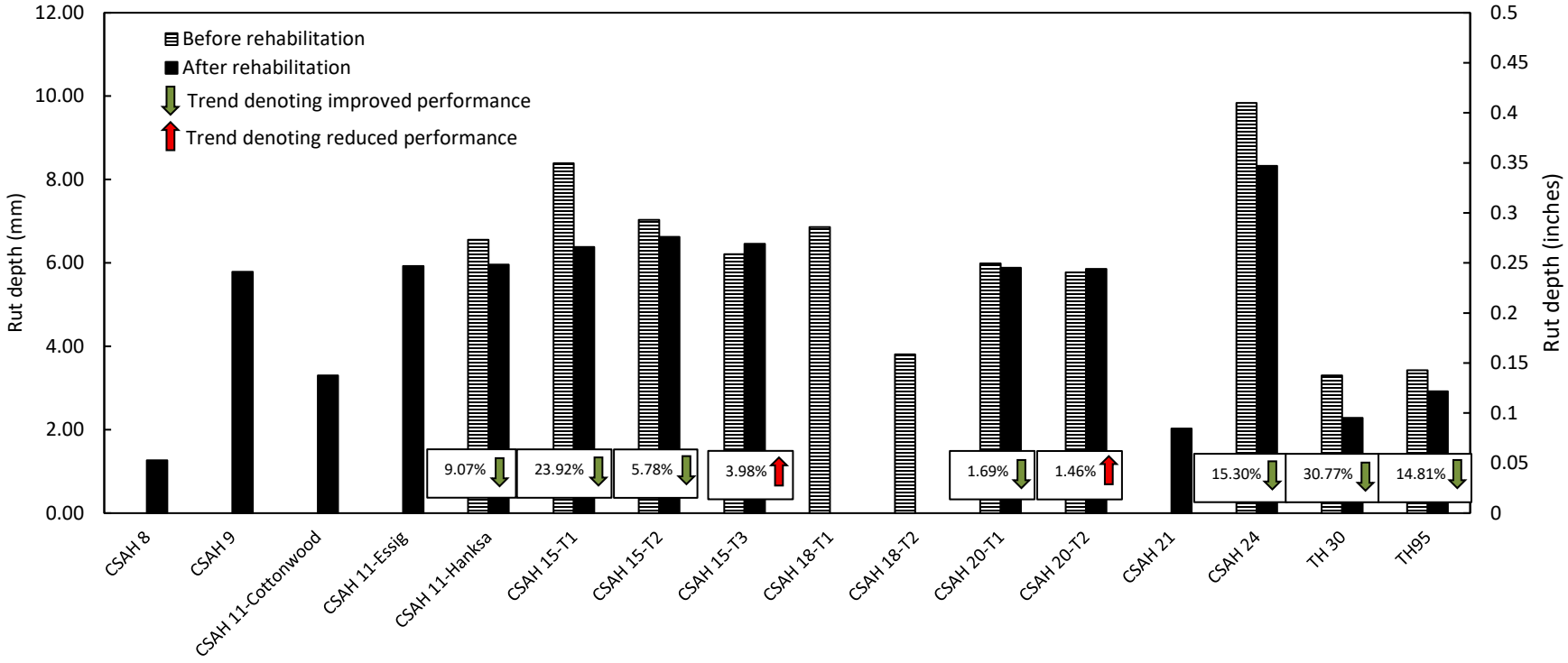

Figure 4-3: Rut depth metrics for all pavement sections

4.1.3 International Roughness Index Results

Figure 4-4 summarizes the average IRI measurements for the field pavement sections. Percentages in boxes represent increase or decrease (alongside arrows depicting increase/decrease trend) in IRI metrics from pavement condition before and after rehabilitation. The average IRI values for all sections are well below 101-inch/mile (1.6 m/km), indicating a very good overall pavement condition. Additionally, all pavement sections show improvements in IRI following rehabilitation, with reductions ranging from approximately 15% to 80%.

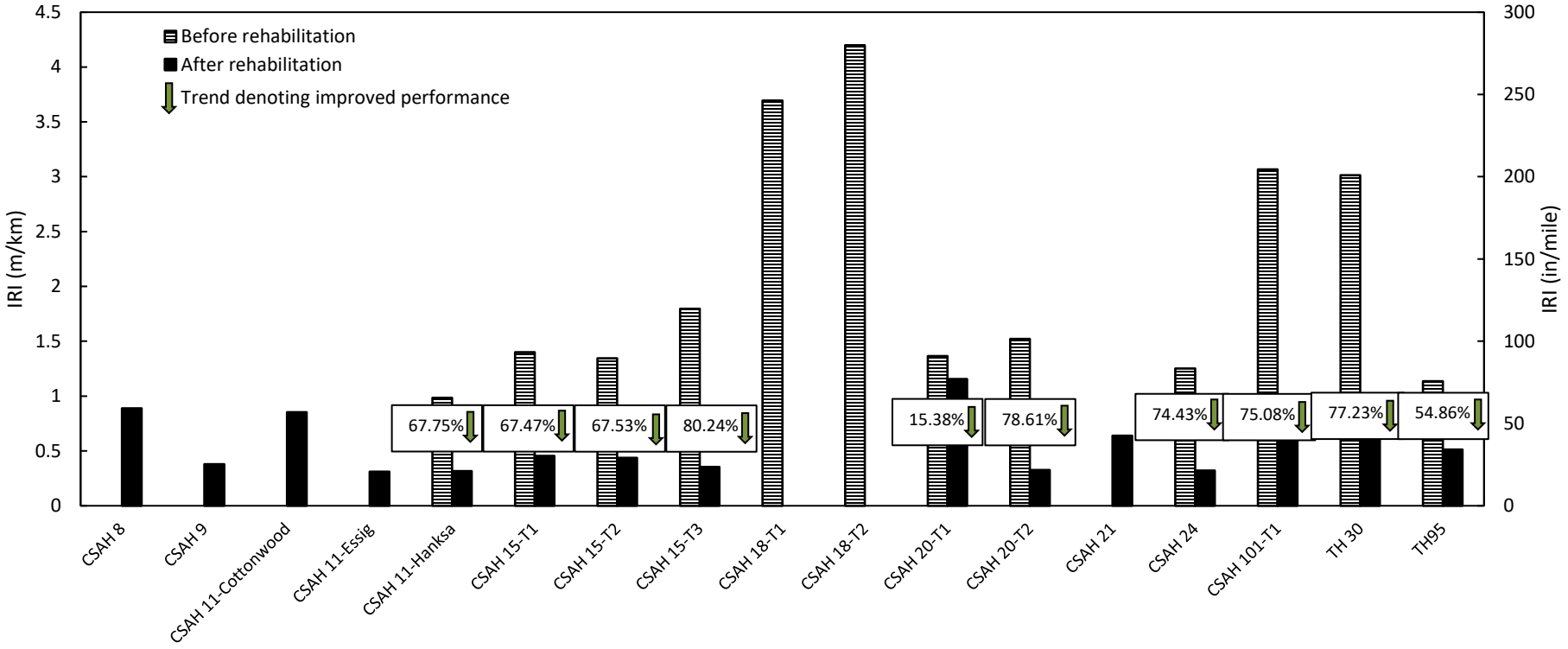

Figure 4-4: IRI metrics for all pavement sections

4.2 Laboratory Assessment Results

A comprehensive understanding of the impact of each mix component or attribute is crucial for mix designers and pavement engineers when utilizing CR materials in pavement structures. This section presents the results of the laboratory tests conducted on the CR mixtures, exploring the effect of mix and non-mix attributes on the mechanical properties. In addition to the CR mixtures processed in this study, twenty-one (21) and five (5) fully cured Engineered emulsion CR mixtures from a preceding study "Evaluation of Curing Effects on Cold In-Place Recycled (CIR) Materials" (Dave et al., 2022) were included for the tensile strength and shear strength analysis, respectively. It should be noted that the five additional shear strength mixtures were tested at confining pressures of 0, 35 and 70kPa. This is not expected to affect the accuracy of the determined failure envelope lines and corresponding shear strength parameter results (Ebels, 2008). The data analysis procedure employed, and the discussion of results are outlined in the following subsections.

4.2.1 Data Analysis Procedure

A brief discussion of the observed properties of the CR mixtures will be presented first where mixtures with comparative attributes, which include stabilizer amount, presence of chemical additive, density, and gradation (%retained 19mm sieve and %passing 4.75mm sieve), are assessed for mix composition variation effects on material properties. This is followed by a stepwise regression analysis in the JMP^{PRO} statistical package to investigate the effect of the mix attributes on the properties of the CR mixtures. This approach typically involves the iterative addition and removal of variables based on predefined criteria, ensuring that only statistically significant attribute(s) are selected while balancing regression complexity and explanatory power (Seber and Lee, 2012). While CR materials, as obtained from the different recycling techniques (CIR, CCPR, and SFDR), are known to share similar mix attributes, the primary difference is typically the method of RAP processing. Given that gradation characteristics are considered a factor in this analysis, all mixtures were combined for the stepwise regression analysis to facilitate a holistic evaluation of the properties of these materials. The result interpretations from the stepwise regression analysis are based on the following.

a. Presence of chemical additive is modelled as a categorical variable and denoted as 0 and 1, where 0 means no chemical additive used, and 1 indicating chemical additive used.
b. The F-ratio from the F-test within the stepwise regression analysis helps explain the variations in the regression analysis. When there is no relationship between the response and any of the predictors/mix attributes, the regression analysis will not explain much of the variation in the response and the F-ratio will be closer or less than 1. If there is explanation of at least some of the variation in the response, the F-ratio will be greater than 1. For context of this analysis, higher F-ratio indicates more significant relationship between the mechanical property and the mix attribute(s).
c. The correlation between the derived mix attribute on the mechanical properties are denoted by either being positive or negative, derived from the regression parameter estimate.
d. The associated p-value from the F-test depicts the statistical significance of the derived F-ratio. A lower p-value validates the F-ratio and indicates a strong influence of the attribute(s). For this

analysis, a significance level (α) of 0.10, corresponding to a 90% confidence level, was used to identify statistically significant attributes.

Table 4-1 outlines the mix attributes and range variables processed in the stepwise regression analysis based on the mix data obtained from the field project sources, the mix variations processed, and the additional mixtures included from the (Dave et al. 2022) study.

Table 4-1: Mixture attributes and variable range considered for analysis.

Material property evaluation [Number of Mixtures]	Mix attribute/Variable	Range of variable
Tensile Strength (kPa) [53 Mixtures]	Stabilizer amount	1.5–5.5%
	Chemical Additive presence [a, b]	NA, Cement/Lime kiln Dust
	Density	1730–2172-kg/m^3
	%Retained on 19-mm sieve (3/4-inches)	2.97–19.02
	%Passing 4.75mm sieve (No. 4)	27.09–55.96
Resilient Modulus (MPa) @ 10°C and 30°C [32 Mixtures]	Stabilizer amount	2.4–5.5%
	Chemical Additive presence [a, b]	NA, Cement
	Density	1730–2172-kg/m^3
	%Retained on 19mm sieve (3/4-inches)	2.97–19.02
	%Passing 4.75mm sieve (No. 4)	27.09–55.96
Shear Strength {Cohesion (kPa), Frictional Angle (°)} [37 Mixtures]	Stabilizer amount	1.5–5.5%
	Chemical Additive presence [a, b]	NA, Cement
	Density	1730–2172-kg/m^3
	%Retained on 19mm sieve (3/4-inches)	2.97–19.02
	%Passing 4.75mm sieve (No. 4)	27.09–55.96
Notes [a] Chemical additive at 0.5 and 1% [b] Not applicable 1-kg/m^3 = 0.062pcf		

4.2.2 Tensile Strength Results

Results of the tensile strength evaluations on the CR mixtures, with average values displayed alongside error bars representing one standard deviation from the mean are depicted in Figure 4-5. Among the mixtures, BelC15-D demonstrates the highest tensile strength. This can be explained by its relatively high emulsion and fines content (based on the %passing the 4.75mm sieve) which creates a cohesive mastic that enhances the tensile strength. Additionally, the high mix density is believed to contribute to this improved property metrics. Similar high tensile strength is observed in mixes CC18-C, BC24-B, BC20-B, and BC11-X, all characterized by high fines content, emulsion levels, and mix density. Conversely, mixtures DT95-A and CMG101-C exhibit the lowest tensile strength, despite similar high fines and

emulsion content. This may be due to the composition of the RAP in these mixes, suggesting that RAP source could play a significant role in the properties of CR mixes. Comparisons of mixtures with similar mix attributes further highlight the influence of RAP source and gradation. For example, CC18-A exhibits lower tensile strength than BC11-B, despite comparable mix attributes, which could be due to the higher coarse RAP content in BC11-B. Similarly, CMG101-C shows reduced tensile strength compared to BelC15-I, which is attributable to differences in RAP source and gradation characteristics. The role of chemical additives is examined in the comparison between BC20-X and BC20-A, as well as BelC15-X and BelC15-D. While BC20-X and BC20-A show comparable tensile strengths, aligning with literature findings that cement addition may primarily only be useful in accelerating curing (Halles & Thenoux, 2009; National Academies of Sciences, 2021), BelC15-D demonstrates higher tensile strength than BelC15-X. This may result from the complementary interaction effect of the chemical additive with the mix's high density. Density also significantly influences tensile strength, as seen in the comparison between BelC15-G and BelC15-H, where BelC15-H, with higher density, exhibits better tensile strength.

The impact of emulsion content can be observed in mixes BelC15-A, BelC15-X, and BelC15-B, where increasing tensile strength correlates with higher emulsion content. This also holds true between mixes BelC15-D and BelC15-L, where BelC15-D exhibits greater tensile strength. To further provide an understanding of the influence of mixture attributes, the results of the stepwise regression analysis is presented in Table 4-2.

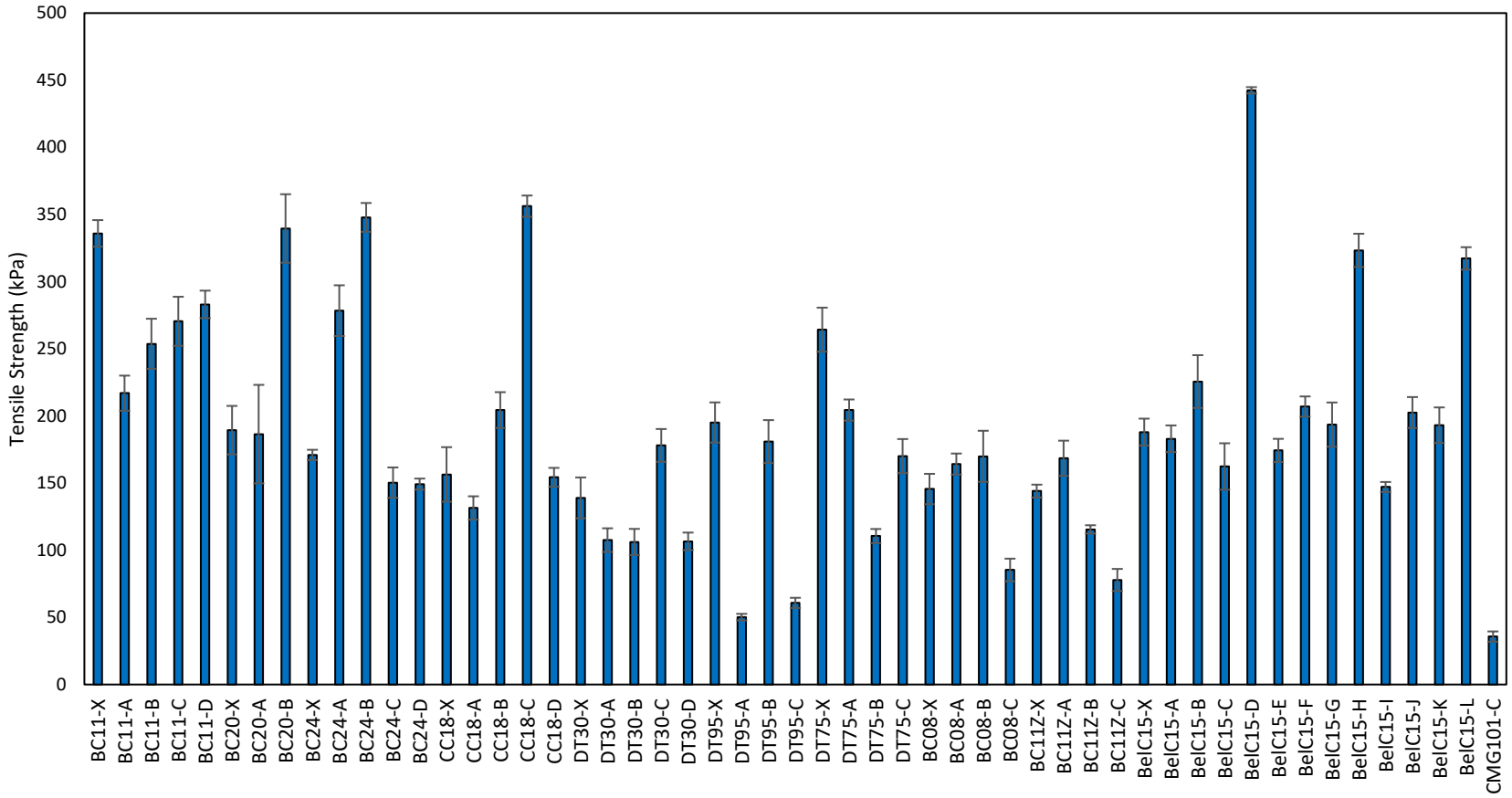

Figure 4-5: Tensile strength results

The results of the analysis indicate that the %Retained on the 19-mm sieve (representing the coarse RAP fraction), mix density, stabilizer content, and %Passing the 4.75-mm sieve are statistically significant factors affecting the tensile strength of the CR mixtures. Notably, the presence of chemical additives was statistically insignificant, with a p-value of 0.82, which does not meet the threshold for significance in this analysis. This finding indicates that chemical additives have a limited direct impact on tensile strength under the conditions studied.

Table 4-2: Significant mix attributes affecting Tensile Strength

Mix Attribute	F Ratio	p-value	Correlation	Significance
%Retained 19-mm	66.75	<.0.0001	Positive	Significant
Density (kg/m^3)	53.13	<.0.0001	Positive	Significant
Stabilizer Amount	36.88	<.0.0001	Positive	Significant
%Passing 4.75-mm	4.67	0.03	Positive	Significant
Chemical Additive	0.05	0.82	-	Not significant

4.2.3 Resilient Modulus Results

Figure 4-6 shows the resilient modulus results of the CR mixtures, with average values displayed alongside error bars representing one standard deviation from the mean. At 10°C, mixtures BC20-B, BC24-B, and BelC15-K exhibit higher resilient modulus on average than all other mixtures. This can be attributed to their mix characteristics, including optimized emulsion content, high density, and well-graded particle distribution. At 30°C, CC18-X demonstrates better average stiffness compared to all other mixtures.

A comparative analysis of mixtures CMG101-C and BelC15-I, with similar mix attributes but differing RAP source and gradation, reveals that BelC15-I consistently achieves a higher resilient modulus on average at both temperatures. This aligns with observations from the tensile strength evaluations, underscoring the influence of RAP source and composition. A variance is however noted when comparing CC18-A and BC11-B. Despite BC11-B's higher coarse RAP content, which should translate to enhanced load distribution and carrying capacity, CC18-A exhibits higher average stiffness at both temperatures. It is hypothesized that the resilient modulus test may not have fully captured the contribution of coarse RAP gradation in this case.

The role of chemical additives is analyzed through mixtures BC20-X and BC20-A as well as BelC15-X and BelC15-D. At both temperatures, BC20-X, which includes no chemical additive, exhibits a higher average resilient modulus than BC20-A. This is, however, not consistent with the tensile strength evaluation. A reverse trend similar to the tensile strength evaluation is observed between BelC15-X and BelC15-D, where BelC15-D consistently outperforms BelC15-X at both temperatures on average, likely due to the increased density complementing the chemical additive. The influence of emulsion content is highlighted in mixtures BelC15-X, BelC15-A, and BelC15-B, which share comparable density and gradation characteristics but vary in emulsion content. At 10°C, a general increase in resilient modulus is observed with higher emulsion content. However, at 30°C, the trend becomes non-linear, suggesting complex interactions between mix components and temperature and/or inability of the resilient

modulus test to capture this effect. In addition, BelC15-D shows higher stiffness on average compared to BelC15-L at both temperatures, further emphasizing the impact of emulsion content on stiffness. A comparison between BelC15-G and BelC15-H additionally demonstrates the influence of density, with BelC15-H, characterized by higher density, showing on average, higher resilient modulus at both temperatures.

Overall, the findings suggest that while the resilient modulus may differentiate the overall performance of the mixes, it may not consistently rank their performance when considered as the only performance assessment criteria. It is also generally observed that all mixtures exhibit temperature sensitivity, with lower resilient modulus values recorded at 30°C compared to 10°C. This underscores the necessity of incorporating temperature considerations in the design and performance assessment of CR mixtures. Further insights into the influence of mixture attributes are provided through Stepwise regression analysis results detailed in Table 4-3.

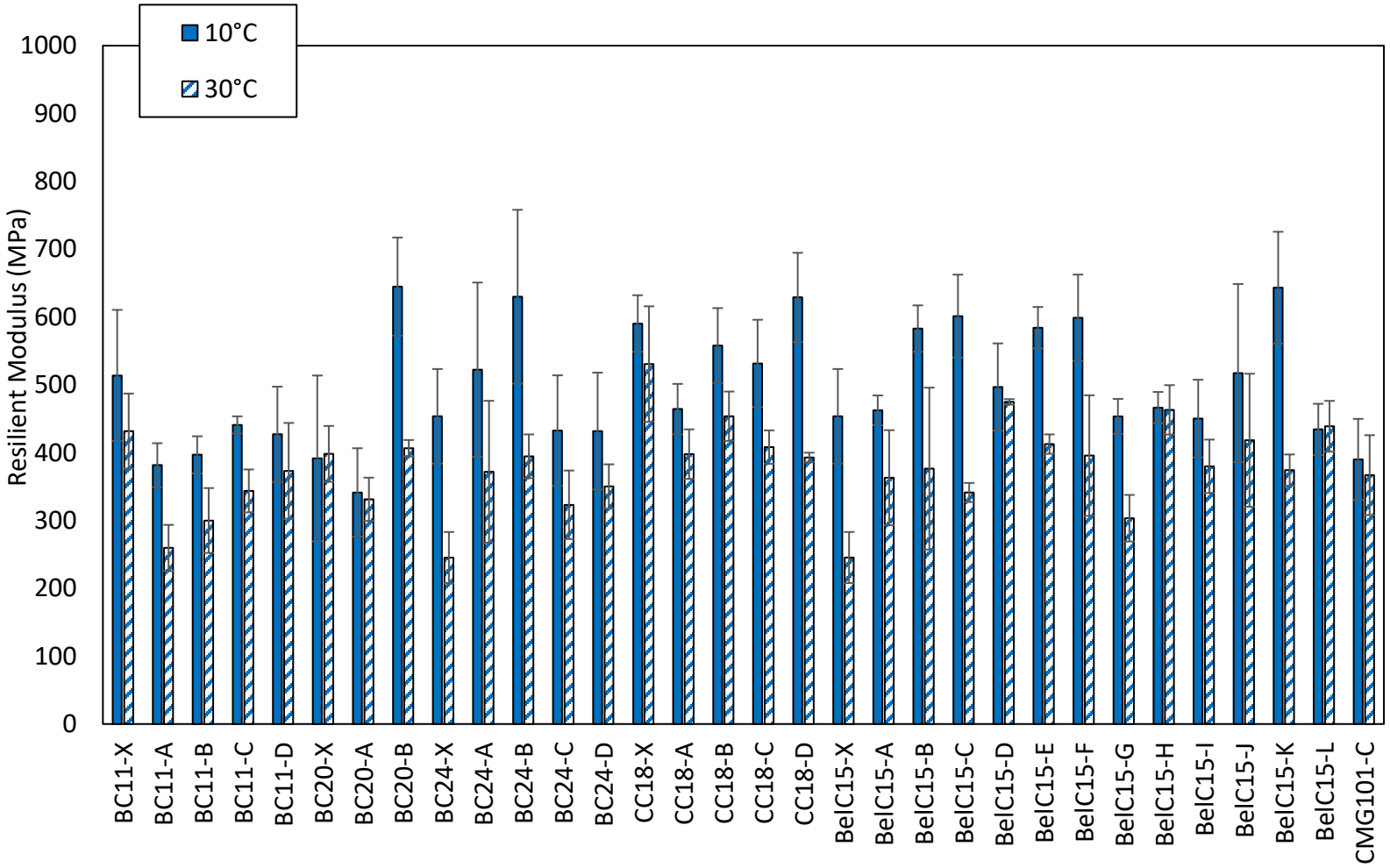

Figure 4-6: Resilient modulus results

At 10°C, the addition of chemical additives negatively impacts the resilient modulus. This is expected since at a lower temperature, the bituminous stabilizing agent creates sufficient stiffening such that chemical additive does not provide additional contribution to stiffness. In contrast, density and stabilizer content emerge as significant factors influencing stiffness at this temperature, emphasizing their critical roles in enhancing the stiffness properties of the CR mixtures. At 30°C, density is identified as the sole significant attribute influencing the resilient modulus. While gradation characteristics at both temperatures was observed to be statistically insignificant, its effect may have been captured through the mix density since gradation strongly influences packing characteristics and thus contributes to the material's overall density. Overall, these findings underscore the necessity of optimizing density and stabilizer content in CR mixtures to achieve desired stiffness properties while recognizing the trade-offs introduced by chemical additives at lower temperatures.

Table 4-3: Significant Mix Attributes affecting Resilient Modulus

Temperature	Mix Attribute	F-Ratio	P-value	Correlation	Significance
10°C	Chemical Additive presence	10.70	0.0015	Negative	Significant
	Stabilizer Amount	4.62	0.034	Positive	Significant
	Density (kg/m^3)	3.85	0.053	Positive	Significant
	%Passing 4.75-mm	1.86	0.177	-	Not Significant
	%Retained 19-mm	1.08	0.30	-	Not Significant
30°C	Density (kg/m^3)	16.45	0.0001	Positive	Significant
	%Passing 4.75-mm	0.19	0.665	-	Not Significant
	Chemical Additive presence	0.04	0.853	-	Not Significant
	Stabilizer Amount	0.01	0.936	-	Not Significant
	%Retained 19-mm	0.00	0.974	-	Not Significant

4.2.4 Shear Strength Results

The shear parameters, cohesion, and frictional angle, derived from the Mohr-Coulomb envelope for CR mixtures are presented in Figure 4-7. The respective coefficients of determination (R^2) are not plotted to allow for better presentation and readability of results, however, R^2 values for all mixtures are provided in Appendix D of this report. Higher cohesion and frictional angles are desirable as they represent strong internal bonding and enhanced resistance to sliding and shear forces. Among the evaluated mixtures, BC11-D demonstrates the highest cohesion, which can be attributed to its emulsion content and mix density. However, this mixture exhibits a relatively low frictional angle compared to others. In contrast, BC11-X, with comparable emulsion content and density, has both high cohesion and a frictional angle, reflecting a balanced internal bonding and shear resistance. The comparison of CMG101-C and BelC15-I highlights the influence of RAP source and gradation characteristics, with BelC15-I exhibiting higher cohesion but a lower frictional angle. This trend aligns with tensile strength evaluations, further demonstrating the effect of RAP source on CR properties. Similarly, in comparing CC18-A and BC11-B, the latter achieves both higher cohesion and a higher frictional angle, consistent with its performance in the tensile strength evaluation.

The role of chemical additives is jointly analyzed through mixtures BC20-X and BC20-A as well as BelC15-X and BelC15-D. BC20-X displays higher cohesion, but a lower frictional angle compared to BC20-A. The reduced cohesion in BC20-A may be explained by the cement's fine particle volume contribution to the mix, which thus reduces surface area coverage by emulsion. Comparison between BelC15-X and BelC15-D is consistent to the findings of the tensile strength and resilient modulus evaluations, where BelC15-D achieves greater cohesion and comparable frictional angle. In addition, emulsion content is observed to affect shear parameters, as evident in the comparison of BelC15-A, BelC15-X, and BelC15-B. An increasing trend in cohesion is observed with higher emulsion content, while frictional angle decreases. Likewise, BelC15-D, compared to BelC15-L, exhibits higher cohesion but a reduced frictional angle. The reduction in frictional angle resulting in an increase in emulsion content is expected as the emulsion introduces more workability for the RAP components. The influence of density is evident in mixtures BelC15-G and BelC15-H, which share identical mix components. BelC15-H, with higher density, exhibits higher cohesion but a reduced frictional angle compared to BelC15-G. To quantify and provide a deeper understanding of the influence of mixture attributes, the results of the stepwise regression analysis are presented in Table 4-4.

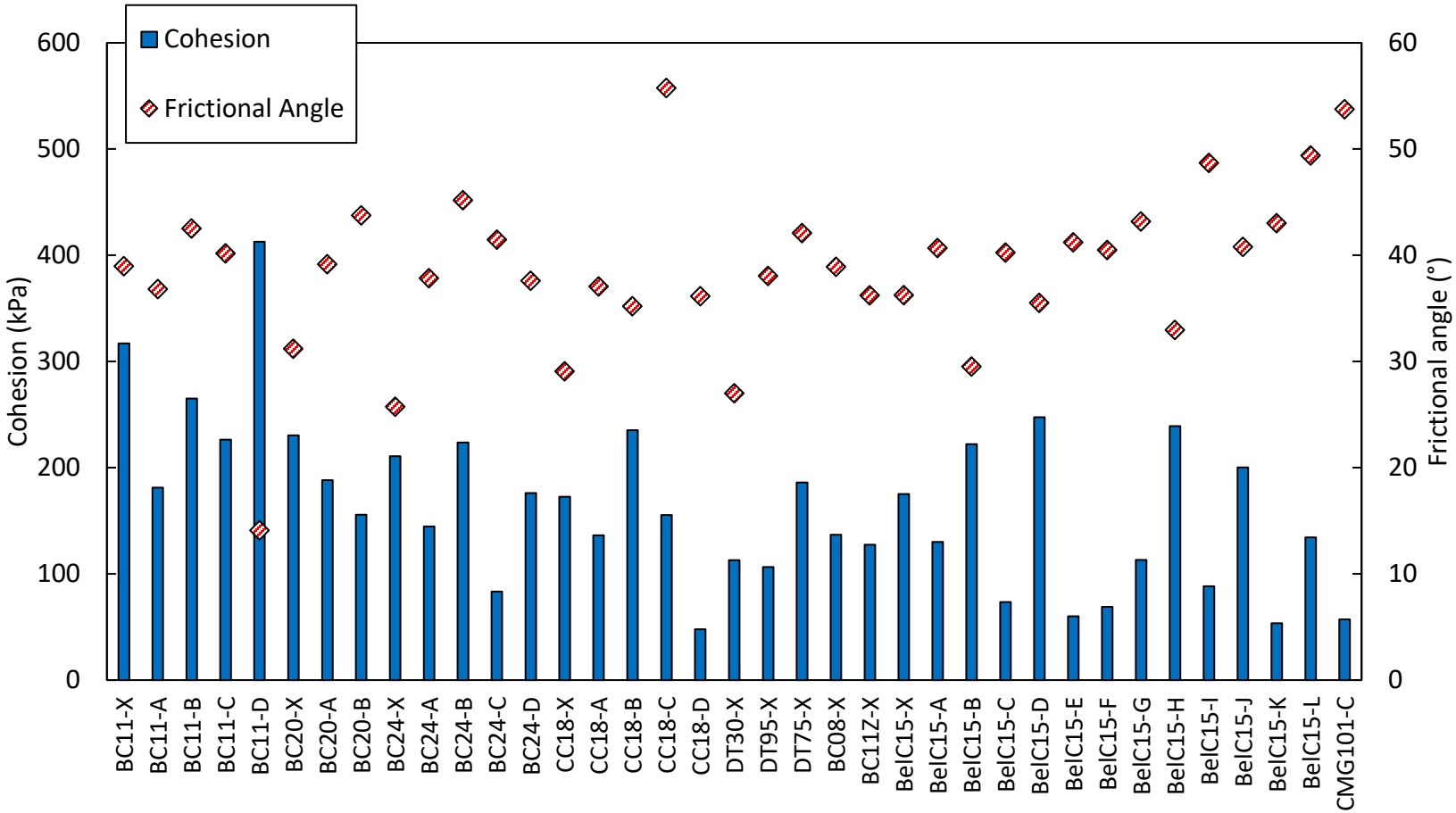

Figure 4-7: Shear parameters Results

The analysis reveals that %Retained on the 19-mm sieve, stabilizer content, and mix density are critical factors influencing the cohesive properties of CR mixtures. These attributes enhance internal bonding by promoting optimal packing and binder distribution within the mix. Additionally, the presence of chemical additives is shown to significantly impact the frictional angle. This is consistent with expectations, as chemical additives enhance interparticle friction and contribute to improved shear strength by creating resistance to sliding action within the mix matrix.

Table 4-4: Significant Mix Attributes affecting Shear parameters

Shear Parameter	Mix Attribute	F-Ratio	P-value	Correlation	Significance
Cohesion	%Retained 19-mm	24.36	<.0.0001	Positive	Significant
	Stabilizer Amount	6.73	0.014	Positive	Significant
	Density (kg/m^3)	5.71	0.023	Positive	Significant
	%Passing 4.75-mm	0.99	0.326	-	Not Significant
	Chemical Additive Presence	0.03	0.867	-	Not Significant
Frictional Angle	Chemical Additive Presence	5.98	0.02	Positive	Significant
	%Retained 19-mm	1.35	0.253	-	Not Significant
	%Passing 4.75-mm	0.77	0.386	-	Not Significant
	Stabilizer Amount	0.54	0.468	-	Not Significant
	Density (kg/m^3)	0.34	0.562	-	Not Significant

4.3 Summary of Field and Laboratory Assessment Results

4.3.1 Field Assessment Result Summary

Primary findings from the in-situ evaluation are summarized below.

1. Peak deflection results from the FWD evaluations indicate that the pavement structures are generally in good condition, with average values consistently below the severe threshold across all test campaigns. Additionally, the analysis reveals an increase in peak deflection values during the spring/summer testing compared to the Fall test campaign, potentially due to moisture accumulation within the pavement layers resulting from freeze-thaw during the preceding winter, which may have influenced the pavement's structural performance.
2. SCI evaluations revealed that the CR layers are in sound condition, as evidenced by the average SCI values below the sound condition threshold. For most pavement sections, the spring/summer evaluations exhibited higher SCI values compared to Fall season evaluations, mirroring the trend observed for peak deflection. This pattern further supports in part, the hypothesis that moisture accumulation resulting from the preceding freeze-thaw event may have influenced the performance of the CR layers.
3. Most pavement sections showed improved performance with respect to reductions in rut depths ranging from 2% to 27% following CR rehabilitation. Two pavement sections, CSAH 15-T3 and CSAH 20-T2, however experienced slight increases in rut depth, which may be as a result of

an additional consolidation and/or compaction of the CR layers. Overall, all sections remain well within the conventional rutting acceptance threshold of 0.5-inches (12.5-mm).

4. The average IRI values for all sections are well below 101-inch/mile (1.6m/km), reflecting very good pavement conditions. Post-rehabilitation, all sections exhibited IRI improvements, with reductions ranging from 15% to 80%.

4.3.2 Laboratory Assessment Result Summary

Laboratory-fabricated mixtures with both as-built properties and variations from these as-built conditions were subjected to tensile strength, resilient modulus and shear strength tests to explore the effect of mix and non-mix attributes on the mechanical properties as well as generate an expanded dataset to be used for the development of the mechanical property prediction model. Tensile and shear strength tests were performed at ambient temperatures (25°C/77°F), while resilient modulus tests were conducted at temperatures corresponding to the average fall and summer temperatures of the CR layer. Initial results from the resilient modulus tests suggest that mixtures may become less dependent on confining pressure after full curing. Drawing from the literature, factors such as emulsion content, presence of chemical additive, mix density, and RAP gradation, were evaluated for their effects on mechanical properties. Results for all mixtures, categorized by laboratory tests conducted, were discussed for observed properties based on mix attribute influenced followed by a stepwise regression analysis to statistically explore the effects of mix components. Table 5-1 summarizes the results presented in terms of mix attributes observed to influence the evaluated mechanical properties.

Table 4-5: Summary of key findings

Mechanical Property	Key Influencing Factors	Key Findings/Effects
Tensile Strength	• Density • Stabilizer Amount • Gradation characteristics	The tensile strength of the CR mixtures is significantly influenced by the emulsion content, mix density, and gradation characteristics, with these factors enhancing cohesive mastic formation. This was additionally confirmed by the stepwise regression analysis indicating these mix attributes as statistically significant components. While chemical additives showed limited direct impact on tensile strength, with statistical insignificance (p-value = 0.82), its interaction with mix density may contribute to improved properties in certain cases. These findings underscore the need for precise specification of mix design parameters to achieve sufficient tensile strength, ensuring enhanced load-bearing capacity and durability in pavement applications.
Resilient Modulus	• Density • Stabilizer Amount • Chemical Additive	The resilient modulus of the CR mixtures is significantly influenced by mix density, and emulsion content, with density emerging as the dominant factor at both 10°C and 30°C. Temperature sensitivity is evident, as all mixtures exhibit lower resilient modulus at 30°C compared to 10°C, emphasizing the need to incorporate temperature considerations in CR mixture design. At 10°C, chemical additives negatively impact resilient modulus due to the brittleness introduced under load application, while stabilizer content and density play critical roles in stiffness improvement. Gradation characteristics were not directly significant at either temperature, likely due to their contribution to density based on its packing characteristics. These findings highlight the importance of optimizing density and stabilizer content while carefully managing chemical additive use to achieve balanced performance.
Shear Strength Parameters	• Density • Stabilizer Amount • Chemical Additive • Gradation characteristics	The shear parameters of CR mixtures, cohesion and frictional angle, are influenced by mix density, gradation (% Retained on the 19 mm sieve), and emulsion content. Higher cohesion is associated with increased emulsion content and density, while frictional angle tends to decrease with higher emulsion content. Chemical additives significantly impact the frictional angle by enhancing interparticle friction, improving shear strength through increased resistance to sliding action, but can reduce cohesion due to increased fine particle volume and reduced emulsion coverage. The RAP source and gradation characteristics also play a critical role, affecting both cohesion and frictional angle, consistent with trends observed in tensile strength evaluations. Overall, these findings underscore the importance of optimizing mix density and stabilizer content while carefully managing emulsion and chemical additive use to achieve balanced internal bonding and shear resistance in CR mixtures.

Chapter 5: Development of Mechanical Property Prediction Model

This chapter provides comprehensive details of the approach undertaken and analyses conducted to develop the mechanical property prediction models. Specifically, information about the mixture database, range of mix attributes/variables, data processing, final variable selection, regression and/or machine learning techniques, and final prediction models transformed to a user-friendly tool are presented. All statistical analyses and model development are performed using the JMP Pro® statistical software.

5.1 Material Database and Data Preprocessing

5.1.1 Material Database

Table 5-1 outlines the range of mixture variables considered for model development. These variables were selected based on their routine availability in cold recycling mix design and construction practices, as well as insights from the *laboratory assessment* section of Chapter 4 of this study. Detailed descriptions of each mix attribute and the corresponding modeling approach are discussed further.

- **Stabilizer (Engineered Emulsion) Amount**: Since the materials used for laboratory investigations were sourced exclusively from projects employing engineered emulsion, model development for each material property was limited to this stabilization method. For the modeled material properties, the corresponding range for this mix attribute is between 1.5% and 5.5% and is treated as a continuous variable.
- **Chemical Additive**: Across the evaluated mixtures, chemical additives were either absent or incorporated at levels of 0.5% and 1%. For the tensile strength evaluations, two types of chemical additives were present: cement and lime kiln dust (LKD). However, for resilient modulus and shear strength evaluations, only cement was present as chemical additive. For model development, and in alignment with MnDOT specifications regarding chemical additive incorporation in CR materials, this variable was modeled as a binary variable, (0) representing the absence of chemical additive and (1) representing the presence of a chemical additive.
- **Density:** The density of the evaluated mixtures ranged from 1730 to 2172 kg/m³ (108 – 136-pcf). As with the stabilizer amount, this variable was treated as a continuous variable.
- **Gradation characteristics**: Two gradation characteristics from a typical sieve analysis were considered for model development. These are, %retained on the 19-mm (¾-inch) sieve which represents the coarse fraction of the CR material and %passing 4.75-mm (No. 4) sieve which represents the fine fraction of the CR material. The range for these variables are between 2.97–19.02% and 27.09–55.96%, respectively and are both modelled as continuous variables.
- **Temperature**: Since the resilient modulus evaluations were conducted at temperatures representative of the in-situ seasonal conditions of the CR layer, temperature was modeled as a continuous variable in the model development. The temperature range for these evaluations

are between 10°C and 30°C (50°F and 86°F). Further details regarding the temperature selection process are provided in Chapter 3.

Table 5-1: Range of mix attributes

Material property evaluation [Total number of data points]	Mix attribute/Variable	Range of variable
Tensile Strength (kPa) [182]	Stabilizer amount	1.5 - 5.5%
	Chemical Additive presence [a, b]	NA, Cement/Lime kiln Dust
	Density	108 – 136 pcf (1730 – 2172-kg/m^3)
	%Retained on 19mm sieve (3/4-in)	2.97 – 19.02
	%Passing 4.75mm sieve (No. 4)	27.09 – 55.96
Resilient Modulus {MPa} [213]	Stabilizer amount	2.4 – 5.5%
	Chemical Additive presence [a, b]	NA, Cement
	Density	108 – 136 pcf (1730 – 2172-kg/m^3)
	%Retained on 19mm sieve (3/4-in)	2.97–19.02
	%Passing 4.75mm sieve (No. 4)	27.09 – 55.96
	Temperature	(50 – 86°F) 10–30°C
Shear Strength {Cohesion (kPa), Frictional Angle (°)} [37][c]	Stabilizer amount	1.5 - 5.5%
	Chemical Additive presence [a, b]	NA, Cement
	Density	108 – 136-pcf (1730 – 2172-kg/m^3)
	%Retained on 19mm sieve (3/4-in)	2.97–19.02
	%Passing 4.75mm sieve (No. 4)	27.09–55.96

Notes
[a] Chemical additive incorporated into the mixtures are at content levels of 0.5% and 1%
[b] Not Applicable
[c] Considering the nature of the testing procedure and amount of material required for this evaluation, it was only feasible to conduct evaluations on single replicates.

5.1.2 Data Preprocessing

5.1.2.1 Mixture Property Distribution

Figure 5-1(a-d) outlines the distribution of the measured values for tensile strength, resilient modulus, and shear parameters (cohesion and friction angle) across the evaluated mixtures. To determine the estimate distribution of these mix properties, several continuous distributions were fit and compared using the corrected Akaike's Information Criteria (AICc) and AICc weights. The best fit is therefore determined as the distribution that results in the lowest AICc and highest AICc weight (Burnham, 2002). Table 2 provides details of this analysis with the best fit distribution for each property highlighted in **bold** and color shaded. The results of the distribution analysis suggest that tensile strength most closely

follows a Normal 3 Mixture distribution, resilient modulus and cohesion are best represented by a Gamma distribution, while the friction angle is most consistent with a student's t-distribution.

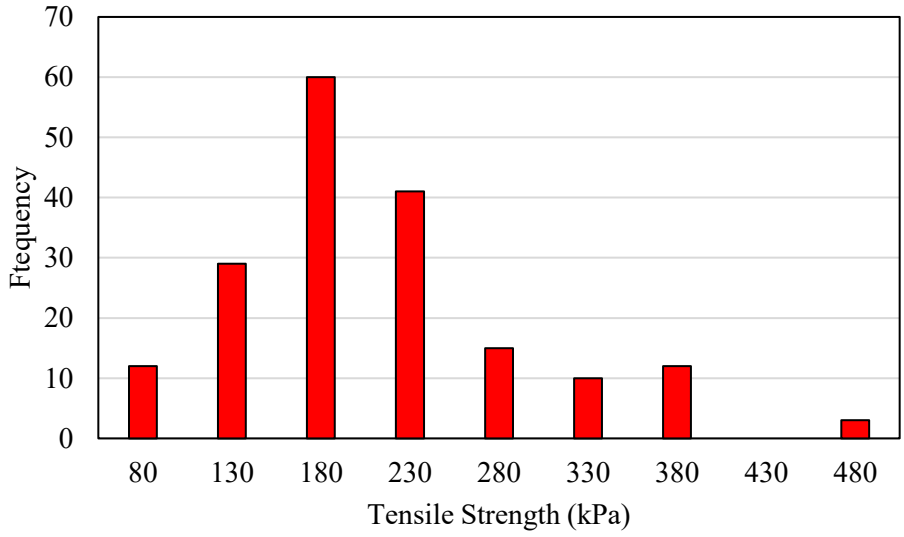

(a)

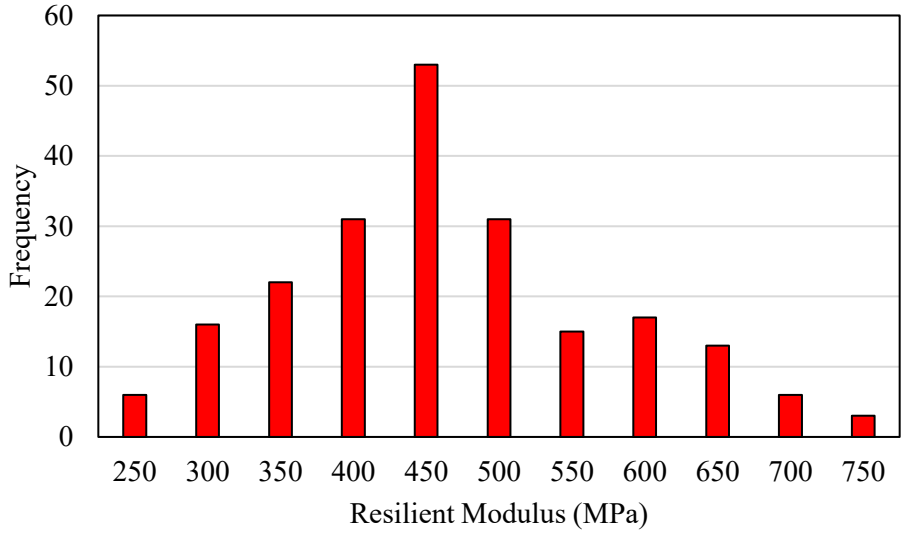

(b)

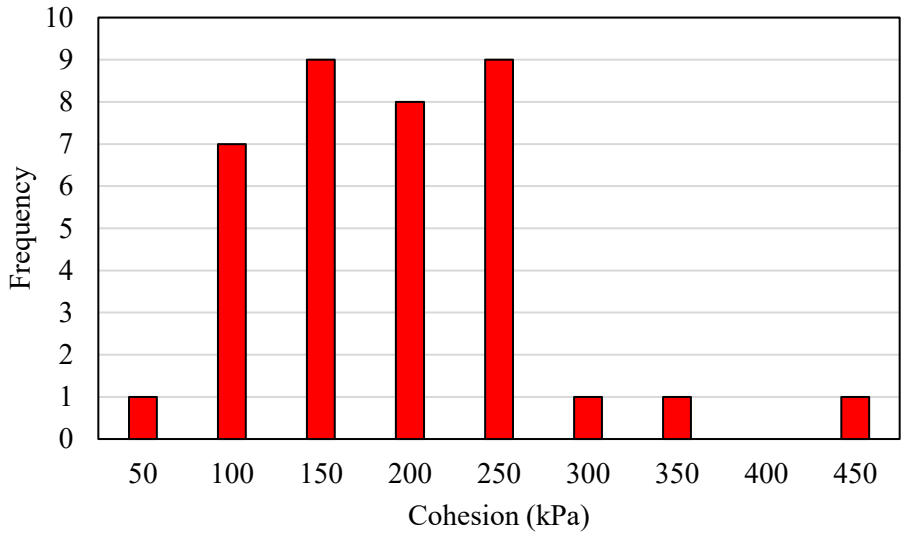

(c)

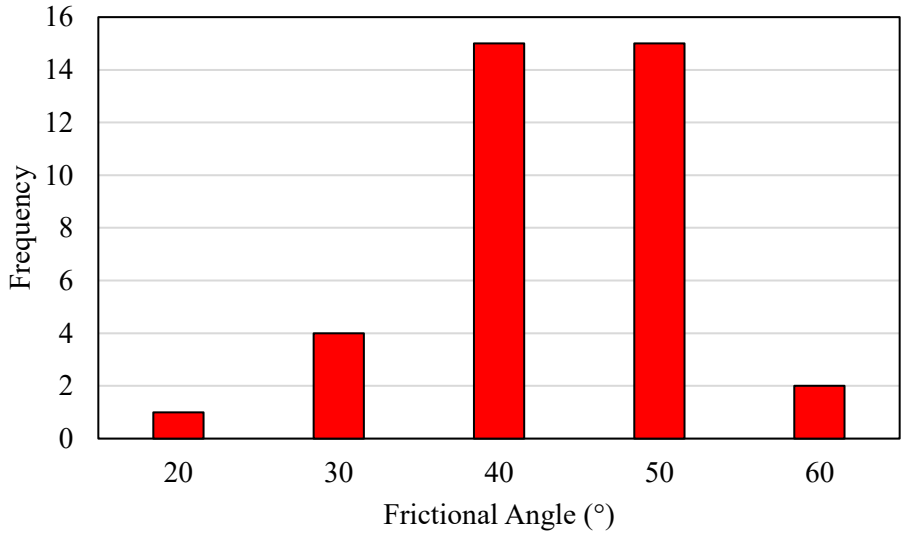

(d)

Figure 5-1: Frequency Distribution of (a) Tensile Strength (b) Resilient Modulus (c) Cohesion (d) Frictional Angle

Table 5-2: Distribution fit results for all mixture properties

Distribution	Tensile Strength (kPa)		Resilient Modulus (MPa)		Cohesion (kPa)		Frictional Angle	
	AICc	AICc weight	AICc	AICc weight	AICc	AICc weight	AICc	AICc weight
Normal	2121.55	0.00	2609.41	0.02	431.72	0.04	259.19	0.09
Cauchy	2140.45	0.00	2673.14	0.00	443.89	0.00	258.34	0.14
Sinh-arcsinh (SHASH)	2099.38	0.01	2606.18	0.08	432.87	0.02	257.54	0.21
ZI SHASH	2101.49	0.00	2608.28	0.03	435.56	0.00	260.23	0.05
Student's t	2118.15	0.00	2611.50	0.01	433.28	0.02	**256.62**	**0.34**
Exponential	2271.08	0.00	3022.01	0.00	453.85	0.00	346.35	0.00
ExGaussian	2100.54	0.01	2606.93	0.06	431.12	0.06	261.55	0.03
Gamma	2101.89	0.00	**2602.43**	**0.54**	**427.31**	**0.39**	265.24	0.00
LogNormal	2112.84	0.00	2605.26	0.53	429.11	0.16	269.96	0.00
Weibull	2108.27	0.00	2617.21	0.00	427.95	0.28	259.07	0.10
Normal 2 Mixture	2094.70	0.09	2605.48	0.12	434.48	0.01	261.95	0.02
Normal 3 Mixture	**2090.01**	**0.90**	2606.73	0.06	444.69	0.00	271.21	0.00
Johnson su	2116.06	0.00	2620.22	0.00	433.36	0.02	260.02	0.06

5.1.2.2 Correlation Analysis on Mix Variables and Mixture Property

To support model development and minimize potential multicollinearity, a correlation analysis was performed to identify suitable predictor variables for each material property. Prior to this analysis, all continuous-type mixture attributes were assessed for normality using the Shapiro-Wilk's test. This step was necessary to guide the selection of the appropriate correlation method, since Pearson's correlation requires the assumption of normally distributed continuous variables and is based on parametric statistical principles while Spearman's correlation coefficient, a non-parametric measure that assesses the strength and direction of monotonic relationships, assumes non-normality. Table 5-4 summarizes the results of the normality test. As shown in the results for all material properties, none of the mixture variables exhibited a normal distribution; therefore, Spearman's correlation was employed to identify suitable predictor variables.

Table 5-3: Results of Shapiro-Wilk test for normality

Material Property	Mix attribute	p-value
Tensile Strength (kPa)	Stabilizer Amount	<.0001
	Density	<.0001
	%Retained 19-mm (3/4-in)	<.0001
	%Passing 4.75-mm (No. 4)	<.0001
Resilient Modulus (MPa)	Stabilizer Amount	<.0001
	Density	<.0001
	%Retained 19-mm (3/4-in)	<.0001
	%Passing 4.75-mm (No. 4)	<.0001
	Temperature	<.0001
Shear Parameters (Cohesion and Frictional Angle)	Stabilizer Amount	0.03
	Density	0.02
	%Retained 19-mm (3/4-in)	<.0001
	%Passing 4.75-mm (No. 4)	<.0001
Note p-value > 0.05; Normally distributed p-value < 0.05; Not normally distributed		

Results of the correlation analysis are depicted in Table 5-5 to Table 5-7. Values with an absolute correlation greater than 0.7 indicate a strong relationship between the variables. Values between 0.3 and 0.7 represent moderate correlations, while values below 0.3 denote weak correlations. Where correlation between attributes exceeds ±0.95, such variables are considered highly collinear; in these cases, the variable showing a lower correlation with the target property is excluded from the model development to eliminate the risk of potential bias.

Table 5-4: Spearman Correlation between attributes and Tensile Strength

	Stabilizer Amount	Density (kg/m³)	%Retained 19-mm	%Passing 4.75-mm	Tensile Strength (kPa)
Stabilizer Amount	1	--	--	--	--
Density	0.34	1	--	--	--
%Retained 19-mm (3/4-in)	-0.42	-0.26	1	--	--
%Passing 4.75-mm (No. 4)	0.59	0.32	-0.63	1	--
Tensile Strength (kPa)	0.37	0.43	0.18	0.13	1

Table 5-5: Spearman Correlation between attributes and Resilient Modulus

	Stabilizer Amount	Density (kg/m³)	%Retained 19-mm	%Passing 4.75-mm	Temperature	Resilient Modulus
Stabilizer Amount	1	--	--	--	--	--
Density	0.44	1	--	--	--	--
%Retained 19-mm (3/4-in)	-0.76	-0.40	1	--	--	--
%Passing 4.75-mm (No. 4)	0.82	0.38	-0.75	1	--	--
Temperature	0.00	0.00	0.00	0.00	1	--
Resilient Modulus	0.17	0.18	-0.17	0.10	-0.53	1

Table 5-6: Spearman Correlation between attributes and Shear parameters (Cohesion and frictional angle)

	Stabilizer Amount	Density (kg/m³)	%Retained 19-mm	%Passing 4.75-mm	Cohesion	Frictional angle
Stabilizer Amount	1	--	--	--	--	--
Density	0.37	1	--	--	--	--
%Retained 19-mm (3/4-in)	-0.58	-0.33	1	--	--	--
%Passing 4.75-mm (No. 4)	0.76	0.32	-0.72	1	--	--
Cohesion	-0.06	0.16	0.46	-0.20	1	--
Frictional angle	0.20	0.18	-0.12	0.15	-0.38	1

The results of this analysis reveal no evidence of multicollinearity among the mixture attributes, based on the predefined ±0.95 threshold. As a result, all identified mix variables were retained and utilized in the model development for each of the evaluated material properties.

5.2 Model Development and Assessment Approach

The aim of prediction model development is to identify the relationship between the predictor (mix variables) and response (material properties) to be able to estimate properties in the absence of lab characterization. This section outlines the machine learning techniques employed, the procedures for data processing into training and testing sets, and the methods used for evaluating model performance.

5.2.1 Machine Learning Techniques

The machine learning techniques employed include the Self-Validating Ensemble Model (SVEM) and Support Vector Regression (SVR). The SVEM represents an advanced machine learning framework that integrates principles of bootstrapping and ensemble modeling to construct validated models. Within the SVEM framework, three multiple linear regression techniques; Forward Selection, Adaptive Least Absolute Shrinkage and Selection Operator (LASSO), and Elastic Net were incorporated alongside a Neural Network algorithm. These methods were selected based on their documented advantages in achieving predictive accuracy when working with limited datasets, as is applicable in this study (Lemkus et al. 2021; Khorshidi et al. 2024). Details of all approaches are discussed in the following subsections.

5.2.1.1 Self-Validating Ensemble Modeling (SVEM)

SVEM is an advanced methodology that integrates principles of bootstrapping and ensemble modeling to construct validated predictive models. The bootstrapping involves generating multiple resampled datasets, each of size N, by randomly sampling with replacement from the original dataset of the same size. Consequently, some observations are selected multiple times, while others may be omitted entirely in each resample. Each observation in a bootstrapped resample is assigned an integer weight (including zero), reflecting the number of times it was selected. Since bootstrapping employs sampling with replacement, certain observations may appear more than once within a given resample. This bootstrapping procedure used within SVEM is termed the fractionally weighted bootstrapping with auto-validation (FWB + AV), which preserves the integrity of the experimental design structure while integrating a weighted resampling scheme.

SVEM employs the fractionally weighted bootstrapping to allocate observations between a training partition and a "self-validation" partition. In the self-validation approach within SVEM, the original dataset serves as the training partition, while an identical copy constitutes the self-validation partition. Each observation in the training set has a corresponding counterpart in the self-validation set. Fractional weights are assigned in pairs such that if an observation in the training partition receives a large weight, its twin in the self-validation partition is assigned a correspondingly small weight, and vice versa. This inverse weighting scheme induces anti-correlation between the two partitions, effectively allowing the self-validation set to function as a surrogate validation set. Each time a fractionally weighted bootstrap sample is generated, observations receive different weight allocations, alternating between higher weights in the training set and higher weights in the validation set. This dynamic weighting strategy mirrors the mechanism used in random forests, where standard bootstrap samples are utilized in bagging.

The fractional weights in SVEM are derived from random samples drawn from an exponential distribution with a mean of 1. The weighting process begins by generating a set of N random values from a uniform distribution over the interval (0,1). These uniform random values are then transformed using the inverse probability transform of the exponential distribution's cumulative distribution function (CDF) with a mean of 1. This transformation ensures that the resulting fractional weights follow the desired exponential distribution. The computation of these weights is formally expressed in Equation 5-1.

$$Generate: u_i \sim U[0,1] \; for \; i = 1 \ldots N$$

$$Training \; FWs: w_{T,i} = \; F^{-1}(u_i) = \log(u_i) \; for \; i = 1 \ldots N$$

$$\boldsymbol{Self - Validation \; FWs: w_{V,i} = \; F^{-1}(1 - u_i) = \log(1 - u_i) \; for \; i = 1 \ldots N}$$

Equation 5-1

Where.
U[0,1] denotes the uniform distribution on (0,1),
F represents the CDF of an exponential distribution with a mean of 1.

The two sets of fractional weights are assigned in pairs to the training and self-validation partitions. This pairing ensures that for each randomly assigned weight $w_{T,i}$ in the training data, there is a corresponding weight $w_{V,i}$ assigned to the same observation in the self-validation data. Due to the inverse weighting scheme, large values of $w_{T,i}$ correspond to small values of $w_{V,i}$, and vice versa. Once the weights are allocated, a model selection algorithm is applied to the training data. The algorithm evaluates different models and selects the one that minimizes the mean squared prediction error (MSPE) on the self-validation set. This process is repeated for a user-specified number of iterations, denoted as n_{Boot}. At each iteration, the selected model is stored, and the final model is constructed by averaging the coefficient estimates from all n_{Boot} iterations. More details on the SVEM algorithm can be found elsewhere (Lemkus et al. 2021). Figure 5-2 provides a schematic representation of the SVEM modeling process.

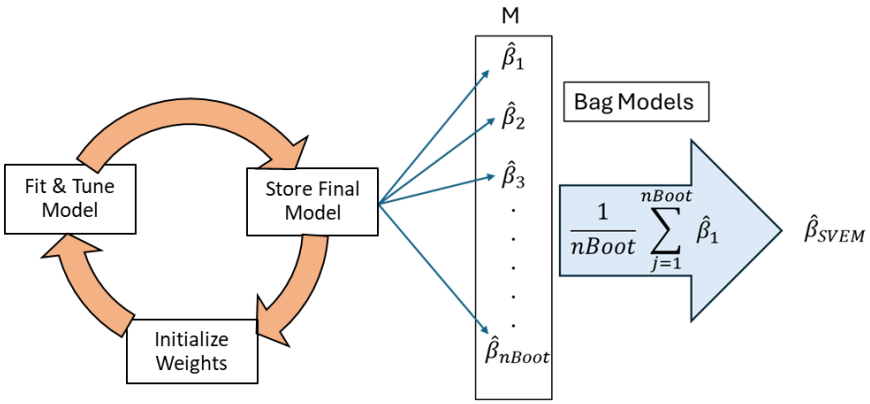

Algorithm 1: SVEM

Result: $\hat{\beta}_{SVEM}$

For *i*=1: *nBoot* **do**

Generate $\overline{w}_T, \overline{w}_V$

Fit model $f(X, \overline{w}_T|Y) = \hat{\hat{f}}(.)$

Calculate $SSE^V(\beta) = \underset{\beta}{argmin} \sum_i w_{V,i} \left(y_i - \hat{f}(X,\beta)\right)^2$;

Select $\hat{\beta} = \underset{\beta}{argmin}[SSE^V(\beta)]$;

$M_i \leftarrow \hat{\beta}$;

End

Bag(M) $\rightarrow \hat{\beta}_{SVEM}$

Figure 5-2: SVEM Workflow (Lemkus et al. 2021)

As part of the SVEM framework, three distinct Multiple Linear Regression (MLR) modeling techniques: Forward Selection (SVEM-FS), Adaptive Least Absolute Shrinkage and Selection Operator (SVEM-AL), and Elastic Net regularization (SVEM-EN) and a Neural Network technique (SVEM-NN) were implemented. Each of the SVEM-MLR methods offers a unique mechanism for variable selection and model regularization while the SVEM-NN approach provides advantages in complex non-linear problems. SVEM-FS sequentially introduces predictors based on statistical significance, while SVEM-AL modifies the standard LASSO by assigning adaptive weights to penalize regression coefficients, improving variable selection consistency. SVEM-EN combines the penalties of LASSO and Ridge regression, offering advantages in handling multicollinearity among predictors. SVEM-NN on the other hand, as inspired by the structure and function of the human brain, consists of interconnected nodes (neurons) that processes input data through weighted connections to produce predictions. Figure 5-3 depicts the typical architecture of the NN model as integrated in the SVEM approach. It is important to note that only 3 hidden nodes were used and was decided upon to reduce computational demands and mitigate the potential for overfitting. The theoretical foundations and computational procedures for each MLR and Neural network method are extensively documented in (James et al. 2013; Shanmuganathan, 2016). For all three MLR techniques, a Full Quadratic Model (FQM) structure was adopted. This model form incorporates the linear (main) effects of the predictor variables, all possible two-way interaction terms, as well as the quadratic (squared) terms of each continuous variable predictor, thereby enabling the exploration of potential non-linear relationships and synergistic effects among input variables. A simplified version of this model with only two experimental factors is shown in Equation 5-2.

$$\boldsymbol{Y = \beta_0 + \beta_1 X_1 + \beta_2 X_2 + \beta_{11} {X_1}^2 + \beta_{22} {X_2}^2 + \beta_{12} X_1 X_2}$$

Equation 5-2

Where:

Y = Response Variable

$X_1 \; and \; X_2$ = Experimental factors

β = Model Coefficients

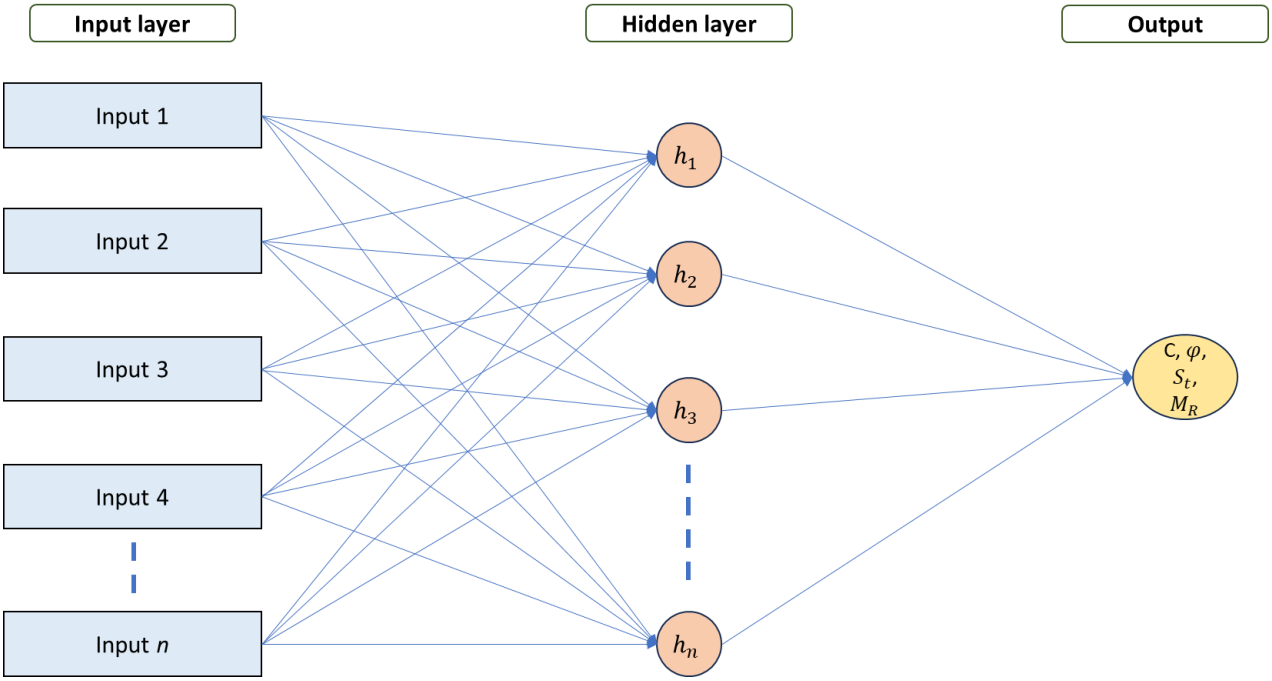

Figure 5-3: Neural Network Architecture

5.2.1.2 Support Vector Regression

Support Vector Regression (SVR), a variant within the broader Support Vector Machine (SVM) framework, also referred to as the Separating Hyperplane method, is a supervised learning technique used for both classification and regression tasks. As introduced by Vapnik et al. (1996), SVR aims to identify a hyperplane in an n-dimensional feature space that best approximates the target function. This is achieved by maximizing the margin around the hyperplane, thereby enhancing the model's ability to generalize and distinguish between varying patterns in the data. SVM is founded on the principle of structural risk minimization (SRM), which seeks to minimize an upper bound on the expected generalization error. This contrasts with empirical risk minimization (ERM), which focuses solely on reducing the training error. The SRM approach enables SVM to achieve better generalization performance, making it more robust to overfitting and improving its ability to perform well on unseen data. (Nazemi & Heidaripanah, 2016). SVM utilizes mapping techniques to transform the original input space into a higher-dimensional feature space, where a linear separating hyperplane can be more effectively identified. Once mapped, SVM determines the optimal decision boundary by maximizing the margin between class boundaries in the transformed space. In SVR, different types of kernel functions can be used to capture complex relationships between input variables and the target variable. These include.

- Linear Kernel: Suitable for linearly separable data
- Radial Basis Function Kernel: Captures non-linear relationships using a Gaussian kernel.
- Polynomial Kernel: Models complex relationships by considering polynomial transformations of the input features.
- Sigmoid: Resembles neural network activation functions and is useful for certain data distributions.

Given a training dataset comprising *n* independent variables x_i and corresponding dependent responses y_i, SVR seeks to determine the optimal hyperplane that best approximates the underlying functional relationship through the formulation and solution of a convex quadratic programming problem (Equation 5-3 and Equation 5-4).

$$\frac{1}{2}\boldsymbol{w}^T\boldsymbol{w} - \boldsymbol{C}\left[\boldsymbol{v\varepsilon} + \frac{1}{\boldsymbol{n}}\sum_{\boldsymbol{i=1}}^{\boldsymbol{n}}(\boldsymbol{\xi_i} + \boldsymbol{\xi_i^*})\right]$$

Equation 5-3

$$\begin{cases} (\boldsymbol{w}^T\emptyset(\boldsymbol{x_i}) + \boldsymbol{b_i}) - \boldsymbol{y_i} \leq \boldsymbol{\varepsilon} + \boldsymbol{\xi_i^*} \\ \boldsymbol{y_i} - ((\boldsymbol{w}^T\emptyset(\boldsymbol{x_i}) + \boldsymbol{b_i}) - \boldsymbol{y_i} \leq \boldsymbol{\varepsilon} + \boldsymbol{\xi_i} \end{cases}$$

Equation 5-4

The selection of an appropriate kernel function in SVR is based on the nature of the dataset, ensuring the best possible fit to the underlying patterns in the data. An extensive detailed description of SVR can be found in (James et al. 2013). In this study, the radial basis function is employed for model development.

5.2.2 Model Development approach

Model development for all ML approaches involved randomly splitting the data into a training and testing set where 85% of the data was employed to develop the model and the remaining 15% of the data were set aside as a true validation set, blind from the model training processes, for the final evaluation. Within the operational framework of the SVEM approach for all training datasets of the multiple linear regression and neural network models, model development involved multiple training iterations to account for variations and enhance robustness. Each model was run for a different number of iterations (50, 100, 150, 200, 250, 300, 400, and 500, 1000), and the final SVEM model was constructed by averaging the predictions obtained from number of iterations that yielded optimum results. As for the SVR approach, *k*-fold cross-validation was implemented within the training dataset to validate the model results. In k-fold cross validation, the dataset is divided into *k* equally sized folds; the model is trained *k* times, each time using a different fold as the validation set and the remaining *k*-1 fold for training. This process ensures that every data point is used for both training and validation, thereby reducing the risk of overfitting and yielding a more stable estimate of model performance. In this study, a 5-fold cross-validation procedure (*k* = 5) was employed.

5.2.3 Model Assessment

The efficiency of all trained models as well as their performance on the test set are evaluated using correlation of determination (R^2), root average square error (RASE) and the mean absolute error (MAE) metrics as shown in Equation 5-5 to Equation 5-7, respectively. R^2 reflects the relationship between the measured and predicted values, with values closer to 1 indicating higher fit. RASE on the other hand gauges the gap between model predictions and actual measurements, with smaller values indicating closer agreement while MAE measures the average of the absolute differences between predicted and actual values, with lower values preferred, giving a clear sense of overall model accuracy.

$$\boldsymbol{R^2 = 1 - \frac{\sum_{i=1}^{n}(M_i - \widehat{P_i})^2}{\sum_{i=1}^{n}(M_i - \overline{M})^2}}$$

Equation 5-5

$$\boldsymbol{RASE = \sqrt{\frac{\sum_{i=1}^{n}(M_i - \widehat{P_i})^2}{n}}}$$

Equation 5-6

$$\boldsymbol{MAE = \frac{1}{n}\sum_{i=1}^{n}|M_i - \widehat{P_i}|}$$

Equation 5-7

Where.
M_i= measured output
$\widehat{P_i}$ = predicted output
$\overline{M}$ = average of measured outputs
n = number of samples

5.3 Tensile Strength Prediction model

Figure 5-4 depicts the model performance in terms of predictive accuracy for all ML models developed for estimating the tensile strength property. The SVR model demonstrated superior accuracy, achieving the highest R^2 of 0.97 in the training set and 0.96 in the test set, coupled with the lowest RASE and MAE values, indicating strong predictive capability and excellent generalization. In comparison, the SVEM-MLR models exhibited moderate training R^2 values ranging from 0.65 to 0.67, and slightly higher test R^2 values between 0.80 and 0.84. On the other hand, the SVEM-NN model yielded a relatively high training R^2 of 0.90 and a slightly lower test R^2 of 0.84, reflecting acceptable generalization with a minor reduction in performance on unseen data. Overall, the SVR consistently outperformed the ensemble models in both accuracy and error reduction, reinforcing its robustness for predicting the tensile strength and is selected as the most reliable model in this context. Figure 5-5 further depicts the SVR model goodness-of-fit plot facilitating visual assessment of prediction accuracy. The diagonal line represents line of

equality (y = x). The visual clustering of data points along the diagonal line shows high consistency between actual and predicted values, supporting its overall excellent predictability.

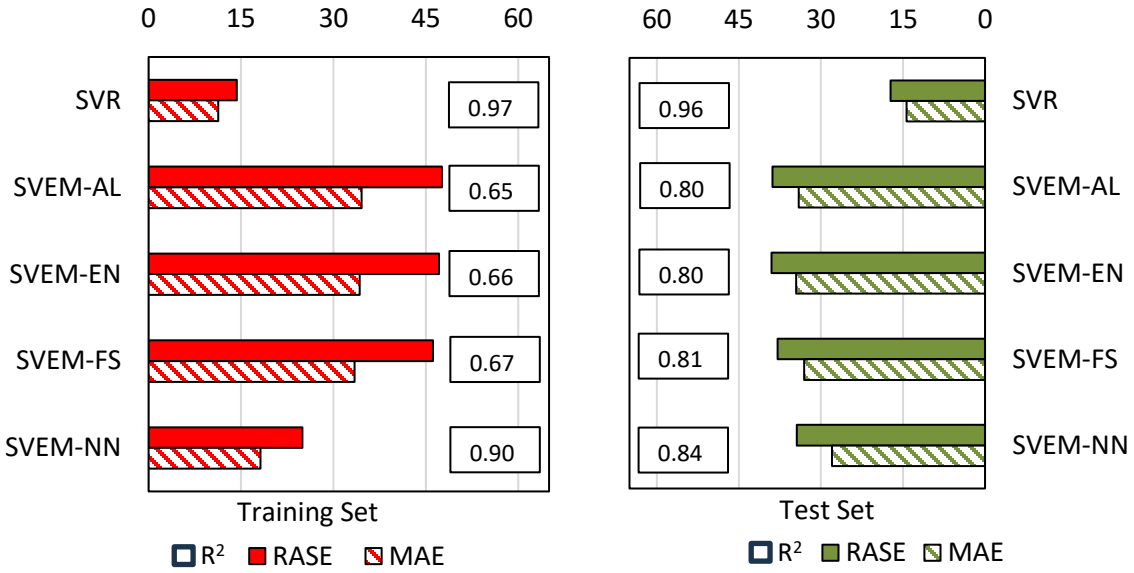

Figure 5-4: Model performance metrics for Tensile Strength

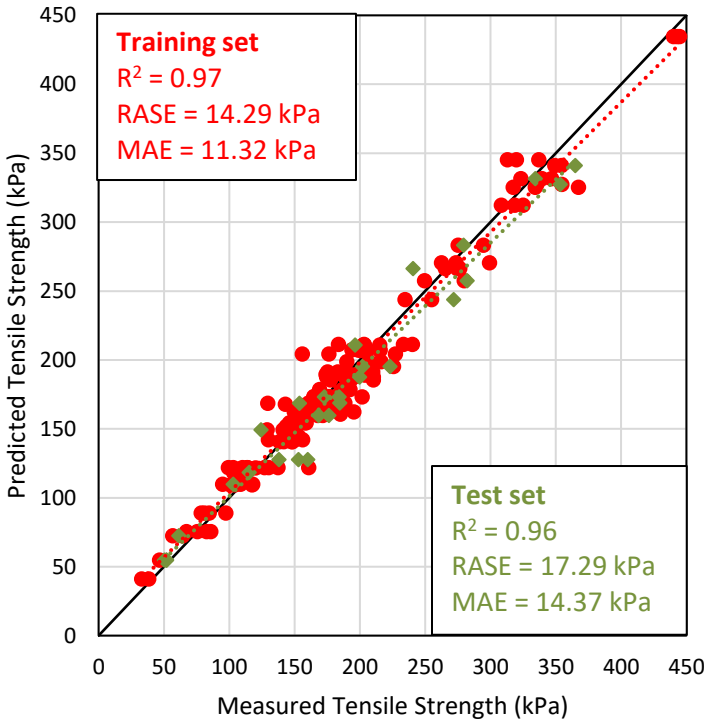

Figure 5-5: SVR Goodness of fit analysis plot for Tensile Strength

The independent variable importance analysis, provided in Figure 5-6, provides insight into the factors that most significantly influence the tensile strength of CR mixtures based on the SVR model. The percentage retained on the 19 mm sieve stands out as the dominant variable, accounting for 24% of the model's predictive power. This highlights the critical role of coarse RAP content in the mixture. Density follows as the second important factor at 16%, emphasizing the importance of proper compaction and material packing in achieving higher tensile strength. In contrast, stabilizer amount and the percentage passing the 4.75 mm sieve contribute minimally (3% each), indicating a relatively low sensitivity of tensile strength to finer material content and additive dosage. Chemical additive presence had the least impact at just 2%, suggesting that while chemical additives may offer supplementary benefits, they are not primary strength drivers in this context. These results point to the importance of optimizing gradation characteristics and compaction in mixture density to achieve desired properties.

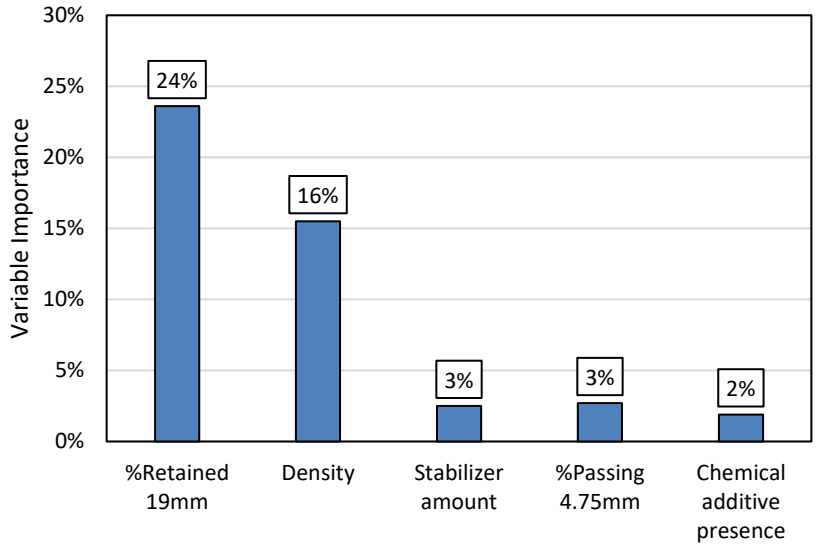

Figure 5-6: Tensile Strength model variable importance analysis

5.4 Resilient Modulus Prediction model

The performance evaluation of the predictive models for estimating the resilient modulus of the CR mixtures, as shown in Figure 5-7, reveals notable differences in their predictive capabilities. On the training set, the SVR and SVEM-NN models exhibit higher moderate R^2 (0.65 and 0.64, respectively), with lower error metrics compared to other SVEM-MLR models. On the test set, SVR maintained better generalization performance (R^2 = 0.42; RASE = 66.11; MAE = 54.76) compared to the SVEM models, suggesting its strength and ability to learn complex patterns. Though the model performance for all models were moderate as analyzed in this context, SVR is selected as the most practicable model for predicting the resilient modulus of the CR mixtures. Figure 5-8 further depicts the SVR model goodness-of-fit plot for the resilient modulus of the CR mixtures. The diagonal line represents the line of equality (y = x), facilitating visual assessment of prediction accuracy. The goodness-of-fit plot shows a reasonable alignment of predicted and measured values, with most data points clustering around the equality line. Despite some scattering, especially in the training set, the SVR model captured the key trends in the data more effectively than all other approaches tested.

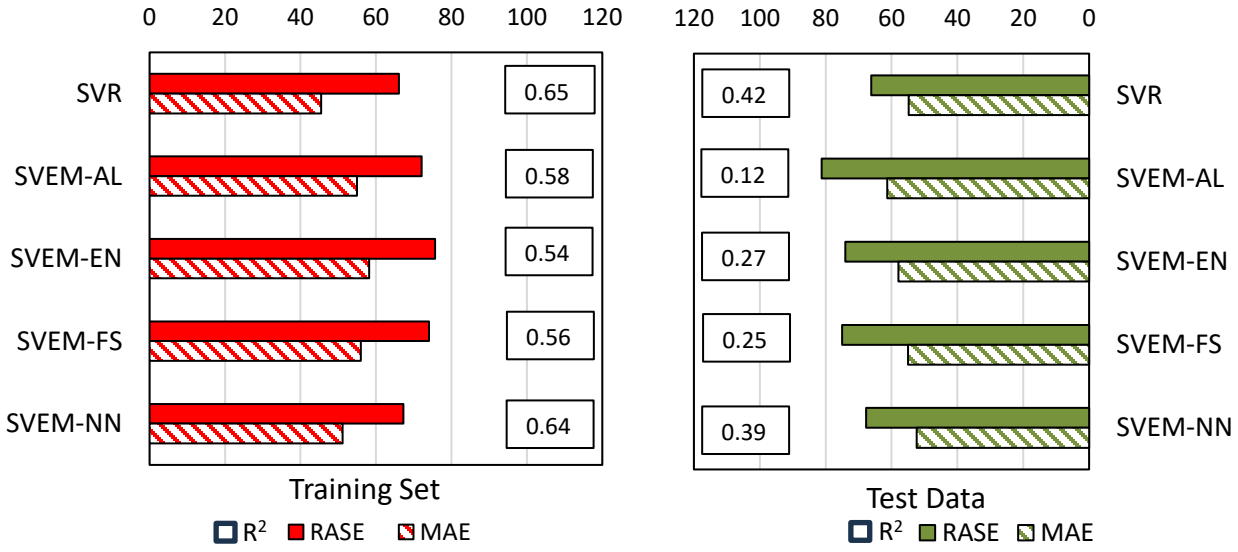

Figure 5-7: Model performance metrics for Resilient Modulus

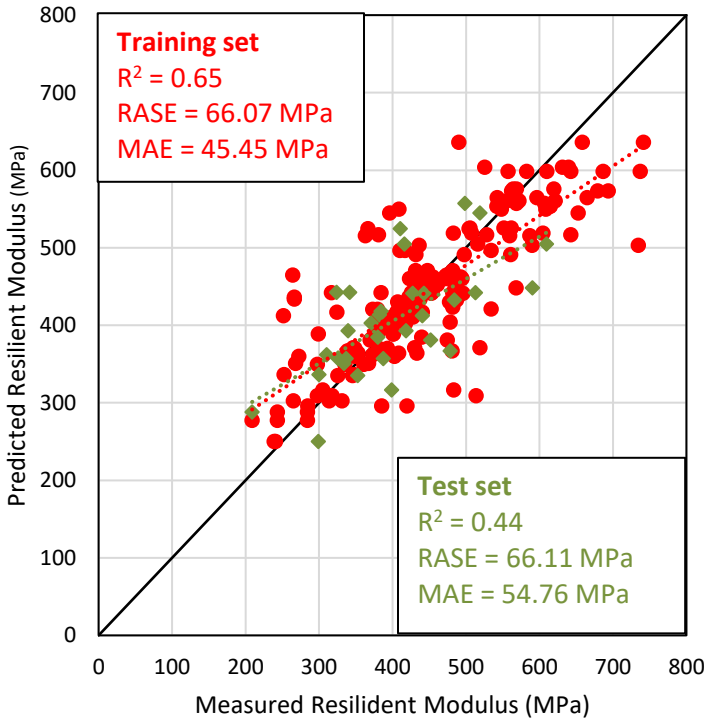

Figure 5-8: Goodness of fit analysis plot for Resilient Modulus

The independent variable importance plot, as provided in Figure 5-9, identifies the most influential factors affecting the resilient modulus of CR mixtures. Temperature appears as the most dominant variable, contributing 19% to the model, indicating that temperature significantly impact modulus outcomes. Density followed with a 14% contribution, reinforcing the role of compaction and material structure in improving load-bearing capacity. The presence of chemical additives also showed a

noticeable influence though at 6%. In contrast, stabilizer amount, fine content (% passing 4.75 mm), and coarse content (% retained on 19-mm) had relatively minor impacts, with contributions ranging from 2% to 4%. These results are consistent with findings from Chapter 4 of this study on the influencing factors affecting the resilient modulus.

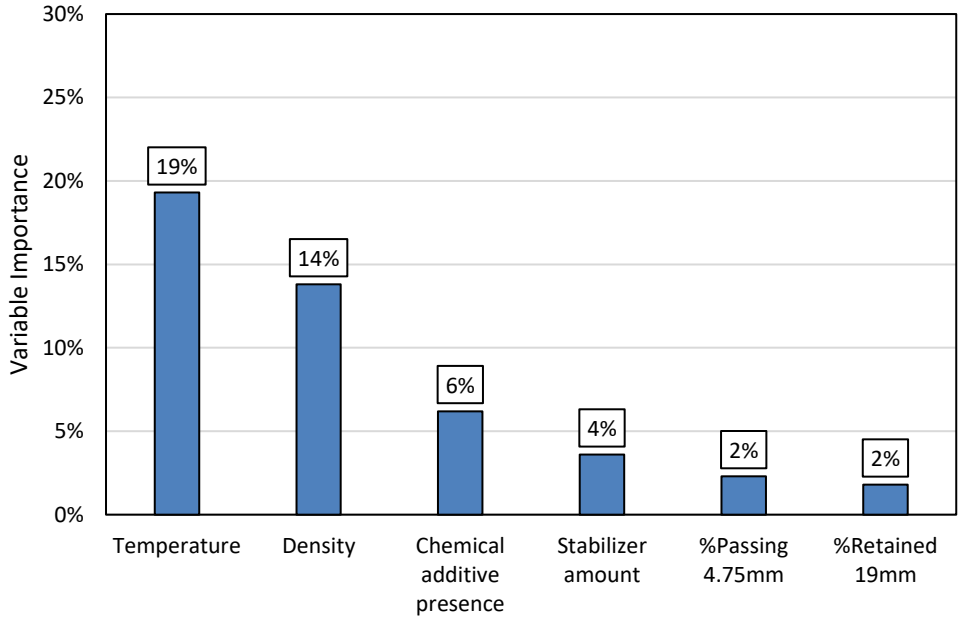

Figure 5-9 : Resilient Modulus model variable importance analysis

To further translate the laboratory-determined resilient modulus to field conditions, the field backcalculated stiffness measurements obtained from the Falling Weight Deflectometer (FWD) tests conducted in Chapter 4 of this study were utilized. Since the FWD tests were performed during the fall and summer seasons, closely aligning with the laboratory testing temperatures, a simple regression model incorporating temperature and the laboratory-estimated resilient modulus as input variables was developed to estimate the field resilient modulus. Where temperature deviations were present in the backcalculated FWD stiffness values, corrections were applied to align them precisely with the designated seasonal temperatures outlined in Chapter 4 of this study—specifically, 10°C for fall and 30°C for summer. These temperature adjustments were performed using Equation 5-8 and Equation 5-9.

$$\boldsymbol{T_{bells3} = 0.95 + 0.892 * T_{surface} + (\log_{10}\left(\frac{H_{ac}}{3}\right) - 1.25) * (-0.448 * T_{surface} + 0.621 * T_{prev.day} + 1.83 * \sin(hr_{18} - 15.5)) + 0.042 * T_{surface} * \sin(hr_{18} - 13.5)}$$

Equation 5-8

$$\boldsymbol{ATAF = 10^{slope(T_r - T_m)}}$$

Equation 5-9

Where.

$T_{surface}$= pavement surface temperature (°C)

$T_{prev.day}$ = average air temperature the day before testing (°C)
$\sin(hr_{18} - 15.5)$ = 18-hr sine function, 15.5 variation.
$\sin(hr_{18} - 13.5)$ = 18-hr sine function, 13.5 variation.
slope = Log (Mr) = intercept + slope T (-0.021 used in this report following LTPP recommendations);
T_r = reference temperature, °C;
T_m = measured temperature, °C

It is important to note that the simple regression model was developed using data from only seven field sections, as only these sections had its lab-compacted materials tested under the controlled temperature conditions during the resilient modulus testing. Equation 5-10 and Equation 5-11 outlines the regression equation (R^2 of 0.64) to estimate the field stiffness from the laboratory measurements based on SI and US metric units, respectively.

$$\boldsymbol{Field\ stiffness\ estimate\ (MPa) = 4581.19 - (87.83 * Temperature) - (3.27 * Lab\ measured\ resilient\ modulus) + 0.23 * ((Lab\ measured\ resilient\ modulus - 420.49) * (Temperature - 20))}$$

Equation 5-10 in °C, [RASE = 620]

$$\boldsymbol{Field\ stiffness\ estimate\ (ksi) = 890.913 - (7.077 * Temperature) - (3.27 * Lab\ measured\ resilient\ modulus) + 0.13 * ((Lab\ measured\ resilient\ modulus - 60.987) * (Temperature - 68))}$$

Equation 5-11 in °F, [RASE = 89.95]

5.5 Shear Parameter Prediction model

5.5.1 Cohesion

The comparative analysis of the models for predicting cohesion (Figure 5-10) demonstrates varied predictive performances across training and test datasets. On the training set, SVR achieved the highest R^2 (0.92) and the lowest RASE (22.35) and MAE (14.45), indicating excellent model fitting and minimal error. SVEM-NN also performed strongly with an R^2 of 0.86 and relatively low errors (RASE = 29.18; MAE = 20.93), while the other ensemble models (SVEM-AL, SVEM-EN, SVEM-FS) showed lower R^2 values (0.53–0.60) and notably higher errors. On the test set, SVR, SVEM-AL, and SVEM-EN achieved similar R^2 values (0.65–0.66) with comparable RASE (42.03–42.63) and MAE (34.11–37.96), suggesting stable generalization performance among these three models. Overall, SVR displayed the best balance of high training accuracy and solid generalization, offering more consistent performance across datasets. Figure 5-11 presents the goodness-of-fit plot of the SVR model for cohesion, demonstrating a strong alignment between the predicted and measured values, as evidenced by the majority of data points clustering closely along the equality line. Despite minor scatter, the SVR model demonstrates a robust capacity to capture the underlying relationships within the dataset.

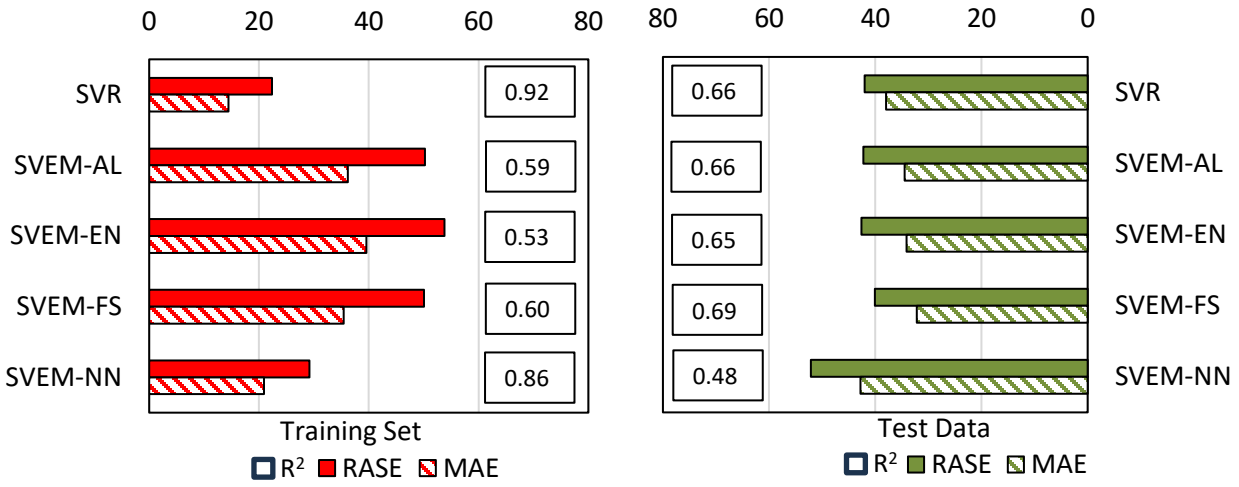

Figure 5-10: Model performance metrics for Cohesion

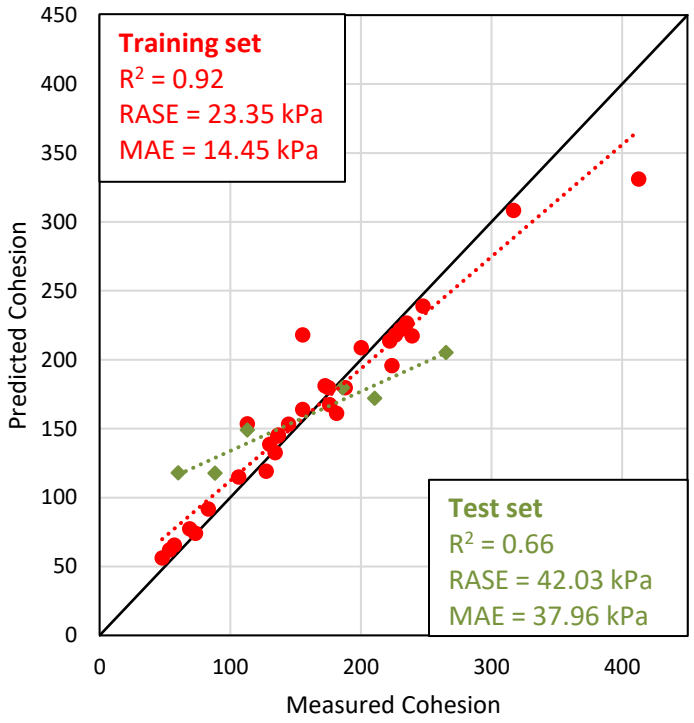

Figure 5-11: Goodness of fit analysis plot for Cohesion

The independent variable importance plot, as shown in Figure 5-12, identifies the percentage retained on the 19mm sieve as the most dominant variable, contributing 24% to the model. This result emphasizes the critical role of coarse fraction content in governing mixture cohesion as these provide a structural skeleton that enhances interlocking. This observation aligns with established findings in cold mix and granular material behavior, where coarse fraction plays a fundamental role in the mechanical performance of the mixture (Pi et al. 2019). The second most influential parameter is the mixture density (4%), which reflects the degree of compaction and packing. Higher density typically implies

reduced void content, leading to stronger interparticle bonding and improved cohesion (Casillas, 2020). Other variables, including stabilizer amount, fine particle content, and chemical additive presence, show minimal impact, each contributing 2% or less, indicating limited influence on overall cohesion. Although these additives can enhance mechanical properties under certain conditions, their lower contribution here suggests that their effects may be secondary or context-dependent within the range of conditions studied.

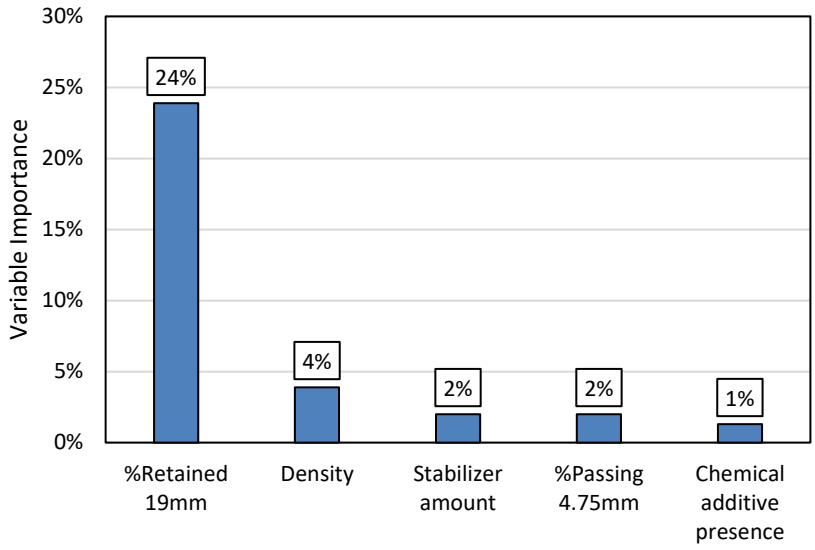

Figure 5-12: Mixture Cohesion model variable importance analysis

5.5.2 Frictional Angle

The performance evaluation of the models for predicting the friction angle of the CR mixtures as shown in Figure 5-13 reveals patterns across training and test sets. On the training set, SVEM-NN achieved the highest R^2 (0.90) and the lowest error metrics (RASE = 2.46; MAE = 1.91), indicating excellent fitting accuracy, followed closely by SVR (R^2 = 0.78; RASE = 3.54; MAE = 2.00). In contrast, the SVEM MLR models (SVEM-AL, SVEM-EN, and SVEM-FS) exhibited substantially lower R^2 values (0.09–0.13) and higher error metrics, suggesting limited learning capacity during training. On the test set, SVR maintained the best predictive performance with an R^2 of 0.53, RASE of 4.81, and MAE of 3.77, showing better generalization capability. SVEM-NN followed with a moderate R^2 of 0.29 and reasonable error levels (RASE = 5.96; MAE = 5.26), though performance declined compared to training. The SVEM-MLR models again showed weak predictive power on the test set, consistent with their poor training results. Overall, SVR demonstrated the most balanced and robust performance across datasets, making it the most reliable model for predicting frictional angle under the evaluated conditions. Figure 5-14 depicts the SVR model goodness-of-fit plot and corresponding model assessment metrics for frictional angle of the CR mixtures. The results show that most predicted points align well with the equality line, though some scattering is visible especially in the test data, the SVR model still effectively captured the key relationships.

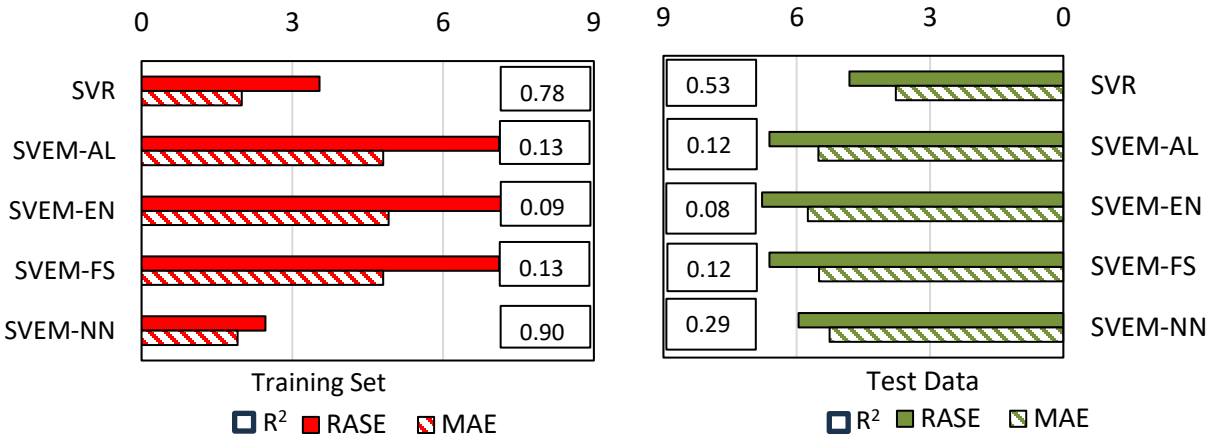

Figure 5-13: Model performance metrics for Frictional angle

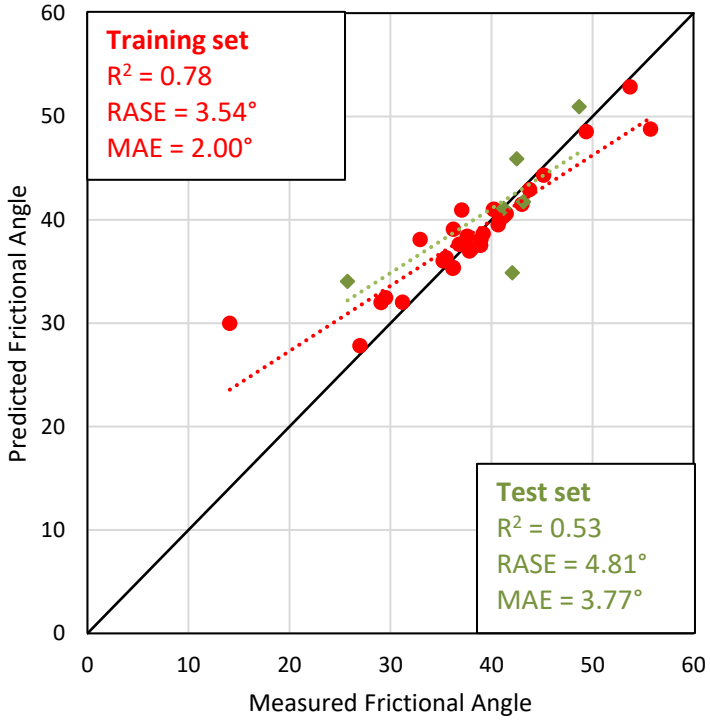

Figure 5-14: Goodness of fit analysis plot for Frictional Angle

The independent variable importance plot, as provided in Figure 5-15, identifies that the stabilizer amount is the most critical factor governing the frictional angle of the CR-EE mixtures, contributing 20% to the model. This highlights the key role of stabilizers in improving interparticle bonding and enhancing shear resistance (Jiang, 2013). Chemical additive presence follows with 10%, indicating its noticeable effect on improving internal friction properties. This influence highlights the critical role that chemical modification plays in altering particle surface properties and enhancing inter-particle bonding, which directly affects the internal friction characteristics (Du, 2015). Density accounts for 8%, reflecting its impact on aggregate packing and contact surface area as denser mixtures generally imply fewer voids

and better mechanical interaction between particles, leading to enhanced shear resistance (Lin et al. 2017). Meanwhile, coarse and fine gradation parameters (% retained 19 mm and % passing 4.75 mm) contribute only minor effects at 4% and 2%, respectively. While gradation parameters are fundamental in determining the structure and load distribution within the mixture, their limited contribution in this context suggests that the influence of finer and coarser aggregate fractions on friction angle may be more indirect or dependent on interaction effects with the stabilizer and chemical modifiers or otherwise captured within the mixture density.

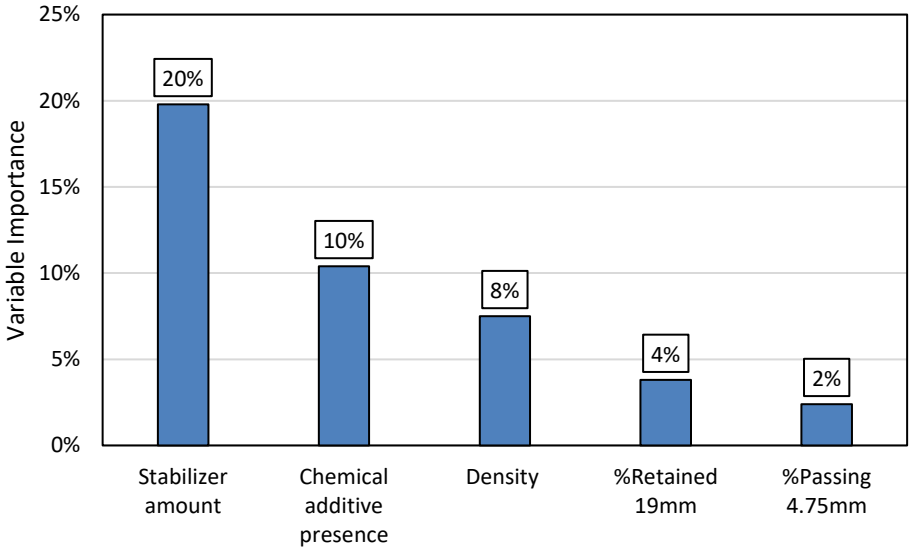

Figure 5-15: Frictional Angle model variable importance analysis

5.6 Implementation Steps

A predictive tool has been developed in the form of a Microsoft excel spreadsheet to support this chapter (Appendix E). This MS Excel-based workbook provides predictive capabilities for estimating the tensile strength, shear parameters (Cohesion and Frictional angle) and resilient modulus of the CR materials. These properties can be utilized in common mix design evaluation and/or performance modelling efforts within mechanistic-empirical analysis of CR pavement structures. The input variables required to estimate tensile strength and shear parameters include the engineered emulsion content, presence of chemical additive, compacted density, and gradation characteristics (percentage retained on the 3/4 in. [19-mm] sieve and percentage passing the No 4. [4.75-mm] sieve). For resilient modulus estimation, temperature is required in addition to the variables used for tensile strength and shear parameters. Mix design data is generally sufficient to estimate these material properties.

The general structure and content of the Excel-based predictive workbook consist of an introductory information tab that outlines the required types and sources of input data, followed by three dedicated tabs containing the prediction models for each material property. The workbook is developed as a macro-enabled Excel file; therefore, users must enable macros to access its full functionality. To maintain the reliability of the predictions, the tool includes built-in data validation features that restrict input values to the ranges used during model development. This is intended to prevent extrapolation

beyond the validated input domain, which is not recommended by the researchers. Additional recommendations are provided following property predictions to support informed engineering decisions and ensure the effective application of the estimated properties.

5.7 Summary of Prediction Model Development

This study task utilized a dataset generated as part of Chapter 4 of this study, consisting of different CIR and SFDR materials to develop material property prediction models. The goal of the prediction model is to estimate the material properties necessary for performance modelling efforts within mechanistic-empirical analysis of CR pavement structures. Several statistical analyses were conducted to process and refine the dataset to ensure accurate delivery of predictive models. The factors incorporated include stabilizer (engineered emulsion) amount, presence of chemical additive, compacted density, gradation characteristics, and temperature, and are all selected based on their routine availability in cold recycling mix design and construction practices. An advanced ML approach called Self-Validating Ensemble Model (SVEM), which integrates principles of bootstrapping and ensemble modeling, and the Support Vector Regression (SVR) technique were employed for model developments. Following model development for each approach, the best model was identified through model performance evaluations (R^2, RASE, MAE) and the final disposition for implementation was provided as a Microsoft excel-based tool for the grand purpose of estimating/predicting the material properties.

Chapter 6: Performance Function Development

This chapter provides details of the CR layer rutting performance function development, facilitating the efficient design of CR pavements. Information regarding the methodology employed to calibrate the rutting performance function as well as the results of the calibration, sensitivity analysis, and design recommendations for the performance function utilization are presented.

6.1 Methodology for Performance Function Development

Building upon the development framework of the Stellenbosch performance function (Equation 2-10) and incorporating key input parameters conceptually indicative of the rutting behavior of such materials within pavement structures, the rutting performance function proposed in this study is formulated as presented in Equation 6-1

$$\boldsymbol{log\ N_R = k_1 + k_2(DevSR) + k_3(\varepsilon_{v\ (CR\ layer)}) + k_4(Density)}$$

Equation 6-1

In which,
N_R = Number of allowable load repetition until rutting failure,
$DevSR$ = deviator stress ratio (Equation 2-9),
ε_v = Vertical Strain on top of the CR layer, derived from LEA,
$Density$ = density of the CR layer, pcf
k_1, k_2, k_3, k_4 = model constants

The number of allowable load repetitions, $log\ N_R$, is considered the outcome of the transfer function, indicating the total amount of allowable load repetitions until failure based on an 18kips ESAL load. This is defined at 0.5 inches [12.5mm], with the assumption that all the rutting in the CR pavement comes from the CR layer. The deviator stress ratio, represented by DevSR, describes the rate of permanent deformation/rutting in the CR layer. As shown in Equation 6-1, this ratio is dependent on factors including the layer stiffness, pavement structure, cohesion, frictional angle as well as the load applied to the pavement. As with any typical rutting performance function, the vertical strain at the top of the CR layer is considered another important variable to describe the deformation of the material within the pavement structure. Density, represented by the compacted density of the material, is considered to describe the density of the CR material/layer in sustaining multiple load repetitions.

The framework for the performance function development is shown in Figure 6-1. Subsequent sub-sections provide detailed information and the data acquisition approach for each input parameter for the calibration process. It is important to note that all calibrations are performed using U.S. customary units.

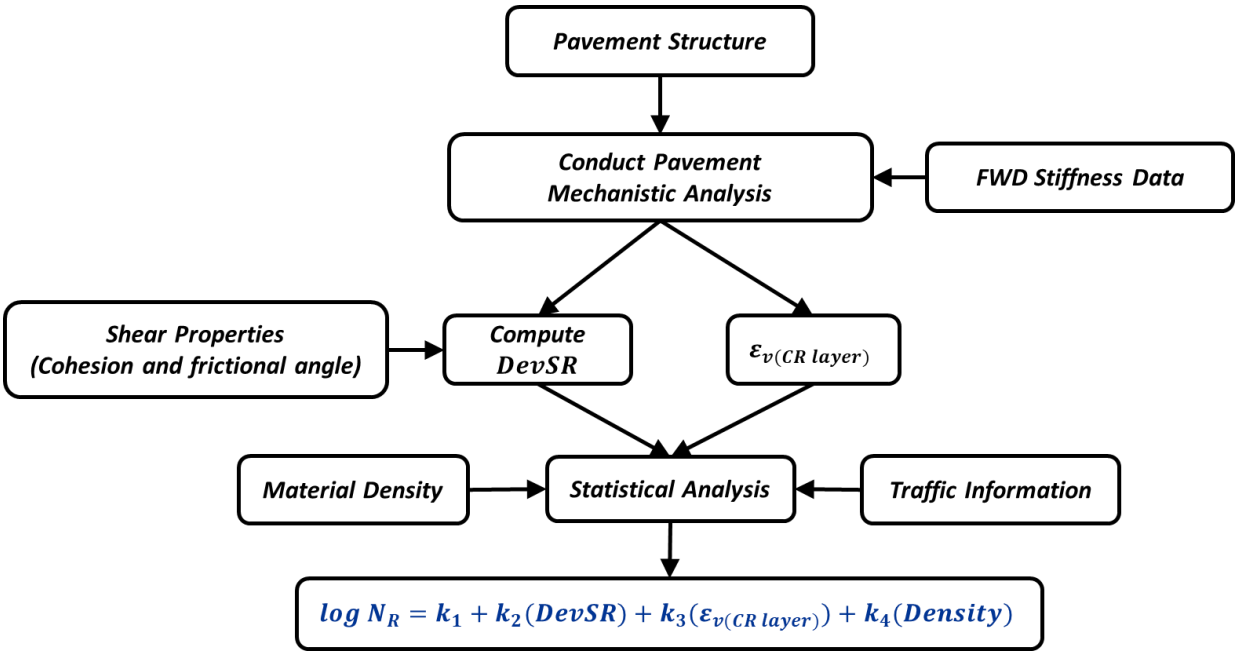

Figure 6-1: Calibration Framework

6.1.1 Data Acquisition

6.1.1.1 Field Projects

Projects outlined in Chapter three along with four select field sections at the MnROAD research facility (Test section 2202, 2203, 2206, and 2207) formed the database for calibration. Only field project CSAH 8 (Table 3-1) was not included due to data unavailability. Since these field sections, as of the time of this report, only have service life of less than 3 years accompanied by limited traffic, the 20-year design ESAL traffic, as indicated in Table 3-1 is considered in this analysis as the number of load repetitions to 0.5 inches (12.5 mm) rutting failure (Huang, 1994) and based on the assumption that the majority, if not all, of the rutting occurs within the CR layer. This assumption is considered reasonable given that the rehabilitated field sections were primarily intended to address functional surface distresses rather than deep-seated structural deficiencies. In cases where traffic data was not readily available, the Minnesota Traffic Mapping Application was used to obtain the class of the roadway, estimate traffic growth rate from two or three successive years of Average Daily Traffic (ADT) and Average Daily Truck Traffic (ADTT) values, which were then used to calculate the 20-year design ESALs.

6.1.1.2 Falling Weight Deflectometer (FWD) Stiffness data

FWD backcalculated stiffness data collected during Chapter 3 of this study, along with FWD data from the MnROAD sections as available to the researchers, were used for the calibration process. Since the FWD tests were conducted across different climatic periods for all field projects, temperature sensitive backcalculated stiffness measurements were corrected to the average +1 standard deviation all-year round CR layer temperature for the calibration process. This was determined to be around 25°C for all field sections which matches the shear parameter lab characterization temperature. The effective temperatures of the HMA and CR temperature sensitive layers were first calculated using the BELLS3

temperature model, as described in Equation 5-8, followed by stiffness adjustment to the 25°C reference temperature using the asphalt temperature adjustment factor (ATAF) proposed by Lukanen et al. (2000), as depicted in Equation 5-9.

6.1.1.3 Laboratory Mixture Attributes [Shear Properties (Cohesion and Frictional Angle) and Density]

Extensive laboratory testing conducted as part of Chapter 4 generated data used to calibrate the rutting performance function. For field sections where laboratory characterization of shear parameters was not possible, the material property prediction tool developed in Chapter 5 was employed to estimate these parameters. The input data required for the prediction tool was obtained from mix design documentation, quality control (QC) records, and construction reports, as available to the research team for these specific field sections.

6.1.1.4 Pavement Structural (Mechanistic) Analysis

Structural analysis is a critical component in calibrating any performance function, as it provides the mechanistic foundation within the Mechanistic-Empirical design framework. In this study, key pavement responses which serve as the mechanistic inputs to the proposed performance function, namely, vertical strain in the CR layer and the stress characteristics used to define the DevSR parameter, were obtained through pavement structural mechanistic modeling. The pavement structure of each field section, as shown in Table 1, was modeled using the MnLAYER Layered Elastic Program, incorporating back-calculated stiffness data (NB: other available Layered Elastic Analysis tool, e.g. WinJULEA, WESLEA may be used for this purpose). Stress characteristics in both the major and minor principal stress were calculated at the top of the CR layer, which were determined as the peak stress characteristics within the layer. While compressive minor principal stresses are typically expected, the LEA model may, in some cases, predict tensile stresses within the CR layer, which would yield no shear resistance. To address this, the minor principal stress is set to zero and the major principal stress is adjusted under the condition that the deviator stress remains constant (Theyse et al. 1996). A graphical representation of this conversion is provided in Figure 6-2. A total 42 critical responses were obtained from the different temperature corrected FWD stiffness data across all field sections.

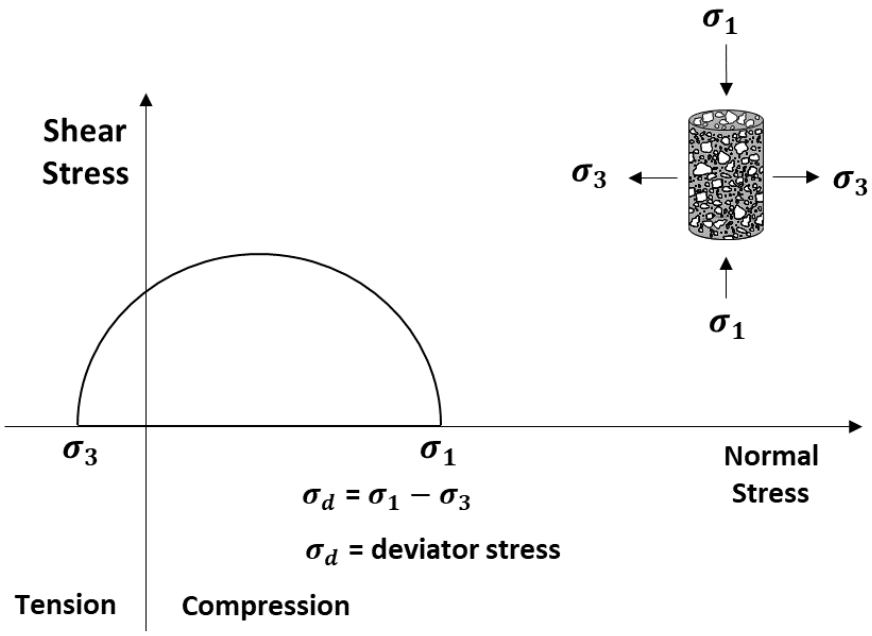

(a)

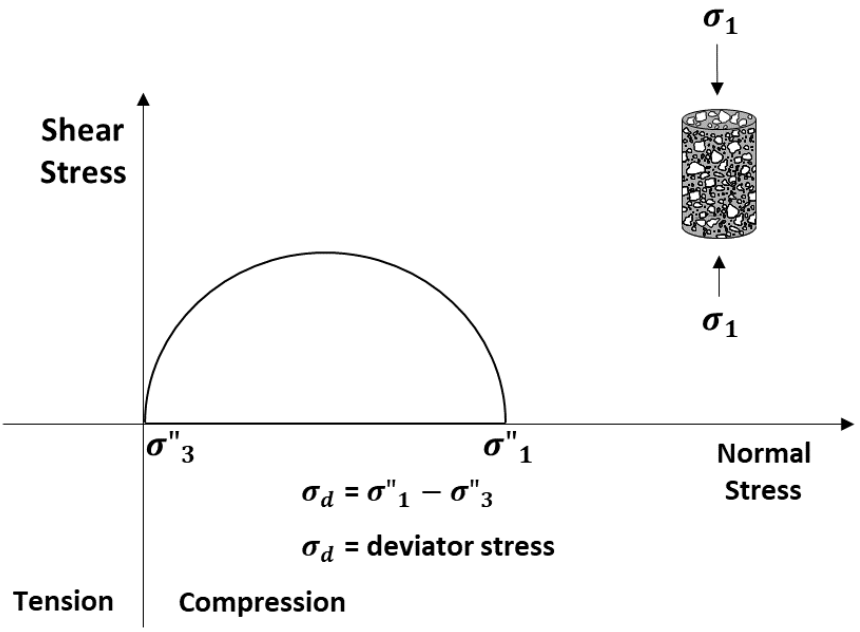

(b)

Figure 6-2: Mohr circle representation (a) minor principal tensile stress (b) adjusted minor principal stress

6.2 Calibrated Performance function

By utilizing the Microsoft Excel solver, model coefficients k_1, k_2, k_3 and k_4 in Equation 4 were derived by minimizing the sum of square error (Equation 6-2) between the measured and predicted Log Nr values. Other model evaluation metrics in R^2, RASE and MAE (Equation 5-5 through Equation 5-7) were used to further evaluate the performance of the calibrated performance function. Equation 6-3 shows the final form of the calibrated performance function (in US customary units) together with the error metrics provided in Table 6-1.

$$SSE = \sum_{i=1}^{n} (M_i - \widehat{P_i})^2$$

Equation 6-2

$$log\ N_R = -8.798 - 1.530(DevSR) - 2.318 \times 10^{-4}(\varepsilon_{v\ (CR\ layer)}) + 0.119(Density)$$

Equation 6-3

Table 6-1: Performance function model statistics

Parameter	Estimate	Standard Error	t-value	Pr (>|t|)
k1	-8.7984	2.5383	-3.466	0.001
k2	-1.5303	0.7113	-2.151	0.038
k3	-2.318E-04	0.0005	-0.445	0.659
k4	0.1192	0.0192	6.224	<.0000
SSE: 11.208 **R^2**: 0.67 **RASE:** 0.516 **MAE:** 0.448				

The model performance metrics as shown in Table 6-1 indicate a reasonably good fit for the rutting performance function, reflecting acceptable prediction accuracy. Among the variables, DevSR emerges as a statistically significant and practically meaningful factor, with a large negative coefficient of -1.530. This indicates that as DevSR increases, rutting life in terms of the allowable number of load repetitions decreases significantly. Similarly, vertical compressive strain in the CR layer also negatively affects rutting performance as indicated by its coefficient of -2.318×10^{-4}. In contrast, the positive coefficient for density (0.119) indicates that increased density improves rutting resistance. Collectively, these statistics validate the reasonableness of the performance function while emphasizing the dominant role of DevSR and density in predicting rutting performance.

6.3 Determination of Threshold values to Control early-life rutting

Rutting measurements collected as part of this study were utilized to define threshold criteria aimed at mitigating early-life rutting in pavement structures. These measurements, obtained approximately one year after construction and exposure to traffic, were derived from 16 field sections as highlighted in Table 6-2. It is important to note that the recorded rut depth represents the total pavement rutting.

However, for the purpose of this analysis as mentioned earlier in this report, it is assumed that the majority, if not all, of the observed rutting is attributable to the CR layer. To thus establish threshold values, statistical analyses were performed leveraging the DevSR parameter identified as most influential in the rutting performance function. Details of the analysis procedure is provided in subsequent sub-sections.

Table 6-2: Field Rut depth measurements

Field Sections	Rut depth (inches)
CSAH 9	0.23
CSAH 11-Essig	0.23
CSAH 11-Hanksa	0.23
CSAH 15-Section 1	0.25
CSAH 15-Section 2	0.26
CSAH 15-Section 3	0.25
CSAH 20-Section 1	0.23
CSAH 20-Section 2	0.23
CSAH 24	0.33
TH 30	0.09
TH 95	0.12
CSAH 21	0.08
CSAH 11-Cottonwood	0.13
MnROAD Section 2203	0.10
MnROAD Section 2206	0.10
MnROAD Section 2208	0.10

6.3.1 Threshold Determination Statistical Analysis Procedure

To categorize the CR material/layer into excellent and poor early life rut performance, an approach involving utilizing a normal distribution function along with verification for accuracy using the Receiver operating characteristics (ROC) classification tool was employed. The ROC is used to evaluate the accuracy of the assessment by indicating the trade-off between sensitivity (true positive rate) and specificity (false positive rate) of the proposed threshold setting. It is particularly valuable since it provides a comprehensive view of how well the assessment distinguishes between classes without being affected by the prevalence of outcomes (Wright, 2005). The steps to the threshold determination and verification are outlined below.

1. Using the mean and standard deviation of rut depth measurements, a normal distribution function is applied to derive the reliability level associated with a rut depth of 0.125 inches. This rut depth value is chosen to be indicative of the early life rut depth limit value for the CR-EE layer and may be adjusted based on designer preference.
2. Utilizing a normal distribution function derived from the mean and standard deviation of the DevSR dataset, the reliability level established in Step 1 is applied to the DevSR distribution to

determine the threshold value, which serves to differentiate between good and poor early-life rutting performance of CR-EE materials.

3. The established DevSR threshold is then verified for accuracy through the ROC quadrant analysis by categorizing the outcomes into true positives (TP), true negatives (TN), false positives (FP), and false negatives (FN).
4. Equation 6-4 through Equation 6-6 is used to assess the accuracy of the proposed threshold.

$$\boldsymbol{True\ Positive\ Rate\ (TPR)} = \frac{\boldsymbol{True\ Positive}}{(\boldsymbol{True\ Positive} + \boldsymbol{False\ Negative})}$$

Equation 6-4

$$\boldsymbol{False\ Positive\ Rate\ (FPR)} = \frac{\boldsymbol{False\ Positve}}{(\boldsymbol{False\ Positive} + \boldsymbol{True\ Negative})}$$

Equation 6-5

$$\boldsymbol{Accuracy} = \frac{\boldsymbol{True\ Positive} + \boldsymbol{True\ Negative}}{\boldsymbol{Total\ population}} \times \mathbf{100}$$

Equation 6-6

Figure 6-3 shows a visual representation of Steps 3 and 4.

$$Accuracy = \frac{True\ Positive + True\ Negative}{Total\ population} \times 100$$

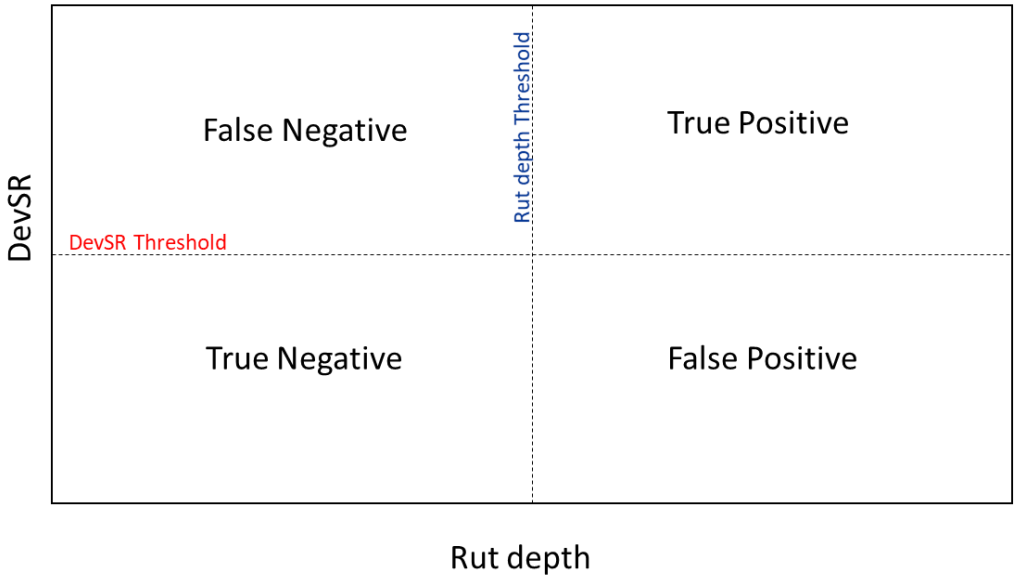

Figure 6-3: ROC accuracy analysis

6.3.2 Determination of Proposed DevSR Rut Threshold

Figure 6-4 shows the frequency and normal distribution for the rut depth. The frequency distribution histogram indicates that most measurements fall within the ranges of 0.10–0.15-inches and 0.20–0.25-

inches. The normal distribution curve shows that the dataset is generally well-represented by a normal distribution with a mean rut depth of approximately 0.2-inches. Based on this observation, it can be inferred that the CR-EE pavement layers experienced about 0.2-inches of rutting within the first year. To thus establish the DevSR threshold to limit rut depth to 0.125-inches, the reliability level corresponding to this rut depth value (determined at 78% reliability level) is mapped to the DevSR distribution (Figure 6-5) to derive the DevSR threshold. This analysis resulted in a DevSR threshold value of 0.31. Hence, CR-EE material/layer DevSR values exceeding this threshold are considered indicative of poor early-life rut performance.

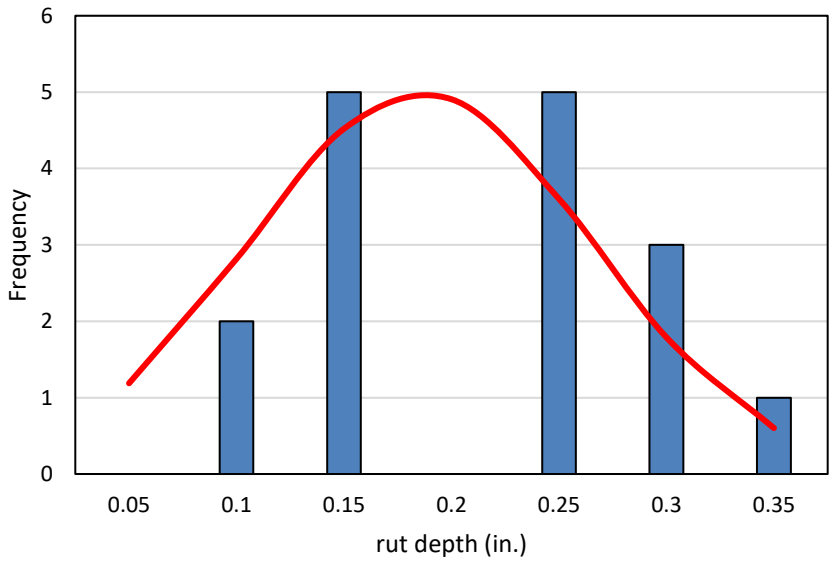

Figure 6-4: Frequency distribution histogram and normal distribution curve for rut depth measurements

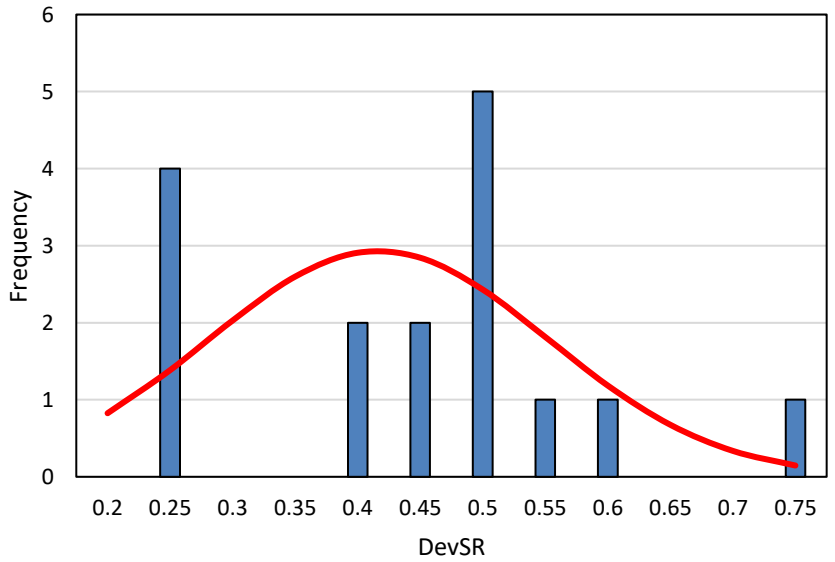

Figure 6-5: Frequency distribution histogram and normal distribution curve for DevSR measurements

Figure 6-6 depicts the quadrant plot assessing the effectiveness of the proposed 0.31 DevSR threshold to classify early-life rutting performance. The following provide interpretations to Figure 7.

- True Positive (TP): CR-EE sections with rut depths exceeding 0.125 inches are correctly associated with DevSR values greater than 0.31.
- False Negative (FN): CR-EE sections with rut depths less than 0.125 inches are incorrectly associated with DevSR values exceeding 0.31.
- False Positive (FP): CR-EE sections with rut depths exceeding 0.125 inches are incorrectly associated with DevSR values less than 0.31.
- True Negative (TN): CR-EE sections with rut depths below 0.125 inches are correctly associated with DevSR values less than 0.31.

The threshold verification results yielded a TPR of 0.75, FPR of 0.25, and an overall classification accuracy of 75%. The TPR of 0.75 indicates that 75% of the field sections with DevSR values exceeding 0.31 was correctly identified as having rut depths greater than 0.125 inches. FPR of 0.25 on the otherhand suggests that 25% of sections with DevSR higher than 0.31 was incorrectly classified as having rut depths below 0.125-inches. The relatively high TPR supports the practical use of DevSR = 0.31 as a threshold to limit early rutting to no more than 0.125-inches.

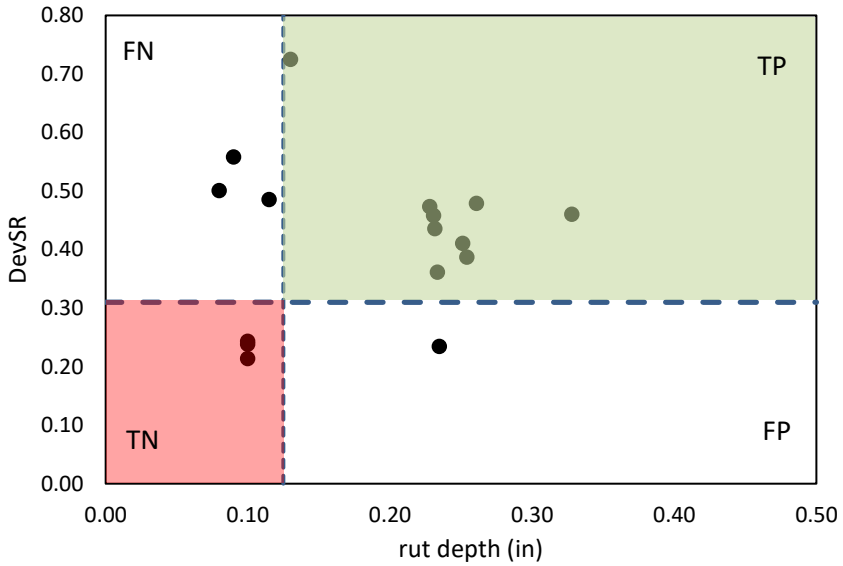

Figure 6-6: Quadrant analysis plot

6.4 Implementation Steps

Figure 6-7 presents a stepwise flowchart developed to evaluate the rutting performance of the CR-EE materials, based on the analytical procedures outlined in this chapter. Within the context of the established DevSR threshold, it is important to note that higher DevSR values are generally associated with an increased rate of permanent deformation/rutting. To maintain DevSR values below or close to

the threshold of 0.31 thereby controlling early-life rutting performance, the following practical construction measures are suggested.

1. Consider improving compaction density (based on insights from Chapter 4 of this report) to improve the cohesion and frictional angle of the material during construction, which would therefore increase its shear strength and resistance to deformation.
2. Given that DevSR depends on the applied stress relative to the material's shear strength, increasing the CR layer thickness (based on the existing in-place HMA layer thickness) and/or surface layer thickness can enhance load distribution and reduce stress concentration on the CR layer.
3. Incorporating chemical additives (cement) during construction can help improve material cohesion & angle of internal friction between RAP aggregates, consequently reducing the DevSR magnitude.
4. For SFDR layers, incorporating crushed gravel may enhance shear strength properties, thus contributing to a reduction in the DevSR.

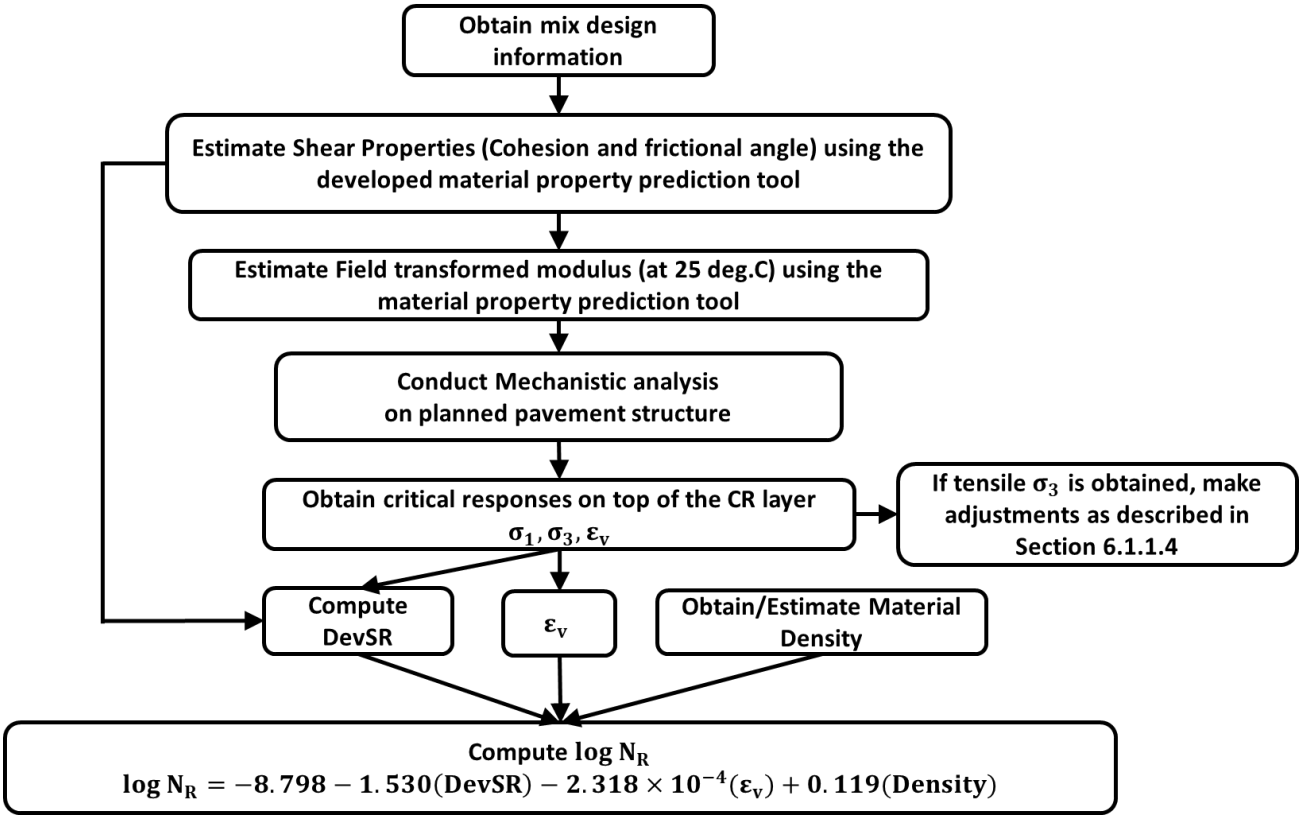

Figure 6-7: Performance function implementation flowchart

6.5 Summary

Dataset generated as part of Chapter 3 to Chapter 5 of this study, consisting of different CIR and SFDR materials, were used to develop CR layer rutting performance functions. A total of 20 field sections across various counties including the MnROAD sections were evaluated using Falling Weight Deflectometer (FWD) data, laboratory-derived shear properties, and mechanistic pavement modeling. Structural responses, including vertical strain and deviator stress ratio (DevSR), were computed through layered elastic analysis. The final calibrated performance function relates the allowable number of load repetitions to rutting failure (defined as 0.5-inches of rut depth) to the three mechanistically relevant variables: DevSR, vertical compressive strain at the top of the CR layer, and CR material/layer density. Among these, DevSR and density were found to be statistically significant, with DevSR exerting the greatest negative influence on rutting life, while density was positively associated with rutting resistance. A statistical analysis of first-year field rutting data was conducted to establish threshold values for early-life rutting performance. A rut depth of 3-mm (0.125-inches) was set as the limiting rut depth value to indicate early-life performance of the CR layer. A DevSR value of 0.31, which yielded a true positive rate (TPR) of 0.75, a false positive rate (FPR) of 0.25, and an accuracy of 75% based on a Receiver Operator Characteristics (ROC) verification analysis, suggesting good practical performance in identifying poor-performing sections, was proposed as the early-life rutting threshold for these CR-EE materials. The developed performance function, supported by both mechanistic analysis and statistical threshold validation, stands a viable tool for evaluating rutting behavior of these CR pavement layers and facilitates more efficient and reliable pavement designs.

Chapter 7: Conclusion & Recommendations

Existing specifications in Minnesota and many other states fail to adequately characterize the properties of cold recycled pavement materials necessary for pavement design procedures. Current assumptions for these materials are not entirely accurate as they often possess complex, non-linear, stress and/or rate dependent material behavior. This can lead to under/overdesigned pavement structures that are not economically and/or environmentally viable. This research was conducted to improve the pavement design procedures for cold recycled pavements, making the design of pavements that include them more efficient. Adequately characterizing the recycled material/layer will ensure that the appropriate thickness of wear course is determined through pavement design with no negative impact on structural capacity or serviceability.

This study, through a series of laboratory and field investigations, successfully developed a material property prediction tool designed to estimate key material parameters essential for quality assurance evaluation and performance modeling within the framework of mechanistic-empirical design of cold recycled pavement systems. In addition, a rutting performance function and an early life rutting failure threshold were established to mitigate the risk of premature rutting in the recycled layer. The comprehensive framework and resulting toolkit offer a practical and adaptable solution that can be readily implemented by state and local transportation agencies. By integrating these tools into pavement design processes, agencies can enhance the durability of cold recycled pavements, thereby extending service life and reducing the frequency and cost of repair and maintenance activities. Moreover, minimizing maintenance interventions will contribute to a reduction in construction-related work zone disruptions, ultimately decreasing the incidence of associated crashes and fatalities.

A few limitations were outlined in this study:

- Model and performance function developments were only possible for engineered emulsion stabilized CIR and SFDR cold recycled pavement sections due to the limited available data during the study.
- Only Engineered Emulsion was used as the bituminous stabilizer in this investigation. Consequently, all findings and model developments are specific to this stabilization approach and may not be directly applicable to other stabilizing agents (e.g. foamed asphalt).
- At the time of the study, the field sections evaluated had been in service for less than three years and experienced relatively low traffic volumes. As a result, rutting performance functions were developed using design traffic projections rather than long-term observed performance data.

Given these constraints, there is substantial opportunity to enhance the accuracy of the material property prediction model, the rutting performance function, and the early life rut threshold. Such improvements will require the collection and analysis of more comprehensive field and laboratory experimental data. Nonetheless, the methodological framework developed in this study provides a valuable foundation for enhancing cold recycling pavement design methodologies. Future studies are encouraged to address these limitations and to further investigate life-cycle assessments particularly focusing on potential reductions in construction-related GHG emissions achieved through the use of the

developed tools and transfer functions from this study, thereby promoting the broader adoption of cold recycling as a sustainable pavement rehabilitation technique.

REFERENCES

American Association of State Highway and Transportation Officials. (2008). *Mechanistic-empirical pavement design guide: A manual of practice.* Washington, DC

Al-Qadi, I., & Ozer, H. (2020, January). *In-place and central-plant recycling of asphalt pavements In Virginia*. Federal Highway Administration. https://www.fhwa.dot.gov/pavement

Arimilli, S., Nagabhushana, M. N., & Jain, P. K. (2018). Comparative mechanistic-empirical analysis for design of alternative cold recycled asphalt technologies with conventional pavement. *Road Materials and Pavement Design, 19*(7), 1595-1616. https://doi.org/10.1080/14680629.2017.1338187

Asphalt Academy. (2020). *Bitumen Stabilised Materials: A guide for the design and construction of bitumen emulsion and foamed bitumen stabilized materials* (3rd ed.). Southern African Bitumen Association. www.asphaltacademy.co.za

Asphalt Recycling and Reclaiming Association. (2015). Basic asphalt recycling manual. In *Federal Highway Administration* (2nd ed., Issue 9). Federal Highway Administration.

Baus, R. L., & Stires, N. R. (2010). *Mechanistic-empirical pavement design guide implementation* (No. FHWA-SC-10-01). University of South Carolina, Department of Civil and Environmental Engineering.

Beesam, V. V., & Torres-Machi, C. (2021). Input parameters for the mechanistic-empirical design of full-depth reclamation projects. *Transportation Research Record, 2675*(11), 384-396. https://doi.org/10.1177/03611981211017916

Bemanian, S., Polish, P., & Maurer, G. (2006). *Cold in-place recycling and full-depth reclamation projects by Nevada Department of Transportation: State of the practice*. *Transportation Research Record, 1949*(1), 54-71.

Bessa, I. S., Almeida, L. R., Vasconcelos, K. L., & Bernucci, L. L. B. (2016). Design of cold recycled mixes with asphalt emulsion and Portland cement. *Canadian Journal of Civil Engineering, 43*(9), 773–782. https://doi.org/10.1139/cjce-2016-0111

Bierman C. R. (2018). *A design function for bitumen stabilised material performance based on laboratory and field evaluation*. MEng (Research), Stellenbosch University, Stellenbosch, South Africa.

Burnham, K. P., & Anderson, D. R. (Eds.). (2002). *Model selection and multimodel inference: a practical information-theoretic approach*. New York, NY: Springer New York.

Caltrans. (2022) *Highway design manual.* California Department of Transportation, Sacramento, California. Retrieved from https://dot.ca.gov/-/media/dot-media/programs/design/documents/hdm-complete-corrected-052022-a11y-020623.pdf

Casillas, S. (2020). *Quantifying workability, compactability, and cohesion gain of asphalt emulsion cold in-place recycling*. University of Arkansas.

Carvajal, M. E., Piratheepan, M., Sebaaly, P. E., Hajj, E. Y., & Hand, A. J. (2021). Structural contribution of cold in-place recycling base layer. *Civil Engineering, 2*(3), 736-746. https://doi.org/10.3390/civileng2030040

Chen, T., Luan, Y., Ma, T., Zhu, J., Huang, X., & Ma, S. (2020). Mechanical and microstructural characteristics of different interfaces in cold recycled mixture containing cement and asphalt emulsion. *Journal of Cleaner Production*, *258*. https://doi.org/10.1016/j.jclepro.2020.120674

Cheng, P., Yi, J., Chen, Z., Luan, H., & Feng, D. (2022). Influence factors of strength and performance of foamed asphalt cold recycled mixture. *Road Materials and Pavement Design, 23*(2), 461-476. https://doi.org/10.1080/14680629.2020.1826343

Čížková, Z., Šedina, J., Valentin, J., & Engels, M. (2016). *Laboratory experience with the application of monotonic triaxial test on the cold recycled asphalt mixes*. Retrieved from https://doi.org/10.14311/ee.2016.220

Collings, D., & Jenkins, K. (2011), The long-term behaviour of bitumen stabilised materials. Paper presented at the 10th Conference on Asphalt Pavements for Southern Africa.

Cross, S. A. (2000). *Evaluation of cold in-place recycled mixtures on US-283* (Final report, No KS-99-4). University of Kansas, Lawrence, KS.

Dal Ben, M., & Jenkins, K. J. (2014). Performance of cold recycling materials with foamed bitumen and increasing percentage of reclaimed asphalt pavement. *Road Materials and Pavement Design*, *15*(2), 348–371. https://doi.org/10.1080/14680629.2013.872051

Dave, E., Sias, J., Ogbo, C., Zegeye, E., & Dai, S. (2022). *Evaluation of curing effects on cold in-place recycled (CIR) materials*. Retrieved from https://www.mndot.gov/research/reports/2022/202211.pdf

Díaz-Sánchez, M. A., Timm, D. H., & Diefenderfer, B. K. (2017). Structural coefficients of cold central-plant recycled asphalt mixtures. *Journal of Transportation Engineering, Part A: Systems, 143*(6), 04017019. http://dx.doi.org/10.1061/JTEPBS.0000005

Diefenderfer, B., Apeagyei, A., Gallo, A., Dougald, L., & Weaver, C. (2012). In-place pavement recycling on I-81 in Virginia. *Transportation Research Record*, *2306*, 21–27. https://doi.org/10.3141/2306-03

Diefenderfer, B. K., & Apeagyei, A. K. (2014). *I-81 in-place pavement recycling project* (No. FHWA/VCTIR 15-R1). Virginia Center for Transportation Innovation and Research.

Diefenderfer, B. K., Bowers, B. F., & Apeagyei, A. K. (2015). Initial performance of Virginia's interstate 81 in-place pavement recycling project. *Transportation Research Record*, *2524*, 152–159. https://doi.org/10.3141/2524-15

Du, S. (2015). Performance characteristic of cold recycled mixture with asphalt emulsion and chemical additives. *Advances in Materials Science and Engineering, 2015*(1), 271596.

Ebels, L. J. (2008). Characterisation of material properties and behaviour of cold bituminous mixtures for road pavements, Doctoral dissertation, Stellenbosch University, Stellenbosch, South Africa.

Bozyurt, O., Keene, A., Tinjum, J., Edil, T., & Fratta, D. (2013, August). Freeze–thaw effects on stiffness of unbound recycled road base. In *Symposium on Mechanical Properties of Frozen Soil* (pp. 3-21). ASTM International.

Kaloush, K. E., Biligiri, K. P., Zeiada, W. A., Rodezno, M. C., & Reed, J. X. (2010). Evaluation of fiber-reinforced asphalt mixtures using advanced material characterization tests. *Journal of Testing and Evaluation*, *38*(4), 400-411.

Fedrigo, W., Núñez, W. P., López, M. A. C., Kleinert, T. R., & Ceratti, J. A. P. (2018). A study on the resilient modulus of cement-treated mixtures of RAP and aggregates using indirect tensile, triaxial and flexural tests. *Construction and Building Materials, 171,* 161-169. https://doi.org/10.1016/j.conbuildmat.2018.03.119

Filho, W. U., Gutiérrez Klinsky, L. M., Motta, R., & Bariani Bernucci, L. L. (2020). Cold recycled asphalt mixture using 100% RAP with emulsified asphalt-recycling agent as a new pavement base course. *Advances in Materials Science and Engineering*, *2020*. https://doi.org/10.1155/2020/5863458

Flores, G., Gallego, J., Miranda, L., & Marcobal, J. R. (2020). Cold asphalt mix with emulsion and 100% rap: Compaction energy and influence of emulsion and cement content. *Construction and Building Materials*, *250*. https://doi.org/10.1016/j.conbuildmat.2020.118804

Fu, P., Jones, D., Harvey, J. T., & Bukhari, S. A. (2009). Laboratory test methods for foamed asphalt mix resilient modulus. *Road Materials and Pavement Design*, *10*(1). https://doi.org/10.1080/14680629.2009.9690187

Graziani, A., Godenzoni, C., Cardone, F., & Bocci, M. (2016). Effect of curing on the physical and mechanical properties of cold-recycled bituminous mixtures. *Materials and Design*, *95*, 358–369. https://doi.org/10.1016/j.matdes.2016.01.094

Gu, F., Sahin, H., Luo, X., Luo, R., & Lytton, R. L. (2015). Estimation of resilient modulus of unbound aggregates using performance-related base course properties. *Journal of Materials in Civil Engineering, 27*(6), 04014188. https://doi.org/10.1061/(ASCE)MT.1943-5533.0001147

Gu, F., Ma, W., West, R. C., Taylor, A. J., & Zhang, Y. (2019). Structural performance and sustainability assessment of cold central-plant and in-place recycled asphalt pavements: A case study. *Journal of Cleaner Production, 208,* 1513-1523. https://doi.org/10.1016/j.jclepro.2018.10.222

Guatimosim, F. V., Vasconcelos, K. L., Bernucci, L. L. B., & Jenkins, K. J. (2018). Laboratory and field evaluation of cold recycling mixture with foamed asphalt. *Road Materials and Pavement Design*, *19*(2), 385–399. https://doi.org/10.1080/14680629.2016.1261726

Halles, F. A., & Thenoux, G. Z. (2009). Degree of influence of active fillers on properties of recycled mixes with foamed asphalt. *Transportation Research Record*, *2095*, 127–135. https://doi.org/10.3141/2095-13

Hill, R., & Braham, A. (2016). Quantifying timing of return to traffic for asphalt cement based full depth reclamation mixtures in the laboratory. *Journal of Testing and Evaluation*, *44*(1). https://doi.org/10.1520/JTE20130288

Horak, E. (2008). Benchmarking the structural condition of flexible pavements with deflection bowl parameters. *Journal of the South African Institution of Civil Engineering, 50*(2), 2-9.

Huang, Y. H. (2004). *Pavement analysis and design* (Vol. 2, pp. 401-409). Upper Saddle River, NJ: Pearson/Prentice Hall.

Iwański, M., & Chomicz-Kowalska, A. (2013). Laboratory study on mechanical parameters of foamed bitumen mixtures in the cold recycling technology. *Procedia Engineering*, *57*, 433–442. https://doi.org/10.1016/j.proeng.2013.04.056

Iwański, M., & Chomicz-Kowalska, A. (2016). Application of the foamed bitumen and bitumen emulsion to the road base mixes in the deep cold recycling technology. *Baltic Journal of Road and Bridge Engineering*, *11*(4), 291–301. https://doi.org/10.3846/bjrbe.2016.34

James, G., Witten, D., Hastie, T., & Tibshirani, R. (2013). *An introduction to statistical learning: With applications in R* (Vol. 103). New York: Springer.

Jenkins, K. J. (2000). Mix design considerations for cold and half-warm bituminous mixes with emphasis of foamed bitumen, Doctoral dissertation, Stellenbosch University, Stellenbosch, South Africa.

Jenkins, K. J., Long, F. M., & Ebels, L. J. (2007). Foamed bitumen mixes = Shear performance? *International Journal of Pavement Engineering*, *8*(2). https://doi.org/10.1080/10298430601149718

Jenkins, K. J., Rudman, C. E., Bierman, C. R., & Carter, A. (2020). Delivering sustainable solutions through improved mix and structural design functions for bitumen stabilised materials. *Advances in Materials Science and Engineering*, *2020*. https://doi.org/10.1155/2020/7460174

Jenkins, K. J., Twagira, M. E., Kelfkens, R. W., & Mulusa, W. K. (2012). New laboratory testing procedures for mix design and classification of bitumen-stabilised materials. In *Road materials and pavement design* (Vol. 13, Issue 4). Retrieved from https://doi.org/10.1080/14680629.2012.742625

Jiang, H. (2013). Mechanism analysis of emulsified asphalt cold recycled mixture. *Applied Mechanics and Materials, 405*, 1761-1766.

Johanneck, L., & Dai, S. (2013). Responses and performance of stabilized full-depth reclaimed pavements at the Minnesota road research facility. *Transportation Research Record, 2368*(1), 114-125. https://doi.org/10.3141/2368-11

Jones, D., Fu, P., Harvey, J. T., & Org, E. (2009). *UC Davis guidelines title full-depth pavement reclamation with foamed asphalt in California: Guidelines for project selection, design, and construction*. Retrieved from https://escholarship.org/uc/item/2px7x2cf

Kandhal, P. S., & Mallick, R. B. (1998). Pavement recycling guidelines for state and local governments: participant's reference book (No. FHWA-SA-98-042).

Kavussi, A., & Modarres, A. (2010). A model for resilient modulus determination of recycled mixes with bitumen emulsion and cement from ITS testing results. *Construction and Building Materials, 24*(11), 2252-2259.

Khorshidi, M., Dave, E., & Sias, J. (2024). Application of machine learning in asphalt and concrete material testing: A comprehensive review. *Građevinski materijali i konstrukcije, 67*(4), 183-200.

Kim, Y. R., & Park, H. (2002). *Use of falling weight deflectometer multi-load data for pavement strength estimation* (No. FHWA/NC/2002-006). North Carolina. Dept. of Transportation.

Kim, Y., Im, S., & Lee, H. (2011). Impacts of curing time and moisture content on engineering properties of cold in-place recycling mixtures using foamed or emulsified asphalt. *Journal of Materials in Civil Engineering*, *23*(5), 542–553. https://doi.org/10.1061/(asce)mt.1943-5533.0000209

Kim, Y., & Lee, H. D. (2012). Performance evaluation of cold in-place recycling mixtures using emulsified asphalt based on dynamic modulus, flow number, flow time, and raveling loss. *KSCE Journal of Civil Engineering, 16*(4), 586-593. https://doi.org/10.1007/s12205-012-1376-0

Konieczna, K., Pokorski, P., Sorociak, W., Radziszewski, P., Żymełka, D., & Król, J. B. (2020). Study of the stiffness of the bitumen emulsion based cold recycling mixes for road base courses. *Materials, 13*(23), 5473.

Kuchiishi, A. K., Vasconcelos, K., & Bariani Bernucci, L. L. (2019). Effect of mixture composition on the mechanical behaviour of cold recycled asphalt mixtures. *International Journal of Pavement Engineering, 22*(8), 984–994. https://doi.org/10.1080/10298436.2019.1655564

Kuchiishi, A. K., Vasconcelos, K., dos Santos Antão, C. C., de Souza, G., Rodrigues de Andrade, L., Dave, E., & Bariani Bernucci, L. L. (2021). Impact of nonlinear elastic behavior of foamed asphalt stabilized mixes on pavement structural performance. *Journal of Materials in Civil Engineering*, *33*(10). https://doi.org/10.1061/(asce)mt.1943-5533.0003919

Lee, H., Kim, Y., & Heitzman, M. (2007). Performance testing for cold in-place recycling with foamed asphalt. In *Fifth International Conference on Maintenance and Rehabilitation of Pavements and Technological Control* (MAIREPAV5), University of Iowa, Iowa City Federal Highway Administration American Society of Civil Engineers Transportation Research Board.

Lekarp, F., Isacsson, U., & Dawson, A. (2000). State of the art. II: Permanent strain response of unbound aggregates. *Journal of Transportation Engineering*, *126*(1). https://doi.org/10.1061/(ASCE)0733-947X(2000)126:1(76)

Lemkus, T., Gotwalt, C., Ramsey, P., & Weese, M. L. (2021). Self-validated ensemble models for design of experiments. *Chemometrics and Intelligent Laboratory Systems, 219,* 104439.

Lewis, D., Jared, D., Torres, H., & Mathews, M. (2006). Georgia's use of cement-stabilized reclaimed base in full-depth reclamation. *Transportation Research Board*, *1952*(1), 125–133. https://doi.org/doi.org/10.1177/0361198106195200114

Li, Z., Hao, P., Liu, H., Xu, J., & Chen, Z. (2016). Investigation of early-stage strength for cold recycled asphalt mixture using foamed asphalt. *Construction and Building Materials*, *127*, 410–417. https://doi.org/10.1016/j.conbuildmat.2016.09.126

Lin, J., Hong, J., & Xiao, Y. (2017). Dynamic characteristics of 100% cold recycled asphalt mixture using asphalt emulsion and cement. *Journal of Cleaner Production, 156*, 337-344.

Loizos, A., Papavasiliou, V., & Plati, C. (2007). Early-life performance of cold-in-place pavement recycling with foamed asphalt technique. *Transportation Research Record, 2005*(1), 36-43. https://doi.org/10.3141/2005-05

Lukanen, E. O., Stubstad, R., & Briggs, R. C. (2000). *Temperature predictions and adjustment factors for asphalt pavement* (No. FHWA-RD-98-085; DBNX94822-D; NTIS-PB2000107444). Turner-Fairbank Highway Research Center.

Ma, T., Wang, H., Zhao, Y., Huang, X., & Pi, Y. (2015). Strength mechanism and influence factors for cold recycled asphalt mixture. *Advances in Materials Science and Engineering*, *2015*. https://doi.org/10.1155/2015/181853

Marquis, B., Peabody, D., Mallick, R., & Soucie, T. (2003). *Determination of structural layer coefficient for roadway recycling using foamed asphalt.* Durham, NH: Recycled Materials Resource Center.

Morian, D. A., Oswalt, J., & Deodhar, A. (2004). Experience with cold in-place recycling as a reflective crack control technique: Twenty years later. *Transportation Research Record, 1869*(1), 47-55.

Meneses, J. P. C., Vasconcelos, K., & Bernucci, L. L. B. (2022). Stiffness assessment of cold recycled asphalt mixtures–Aspects related to filler type, stress state, viscoelasticity, and suction. *Construction and Building Materials, 318,* 126003. https://doi.org/10.1016/j.conbuildmat.2021.126003

Minnesota Department of Transportation. (2019). *MnDOT pavement design Manual*. Minnesota Department of Transportation. http://www.dot.state.mn.us/materials/pvmtdesign/manual.html

Minnesota Department of Transportation. (2024). *MnPAVE* flexible 6.5. Minnesota Department of Transportation. Retrieved from http://www.dot.state.mn.us/app/mnpave/

Minnesota Department of Transportation. (2022). Geotechnical section grading and base unit. *Grading and base manual*. Minnesota Department of Transportation. Retrieved from https://www.dot.state.mn.us/materials/gbmanual.html

Minnesota Department of Transportation. (2023) MnROAD Test sections "*low volume road*". Minnesota Department of Transportation. Retrieved from https://www.dot.state.mn.us/mnroad/test-cells/lowvolume.html

Mulusa, W. K. (2009). Development of a simple triaxial test for characterizing bitumen stabilised Materials, master's thesis, University of Stellenbosch, Stellenbosch, South Africa.

Nazemi, M., & Heidaripanah, A. (2016). Support vector machine to predict the indirect tensile strength of foamed bitumen-stabilised base course materials. *Road Materials and Pavement Design, 17*(3), 768-778.

Nemati, R., Dave, E. V., & Sias, J. E. (2022). Generalized methodology to develop mechanistically informed asphalt mixture layer coefficients for AASHTO 1993 pavement design approach. *Transportation Research Record, 2676*(2), 312-324. https://doi.org/10.1177/03611981211041597

Ogbo, C., Dave, E. V., Sias, J. E., & Zegeye, E. (2022). Correlating field and laboratory evolution of curing in cold in-place recycled (CIR) materials. *Construction and Building Materials*, *345*. https://doi.org/10.1016/j.conbuildmat.2022.128352

Orosa, P., Pérez, I., & Pasandín, A. R. (2023). Evaluation of water loss and stiffness increase in cold recycled mixes during curing. *Case Studies in Construction Materials*, *18,* e01877. https://doi.org/10.1016/j.cscm.2023.e01877

PPRA. (2022). *Cold in-place recycling*. Pavement Preservation & Recycling Alliance. https://roadresource.org/treatment_resources/cold_in_place_recycling

Pi, Y., Li, Y., Pi, Y., Huang, Z., & Li, Z. (2019). Strength and micro-mechanism analysis of cement-emulsified asphalt cold recycled mixture. *Materials, 13*(1), 128.

Preti, F., Dave, E. V., Romeo, E., Tebaldi, G., & Sias, J. E. (2021). Plasticity-based method for the design and analysis of cold recycled pavement layers. *Journal of Testing and Evaluation, 50*(2). https://doi.org/10.1520/JTE20210198

Rahman, M., & Vargas-Nordcbeck, A. (2019). Effect of thin overlays on the structural performance of cold recycled bases for high traffic volume roads. In *Technology Pkwy*, 277. https://doi.org/10.1061/9780784482452.020

Raschia, S., Mignini, C., Graziani, A., Carter, A., Perraton, D., & Vaillancourt, M. (2019). Effect of gradation on volumetric and mechanical properties of cold recycled mixtures (CRM). *Road Materials and Pavement Design*, *20*(sup2), S740–S754. https://doi.org/10.1080/14680629.2019.1633754

Raschia, S., Perraton, D., Graziani, A., & Carter, A. (2020). Influence of low production temperatures on compactability and mechanical properties of cold recycled mixtures. *Construction and Building Materials*, *232*. https://doi.org/10.1016/j.conbuildmat.2019.117169

Ren, J., Wang, S., & Zang, G. (2020). Effects of recycled aggregate composition on the mechanical characteristics and material design of cement stabilized cold recycling mixtures using road milling materials. *Construction and Building Materials*, *244*. https://doi.org/10.1016/j.conbuildmat.2020.118329

Romanoschi, S. A., Hossain, M., Gisi, A., & Heitzman, M. (2004). Accelerated pavement testing evaluation of the structural contribution of full-depth reclamation material stabilized with foamed asphalt. *Transportation Research Record*, *1896*. https://doi.org/10.3141/1896-20

Santagata, E., Chiappinelli, G., Riviera, P. P., & Baglieri, O. (2010). Triaxial testing for the short term evaluation of cold-recycled bituminous mixtures. *Road Materials and Pavement Design, 11*(1), 123-147. https://doi.org/10.1080/14680629.2010.9690263

Schwartz, C., Diefenderfer, B., & Bowers, B. (2017). *Material properties of cold in place recycled and full-depth reclamation asphalt concrete*. Retrieved from https://doi.org/https://dx.doi.org/10.17226/24902

Sebaaly, P. E., Bazi, G., Hitti, E., Weitzel, D., & Bemanian, S. (2004). Performance of cold in-place recycling in Nevada. *Transportation Research Record*, *1896*. https://doi.org/10.3141/1896-16

Seber, G. A., & Lee, A. J. (2003). *Linear regression analysis.* John Wiley & Sons.

Shanmuganathan, S. (2016). Artificial neural network modelling: An introduction. In *Artificial neural network modelling* (pp. 1-14). Cham: Springer International Publishing.

Smith, S., & Braham, A. (2018). Comparing layer types for the use of PavementME for asphalt emulsion full depth reclamation design. *Construction and Building Materials, 158,* 481-489. https://doi.org/10.1016/j.conbuildmat.2017.10.054

Stroup-Gardiner, M. (2011). *Recycling and reclamation of asphalt pavements using in-place methods. NCHRP Synthesis*. (No. Project 20-05 (Topic 40-13)). Washington, DC: The National Academies Press.

Stroup-Gardiner, M. (2021). *Practice and performance of cold in-place recycling and cold central plant recycling* (No. NCHRP Project 20-05, Topic 51-08). https://nap.nationalacademies.org/catalog/26319.

Tebaldi, G., Dave, E. V., Marsac, P., Muraya, P., Hugener, M., Pasetto, M., Graziani, A., Grilli, A., Bocci, M., Marradi, A., Wendling, L., Gaudefroy, V., Jenkins, K., Loizos, A., & Canestrari, F. (2014). Synthesis of standards and procedures for specimen preparation and in-field evaluation of cold-recycled asphalt mixtures. *Road Materials and Pavement Design*, *15*(2), 272–299. https://doi.org/10.1080/14680629.2013.866707

Theyse, H. L., De Beer, M., & Rust, F. C. (1996). Overview of South African mechanistic pavement design method. *Transportation Research Record, 1539*(1), 6-17

Theyse, H. L., Sadzik, E., & Notnagel, J. P. (2000). A design model for waterbound macadam based on heavy vehicle simulator and laboratory test results. South African Transport Conference. Pretoria.

Thompson, M. R. (1996). Mechanistic-empirical flexible pavement design: An overview. *Transportation Research Record, 1539*(1), 1-5. https://doi.org/10.1177/0361198196153900101

Tia, M., & Wood, L. E. (1983). Use of asphalt emulsion and foamed asphalt in cold-recycled asphalt paving mixtures. *Transportation Research Record, 898,* 315-321.

Timm, D. H., Diefenderfer, B. K., & Bowers, B. F. (2018). Cold central plant recycled asphalt pavements in high traffic applications. *Transportation Research Record*, *2672*(40), 291–303. https://doi.org/10.1177/0361198118801347

Ullidtz, P., Harvey, J., Basheer, I., Jones, D., Wu, R., Lea, J., & Lu, Q. (2010). CalME, a mechanistic–empirical program to analyze and design flexible pavement rehabilitation. *Transportation Research Record, 2153*(1), 143-152. https://doi.org/10.3141/2153-16

Valdés, G., Pérez-Jiménez, F., Miró, R., Martínez, A., & Botella, R. (2011). Experimental study of recycled asphalt mixtures with high percentages of reclaimed asphalt pavement (RAP). *Construction and Building Materials*, *25*(3), 1289–1297. https://doi.org/10.1016/j.conbuildmat.2010.09.016

Valentin, J., Čížková, Z., Suda, J., Batista, F., Mollenhauer, K., & Simnofske, D. (2016). Stiffness characterization of cold recycled mixtures. *Transportation Research Procedia*, *14*, 758–767. https://doi.org/10.1016/j.trpro.2016.05.065

van Nierkerk, A. (2002). Mechanical behavior and performance of granular bases and sub-bases in pavements, doctoral dissertation, Technical University Delft, Delft, Netherlands.

Van Wijk, A. & Wood, L. E. (1983). Use of foamed asphalt in recycling of an asphalt pavement. *Transportation Research Record, 911*, 96-103.

Van Wyk, A., Yoder, E. J., & Wood, L. E. (1983). Determination of structural equivalency factors of recycled layers by using field data. *Transportation Research Record, 898*(898-902), 122.

Vapnik, V., Golowich, S., & Smola, A. (1996). Support vector method for function approximation, regression estimation and signal processing. *Advances in Neural Information Processing Systems,* 9.

Vavrik, W. R., Pine, W. J., & Carpenter, S. H. (2002). Aggregate blending for asphalt mix design: Bailey method. *Transportation Research Record, 1789*(1), 146-153.

Vrtis M. (2023) Stabilized full depth reclamation test sections. NRRA Newsletter: February 2019. Minnesota Department of Transportation. Retrieved https://www.dot.state.mn.us/mnroad/nrra/newsletter/2019/february.html

Werkmeister, S. (2003). *Permanent deformation Behaviour of unbound granular materials in pavement constructions*. Technical University of Dresden, Dresden.

Wirtgen GMBH, (2012). Cold recycling – Wirtgen cold recycling technology. Windhagen: Wirtgen GMBH. Manual.

Wright, D. B. (2005). Receiver operating characteristics curves. *Encyclopedia of Statistics in Behavioral Science, 4*, 1718-1721.

Xiao, Y., Tutumluer, E., & Siekmeier, J. (2011). Mechanistic–empirical evaluation of aggregate base and granular subbase quality affecting flexible pavement performance in Minnesota. *Transportation Research Record, 2227*(1), 97-106.

Xiao, F., Yao, S., Wang, J., Li, X., & Amirkhanian, S. (2018). A literature review on cold recycling technology of asphalt pavement. *Construction and Building Materials*, *180*, 579–604. https://doi.org/10.1016/j.conbuildmat.2018.06.006

Xie, Y., Liu, G., Pan, Y., Chen, Z., & Zhao, Y. (2021). Long-term effects of RAP on the mechanical properties of cold recycled mixtures. *International Journal of Pavement Engineering, 23*(14). https://doi.org/10.1080/10298436.2021.1985117

Yang, W., Ouyang, J., Meng, Y., Han, B., & Sha, Y. (2021). Effect of curing and compaction on volumetric and mechanical properties of cold-recycled mixture with asphalt emulsion under different cement contents. *Construction and Building Materials*, *297*. https://doi.org/10.1016/j.conbuildmat.2021.123699

Zhang, J., Guo, C., Chen, T., Zhang, W., Yao, K., Fan, C., Liang, M., Guo, C., & Yao, Z. (2021). Evaluation on the mechanical performance of recycled asphalt mixtures incorporated with high percentage of RAP and self-developed rejuvenators. *Construction and Building Materials*, *269*. https://doi.org/10.1016/j.conbuildmat.2020.121337

Zhu, C., Zhang, H., Huang, L., & Wei, C. (2019). Long-term performance and microstructure of asphalt emulsion cold recycled mixture with different gradations. *Journal of Cleaner Production*, *215*, 944–951. https://doi.org/10.1016/j.jclepro.2019.01.103

APPENDIX A
Survey

IMPROVING AND DEVELOPING PAVEMENT DESIGN INPUTS AND PERFORMANCE FUNCTIONS FOR COLD RECYCLED LAYERS IN MINNESOTA

This survey is being conducted to understand the current pavement design methodologies used by stakeholders for Cold Recycled layers as part of the MnDOT and Minnesota Local Road Research Board (LRRB) study on "Improving and developing pavement design inputs ad performance functions for Cold recycled layers in Minnesota".

If you have any questions or concerns, please contact project PI Eshan Dave (eshan.dave@unh.edu), co-PI Jo Sias (jo.sias@unh.edu) or Graduate researcher Ebube Al-Ihekwaba (ebubechukwu.al-ihekwaba@unh.edu).

Click "Next" to begin.

2 **Agency**

_____

3 **Full Name**

_____

4 **Affiliation**

_____

5 **Contact**

Phone _____

e-mail address_____

6 **Has your agency utilized cold recycling techniques in rehabilitation of your pavements in last 5 years?**

- ○ Yes
- ○ No

Display This Question:

If Has your agency utilized cold recycling techniques in rehabilitation of your pavements in last 5... = Yes

7 **Which cold recycling technique(s) have been used by your agency in last 5 years? (Select all that apply)**

- ☐ CCPR
- ☐ CIR
- ☐ FDR/SFDR

Display This Question:

If Which cold recycling technique(s) have been used by your agency in last 5 years? (Select all that... = CCPR

8 **What pavement design approach is utilized to design thicknesses of cold recycled layer and wearing course/overlay by your agency for CCPR? (Select all that apply)**

- ☐ AASHTO 1993
- ☐ AASHTOWare PEMD
- ☐ In-house Design (Please specify)

  _____
- ☐ Others (Please specify)

  _____

Display This Question:

If Which cold recycling technique(s) have been used by your agency in last 5 years? (Select all that... = CIR

9 **What pavement design approach is utilized to design thicknesses of cold recycled layer and wearing course/overlay by your agency for CIR? (Select all that apply)**

- ☐ AASHTO 1993
- ☐ AASHTOWare PEMD
- ☐ In-house Design (Please specify)

  _____
- ☐ Other (Please Specify)

  _____

Display This Question:

If Which cold recycling technique(s) have been used by your agency in last 5 years? (Select all that... = FDR/SFDR

10 **What pavement design approach is utilized to design thicknesses of cold recycled layer and wearing course/overlay by your agency for FDR/SFDR? (Select all that apply)**

- ☐ AASHTO 1993
- ☐ AASHTOWare PEMD
- ☐ In-house Design (Please specify)

  _____
- ☐ Other (Please Specify)

  _____

Display This Question:

If Which cold recycling technique(s) have been used by your agency in last 5 years? (Select all that... = CCPR

11 **Are there any challenges with employing the current design methodology in designing thicknesses of CCPR layer and wearing course/overlay by your agency? (e.g determining layer coefficient) Please specify**

_____

Display This Question:

If Which cold recycling technique(s) have been used by your agency in last 5 years? (Select all that... = CIR

12 **Are there any challenges with employing the current design methodology in designing thicknesses of CIR layer and wearing course/overlay by your agency? (e.g determining layer coefficient) Please specify**

_____

Display This Question:

If Which cold recycling technique(s) have been used by your agency in last 5 years? (Select all that... = FDR/SFDR

13 **Are there any challenges with employing the current design methodology in designing thicknesses of FDR/SFDR layer and wearing course/overlay by your agency? (e.g determining layer coefficient) Please specify**

_____

Display This Question:

If Which cold recycling technique(s) have been used by your agency in last 5 years? (Select all that... = CCPR

14 **Please provide links of design methods/standards used by your agency for CCPR treated pavements (If there are no links, move to "next" to upload file)**

_____

Display This Question:

If Which cold recycling technique(s) have been used by your agency in last 5 years? (Select all that... = CCPR

And And Please provide links of design methods/standards used by your agency for CCPR treated pavements (... Text Response Is Empty

15 **Please upload design methods/standards used by your agency for CCPR treated pavements**

Display This Question:

If Which cold recycling technique(s) have been used by your agency in last 5 years? (Select all that... = CIR

16 **Please provide links of design methods/standards used by your agency for CIR treated pavements (If there are no links, move to "next" to upload file)**

_____

Display This Question:

If Which cold recycling technique(s) have been used by your agency in last 5 years? (Select all that... = CIR

And And Please provide links of design methods/standards used by your agency for CIR treated pavements (I... Text Response Is Empty

17 **Please upload design methods/standards used by your agency for CIR treated pavements**

Display This Question:

If Which cold recycling technique(s) have been used by your agency in last 5 years? (Select all that... = FDR/SFDR

18 **Please provide links of design methods/standards used by your agency for FDR/SFDR treated pavements (If there are no links, move to "next" to upload file)**

Display This Question:

If Which cold recycling technique(s) have been used by your agency in last 5 years? (Select all that... = FDR/SFDR

And And Please provide links of design methods/standards used by your agency for FDR/SFDR treated pavemen... Text Response Is Empty

19 **Please upload design methods/standards used by your agency for FDR/SFDR treated pavements**

Display This Question:

If Which cold recycling technique(s) have been used by your agency in last 5 years? (Select all that... = CCPR

20 **What is your agency's process for selecting CCPR as pavement rehabilitation technique (for example, pavement attributes/distresses that would result in CCPR to be considered)?**

_____

Display This Question:

If Which cold recycling technique(s) have been used by your agency in last 5 years? (Select all that... = CIR

21 **What is your agency's process for selecting CIR as pavement rehabilitation technique (for example, pavement attributes/distresses that would result in CIR to be considered)?**

Display This Question:

If Which cold recycling technique(s) have been used by your agency in last 5 years? (Select all that... = FDR/SFDR

22 **What is your agency's process for selecting FDR/SFDR as pavement rehabilitation technique (for example, pavement attributes/distresses that would result in FDR/SFDR to be considered)?**

_____

Display This Question:

If Which cold recycling technique(s) have been used by your agency in last 5 years? (Select all that... = CCPR

23 **On roads that are treated using the CCPR process, what type of stabilizing agent is used most commonly?**

- ○ Asphalt Emulsion
- ○ Foamed Asphalt
- ○ Both (according to needs of specific projects)

Display This Question:

If Which cold recycling technique(s) have been used by your agency in last 5 years? (Select all that... = CCPR

24 **On roads that are treated using the CCPR process, what non-asphalt (active fillers) stabilizing agent is used most commonly? (Select all that apply)**

- ☐ Portland Cement
- ☐ Quicklime
- ☐ Lime (including lime kiln dust)
- ☐ Other (Please specify)

_____

Display This Question:

If Which cold recycling technique(s) have been used by your agency in last 5 years? (Select all that... = CIR

25 **On roads that are treated using the CIR process, what type of stabilizing agent is used most commonly?**

- ○ Asphalt Emulsion
- ○ Foamed Asphalt
- ○ Both (according to needs of specific projects)

Display This Question:

If Which cold recycling technique(s) have been used by your agency in last 5 years? (Select all that... = CIR

26 **On roads that are treated using the CIR process, what non-asphalt (active fillers) stabilizing agent is used most commonly? (Select all that apply)**

- ☐ Portland Cement
- ☐ Quicklime
- ☐ Lime (including lime kiln dust)
- ☐ Other (Please specify)

_____

Display This Question:

If Which cold recycling technique(s) have been used by your agency in last 5 years? (Select all that... = FDR/SFDR

27 **On roads that are treated using the FDR/SFDR process, what type of stabilizing agent is used most commonly?**

- ○ Asphalt Emulsion
- ○ Foamed Asphalt
- ○ Both (according to needs of specific projects)

Display This Question:

If Which cold recycling technique(s) have been used by your agency in last 5 years? (Select all that... = FDR/SFDR

28 **On roads that are treated using the FDR/SFDR process, what non-asphalt (active fillers) stabilizing agent is used most commonly? (Select all that apply)**

- ☐ Portland Cement
- ☐ Quicklime
- ☐ Lime (including lime kiln dust)
- ☐ Other (Please specify)

_____

Display This Question:

If Which cold recycling technique(s) have been used by your agency in last 5 years? (Select all that... = FDR/SFDR

29 **What percentage of roads utilizing the FDR/SFDR process is just reclamation without any added materials or stabilizing agent?**

_____

Display This Question:

If Which cold recycling technique(s) have been used by your agency in last 5 years? (Select all that... = CCPR

30 **Has your agency used any proprietary material in CCPR treated pavement? (such as, recycling agents)**

- ○ Yes
- ○ No

Display This Question:

If Which cold recycling technique(s) have been used by your agency in last 5 years? (Select all that... = CIR

31 **Has your agency used any proprietary material in CIR treated pavement? (such as, recycling agents)**

- ○ Yes
- ○ No

Display This Question:

If Which cold recycling technique(s) have been used by your agency in last 5 years? (Select all that... = FDR/SFDR

32 **Has your agency used any proprietary material in FDR/SFDR treated pavement? (such as, recycling agents)**

- ○ Yes
- ○ No

Display This Question:

If Has your agency used any proprietary material in CCPR treated pavement? (such as, recycling agents) = Yes

33 **Please provide name(s) of proprietary material used in CCPR treated pavements and indicate their purpose.**

- ○ Material _____
- ○ Purpose _____

Display This Question:

If Has your agency used any proprietary material in CIR treated pavement? (such as, recycling agents) = Yes

34 **Please provide name(s) of proprietary material used in CIR treated pavements and indicate their purpose.**

- ○ Material_____
- ○ Purpose_____

Display This Question:

If Has your agency used any proprietary material in FDR/SFDR treated pavement? (such as, recycling a... = Yes

35 **Please provide name(s) of proprietary material used in FDR/SFDR treated pavements and indicate their purpose.**

- ○ Material_____
- ○ Purpose _____

Display This Question:

If Which cold recycling technique(s) have been used by your agency in last 5 years? (Select all that... = CCPR

36 **Are there any specific structural distresses observed on the CCPR treated pavements? (Please Specify)**

_____

Display This Question:

If Which cold recycling technique(s) have been used by your agency in last 5 years? (Select all that... = CIR

37 **Are there any specific structural distresses observed on the CIR treated pavements? (Please Specify)**

_____

Display This Question:

If Which cold recycling technique(s) have been used by your agency in last 5 years? (Select all that... = FDR/SFDR

38 **Are there any specific structural distresses observed on the FDR/SFDR treated pavements? (Please Specify)**

_____

Display This Question:

If Which cold recycling technique(s) have been used by your agency in last 5 years? (Select all that... = CCPR

39 **What is the current average life of the CCPR treated pavement? (Please indicate)**

_____

Display This Question:

If Which cold recycling technique(s) have been used by your agency in last 5 years? (Select all that... = CIR

40 **What is the current average life of the CIR treated pavement? (Please indicate)**

_____

Display This Question:

If Which cold recycling technique(s) have been used by your agency in last 5 years? (Select all that... = FDR/SFDR

41 **What is the current average life of the FDR/SFDR treated pavement? (Please indicate)**

_____

Display This Question:

If Which cold recycling technique(s) have been used by your agency in last 5 years? (Select all that... = CCPR

42 **What rehabilitation techniques does your agency commonly use or plan to use on CCPR treated roads when they reach end of life?**

_____

Display This Question:

If Which cold recycling technique(s) have been used by your agency in last 5 years? (Select all that... = CIR

43 **What rehabilitation techniques does your agency commonly use or plan to use on CIR treated roads when they reach end of life?**

_____

Display This Question:

If Which cold recycling technique(s) have been used by your agency in last 5 years? (Select all that... = FDR/SFDR

44 **What rehabilitation techniques does your agency commonly use or plan to use on FDR/SFDR treated roads when they reach end of life?**

_____

Display This Question:

If Has your agency utilized cold recycling techniques in rehabilitation of your pavements in last 5... = Yes

45 **Has your agency undertaken any efforts to track field performances of cold recycling treated pavements in any projects?**

- ○ Yes
- ○ No

Display This Question:

If Has your agency undertaken any efforts to track field performances of cold recycling treated pave... = Yes

X→

46 **If reports/data from performance tracking projects are available on the internet, we would appreciate if you would share those links with us.**
Please first select number of weblinks that you wish to share.

- ○ 0
- ○ 1
- ○ 2
- ○ 3
- ○ 4
- ○ 5

Display This Question:

If If reports/data from performance tracking projects are available on the internet, we would apprec... != 0

47 **Please provide weblink of a report related to a project tracking performance of CIR,CCPR, FDR/SFDR (please provide link in this format "Name of project - link").**

_____

Display This Question:

If Has your agency undertaken any efforts to track field performances of cold recycling treated pave... = Yes

48 **If you wish to upload reports/data with the performance tracking project(s), please select below the number of reports/files that you wish to upload**

- ○ 0
- ○ 1
- ○ 2
- ○ 3
- ○ 4
- ○ 5

49 **Please upload report(s) related to these project(s)**

50 **Can we contact you to obtain further information?**

- ○ Yes
- ○ No

Display This Question:

If Can we contact you to obtain further information? = Yes

51 **What communication methods are preferred (Select all that apply)?**

- ☐ Zoom
- ☐ Phone Call
- ☐ Email
- ☐ Microsoft Teams

52

This is the end of the survey. Thank you for participating in this MnDOT and Minnesota Local Road Research Board (LRRB) survey for the study on "Improving and developing pavement design inputs ad performance functions for Cold Recycled Layers in Minnesota".

If you have any questions or concerns, please contact project PI Eshan Dave (eshan.dave@unh.edu), co-PI Jo Sias (jo.sias@unh.edu) or Graduate researcher Ebube Al-Ihekwaba (ebubechukwu.al-ihekwaba@unh.edu).

If you are ready to submit the survey responses, please press "next

Agency Design document will be made available upon request.

APPENDIX B
Material Sampling & Construction Details

B.1 Beltrami County Highway Department

B.1.1 CSAH 15 (From CSAH 26 to CSAH 32)

Existing Pavement Condition: A visual examination of the pavement revealed significant transverse cracking (see Figure B 1). Additionally, moderate severity longitudinal cracks were observed.

Figure B 1: CSAH 15 pavement condition prior to construction

Construction: CSAH 15 involved the application of SFDR along its 6.67-mile (10.73 kilometer) length. The SFDR treatment process involved the removal of two inches of asphalt wear course, followed by 7-inch FDR on the remaining pavement structure. The reclaimed section was thereafter treated with a 6-inch SFDR prior to the application of an asphalt overlay. The recycling train setup is shown in Figure B 2. The final pavement cross section is shown in Figure B 3.

Figure B 2: CSAH 15 recycling train setup

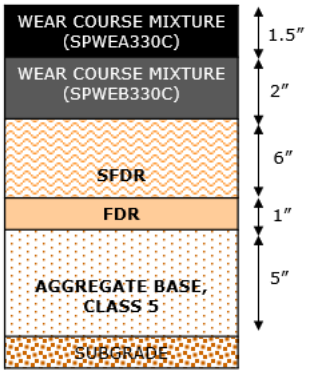

Figure B 3: CSAH 15 final pavement cross-section

Test Section description and sampling: Through discussions with the county engineer and project consultants, two mix design variations were recommended and subsequently constructed on defined sections along the project length. These sections (with varying emulsion content) in addition to the as-built mix design section are located on the northbound lane of the roadway and are shown in Figure B 4. These sections included 1000-ft (305m) of the initial mix design and 500-ft (152m) each of mix designs with varying emulsion content. Table B 1 provides details on the as-built job mix for each test section. RAP, engineered emulsion and samples of SFDR loose mix were collected from these sections to aid replicating the as-built conditions in the laboratory. RAP was sampled following the initial 7-inch reclamation and prior to the 6-inch stabilization. Figure B 5 shows the material sampling and storage/packaging process for transportation to the laboratory.

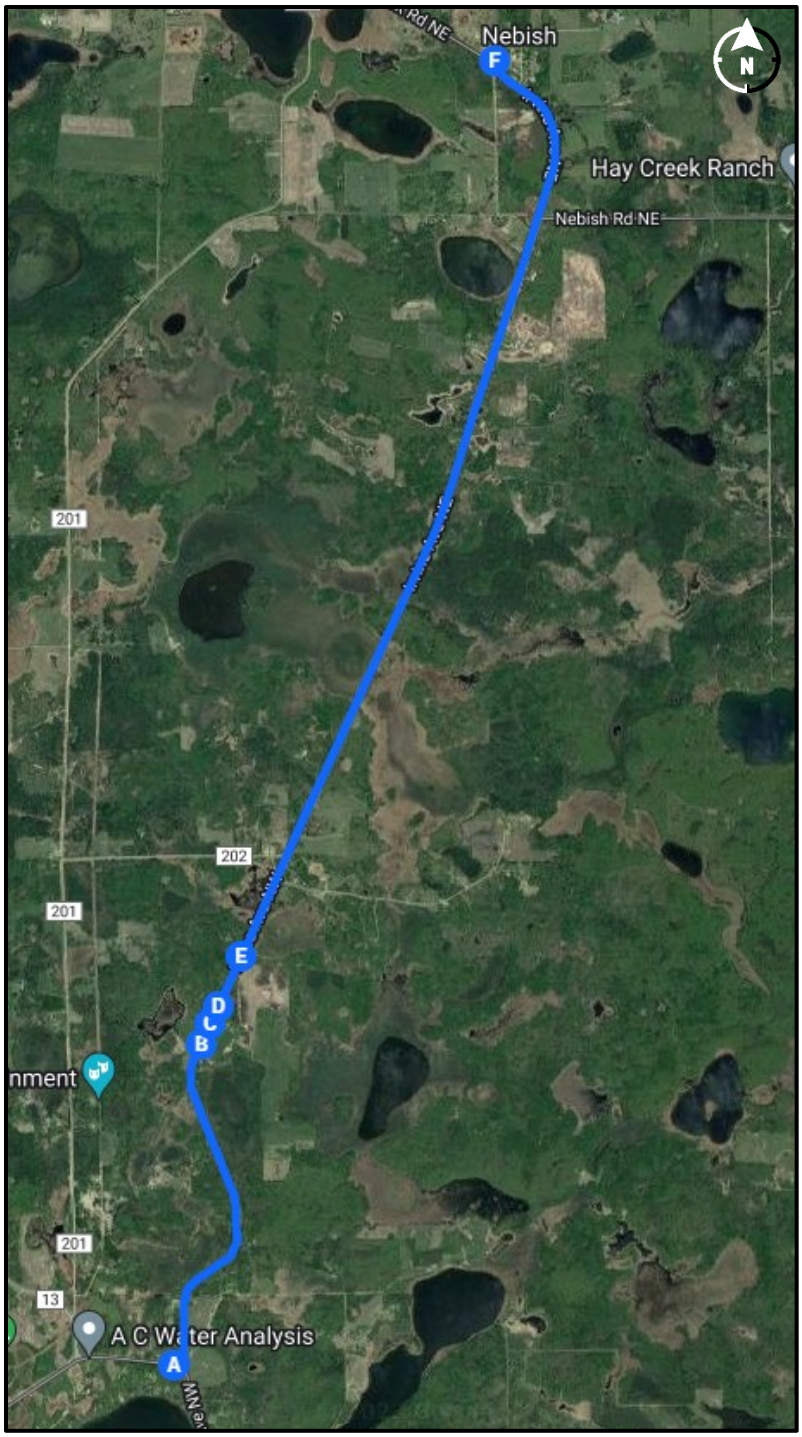

Figure B 4: Map of defined sections on CSAH 15 (Section B-C: 4.5% Emulsion, Section C-D: 5.5% Emulsion, Section D-E: 5% Emulsion)

Figure B 5: CSAH 15 Material Sampling and Storage/Packaging

Table B 1: CSAH 15 As-built job mix formulas

Parameters	Attributes		
	Section D-E (T1)	Section B-C (T2)	Section C-D (T3)
Method of Binder Delivery	Engineered Emulsion (EE)		
Grade of Emulsion	PG 58-28 Base Binder		
Amount of Bituminous Material	5%	4.5%	5.5%
Length	1000-ft (305m)	500-ft (152m)	500-ft (152m)
Type and Amount of Chemical Additive	N/A		
Target Density	2098.4kg/m^3 (131-pcf)		

T1: Test section 1 (Original Mix design)
T2: Test section 2 (Mix design variation 1)
T3: Test section 3 (Mix design variation 2)

B.2 Brown County Highway Department

Five projects in Brown County were identified, all of which have CIR treatments. Due to logistics and other unforeseen circumstances, material was only sampled from three of the five projects. Details on each project are presented in the following sub-sections.

B.2.1 CSAH 11 (From CSAH 6 to CSAH 20)

Existing Pavement Condition: Severe transverse cracking was observed in the existing pavement structure prior to construction, as determined by a visual distress survey (refer to Figure B 6). The mean distance between these transverse cracks was 5-ft (1.5m). Longitudinal cracks were also identified at the center of the lane.

Figure B 6: CSAH 11 pavement condition prior to construction

Construction: CSAH 11 involved the application of CIR along its 4.06-mile (6.54 kilometer) length. The CIR treatment process involved the re-recycling of the existing CIR into a 4-inch CIR layer followed by the application of an asphalt overlay which occurred at a later date. The recycling train setup is as shown in Figure B 7. The final pavement cross section is shown in Figure B 8.

Figure B 7: CSAH 11 recycling train setup

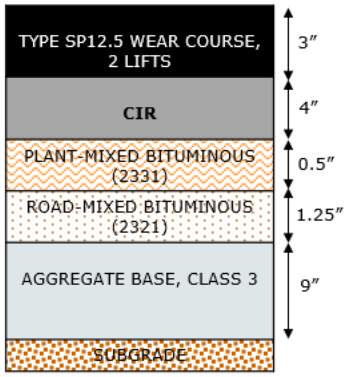

Figure B 8: CSAH 11 (CSAH 6 to CSAH 20) final pavement cross section

Test Section description and sampling: The identified section for field testing was located on the northbound lane of the roadway at a length of 1000-ft (305m). Figure B 9 shows the length and location

of the defined section. RAP, engineered emulsion and samples of CIR loose mix were collected from these sections to aid replicating the as-built conditions in the laboratory. Figure B 10 shows the material sampling and storage/packaging process for transportation to the laboratory for further investigations. Table B 2 provides details of the as-built job mix obtained from the quality control report provided to the researchers.

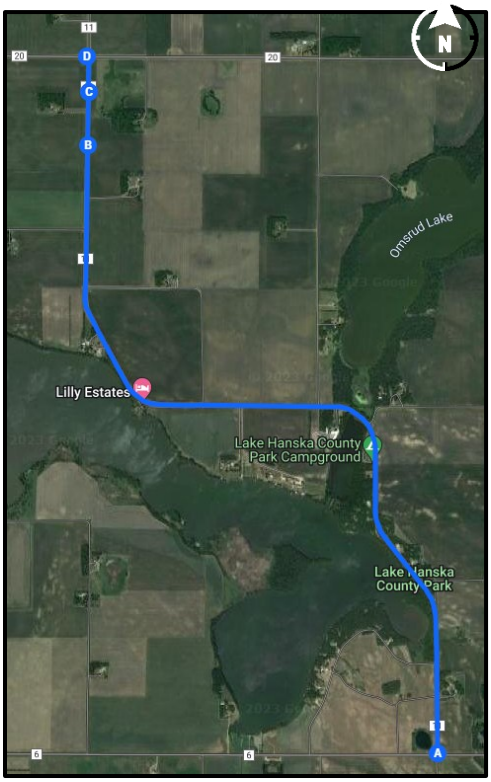

Figure B 9: CSAH 11 (CSAH 6 to CSAH 20) project map (Start of defined section denoted as B and end denoted as C)

Figure B 10: CSAH 11 material sampling and storage/packaging

Table B 2: CSAH 11 As-built job mix formula

Parameters	Attributes
Method of Binder Delivery	Engineered Emulsion (EE)
Grade of Emulsion	PG XX-28 Base Binder
Target Amount of Bituminous Material	3.1%
Type and Amount of Chemical Additive	N/A
Target Density	1974-kg/m^3 (123.2-pcf)

B.2.2 CSAH 20 (From CSAH 8 to TH 4)

Existing Pavement Condition: The pavement section prior to construction had potholes at different locations along the project length. Also visible were medium severity fatigue cracking, longitudinal cracking on the centerline, and edge cracking on varying locations along the length (see Figure B 11).

Figure B 11: CSAH 20 pavement condition prior to construction

Construction: CSAH 20 involved the application of CIR along its 4.71-mile (7.58 kilometer) length. This roadway is divided into two sections with different existing pavement structures, both consisting of a CIR layer. Figure B 12 and Figure B 13 depict the project location map and the pavement structure cross-section prior to construction, respectively. In particular, section A-B represents a pavement cross-section spanning a length of 1.31 miles (2.1 kilometers). The CIR treatment process involved the reclamation of the existing surface treatment + CIR layer into a 3-inch CIR layer followed by the application of an asphalt overlay which occurred later. The recycling train setup is as shown in Figure B 14. The final pavement cross section is shown in Figure B 15.

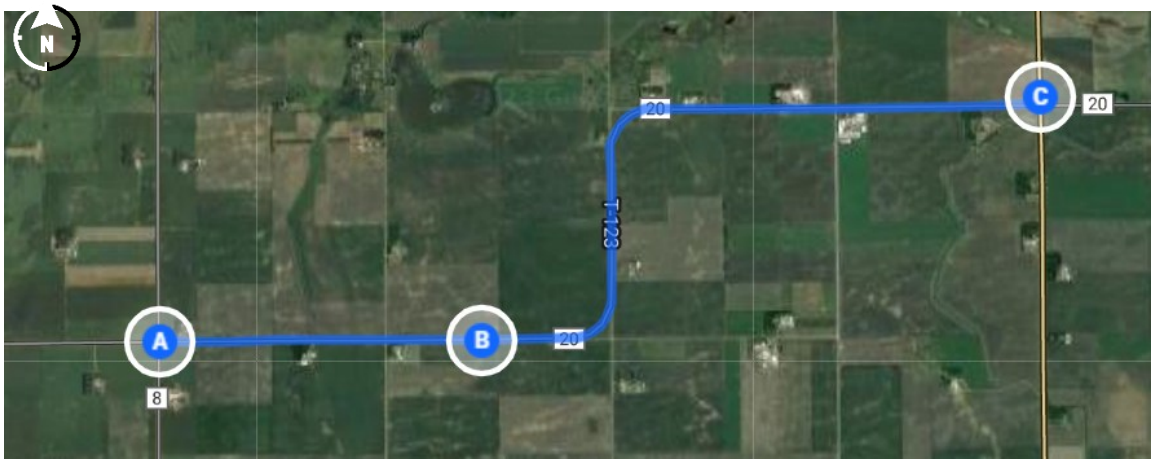

Figure B 12: CSAH 20 project map (Different pavement cross-section represented by length A-B and B-C)

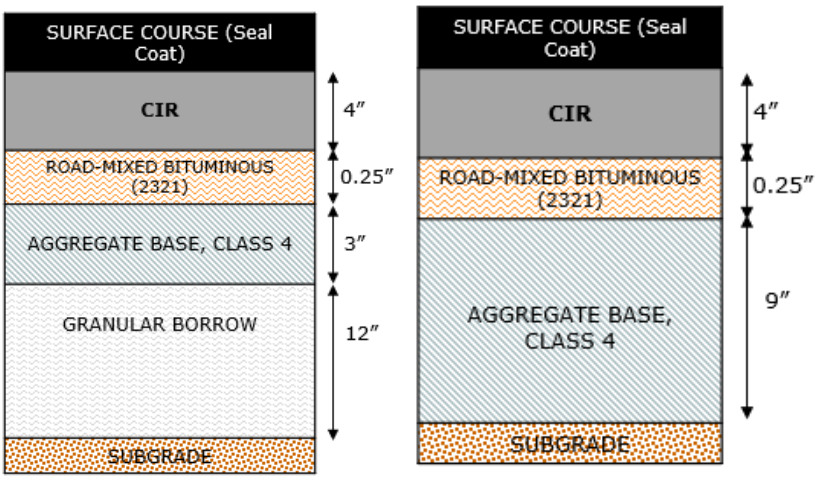

Figure B 13: CSAH 20 pavement cross section prior to construction (a) Section A-B on Figure B 12 (d) Section B-C on Figure B 12

Figure B 14: CSAH 20 Recycling Train Setup

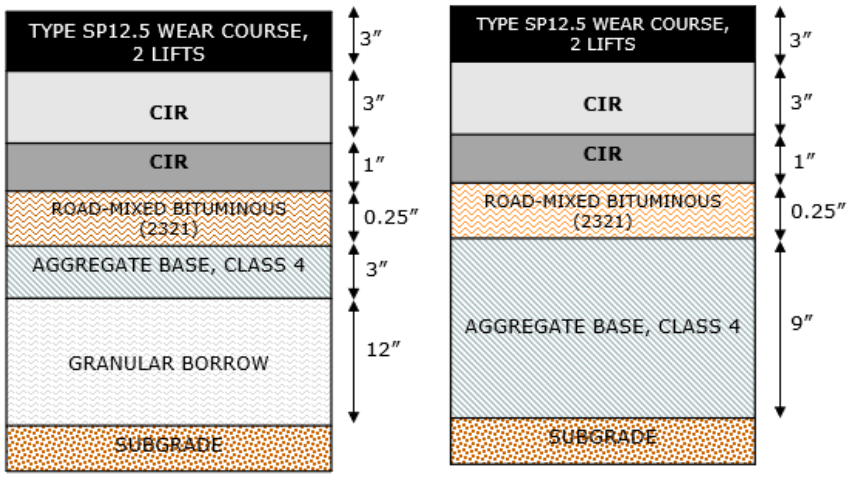

Figure B 15: CSAH 20 final pavement cross section (a) Section A-B on Figure B 12 (d) Section B-C on Figure B 12

Test Section description and sampling: The identified sections for field testing were located on the eastbound lane of the roadway at a length of 1000-ft (305m) each. Figure B 16 illustrates the length and location of the defined sections. As a result of construction schedule and logistics, RAP, engineered emulsion and samples of CIR loose mix were retrieved from section D-E (see Figure B 16) to aid replicating the as-built conditions in the laboratory. Figure B 17 shows the material sampling and storage/packaging process for transportation to the laboratory for further investigations. Table B 3 provides details on the as-built job mix obtained from the quality control report provided to the researchers.

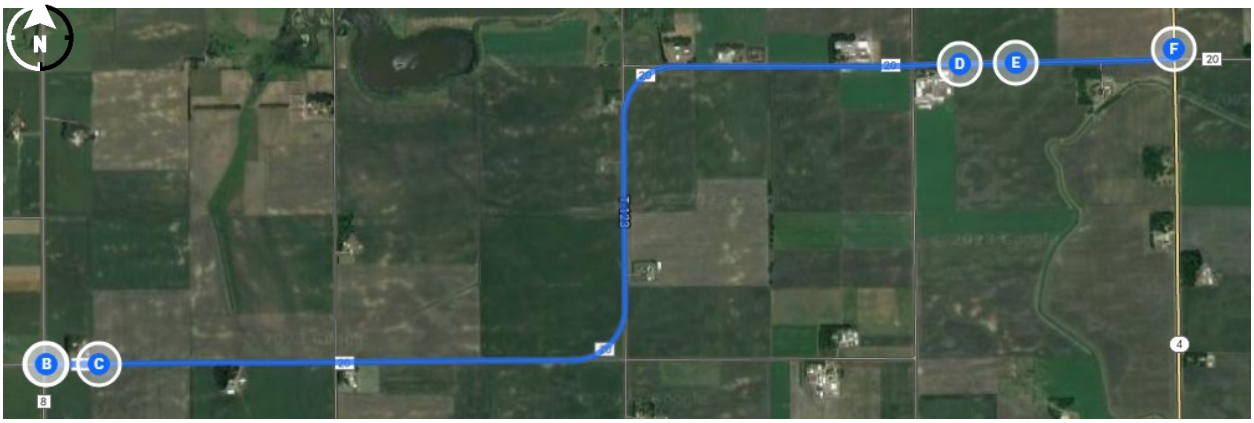

Figure B 16: CSAH 20 Project Map defined sections: Section B-C; Section D-E)

Figure B 17: CSAH 20 material sampling and storage/packaging

Table B 3: CSAH 20 As-built job mix formula

Parameters	Attributes
Method of Binder Delivery	Engineered Emulsion (EE)
Grade of Emulsion	CIR-EE (PG XX-28 Base Binder)
Target Amount of Bituminous Material	2.5%
Type and Amount of Chemical Additive	N/A
Target Density	1922-kg/m^3 (120-pcf)

B.2.3 CSAH 24 (From CSAH 13 to TH 15)

Existing Pavement Condition: A combination of distresses was observed on the pavement structure prior to construction. Amongst these distresses along the length of the project were low-high severity fatigue cracking, wheel ruts, longitudinal cracking on the wheel path, transverse cracking with weed propagation from these cracks, and potholes (see Figure B 18).

Figure B 18: CSAH 24 pavement condition prior to construction

Construction: CSAH 24 spanning 3.01 miles (4.85 kilometers) in length involved the reclamation of the existing asphalt layer into a 4-inch CIR layer followed by the application of an asphalt overlay which occurred at a later date. The recycling train setup is as shown in Figure B 19. The final pavement cross section is shown in Figure B 20.

Figure B 19: CSAH 24 recycling train setup

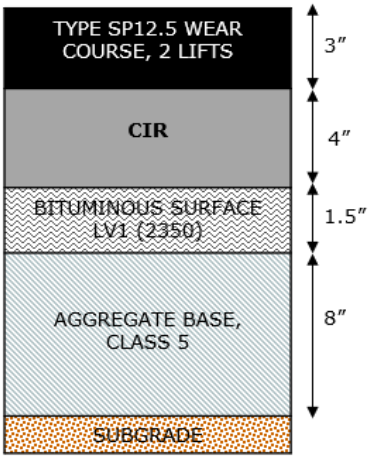

Figure B 20: CSAH 24 final pavement cross section

Test Section description and sampling: The identified section for field testing along the CIR portion of the roadway was located on the eastbound lane of the roadway at a length of 1000-ft (305m). Figure B

21 shows the length and location of the defined section on this CIR constructed section of the project. RAP materials, along with samples of CIR loose mix, were collected from these sections to aid replicating the as-built conditions in the laboratory. Figure B 22 shows the material sampled and stored for transportation to the laboratory for further investigations. Table B 4 provides details on the as-built job mix obtained from the quality control report provided to the researchers.

Figure B 21: CSAH 24 project map (Start of defined section denoted as B and end denoted as C)

Figure B 22: CSAH 24 sampled materials

Table B 4: CSAH 24 As-built job mix formula

Parameters	Attributes
Method of Binder Delivery	Engineered Emulsion (EE)
Grade of Emulsion	PG XX-28 Base Binder
Target Amount of Bituminous Material	2.4%
Type and Amount of Chemical Additive	N/A
Target Density	1893-kg/m^3 (118.2-pcf)

B.3 Clay County Highway Department

B.3.1 CSAH 18 (from CSAH 11 to the intersection of CSAH 18 & TH 9)

Test section description and sampling: With two sections, both consisting of a CIR layer, the designated areas for field testing were at lengths of 1000-ft (305 meters) along the eastbound lane of the roadway. Figure B 23 shows the length and location of the defined sections. As a result of construction schedule and logistics constraints, CIR loose mix were not obtained from this project though samples of RAP materials were retrieved alongside quality control report to aid replicating the as-built conditions in the laboratory. Figure B 24 shows the material sampled and stored for transportation to the laboratory for further investigations. The final pavement cross-section of both CIR sections is depicted in Figure B 25. Table B 5 provides details on the as-built job mix obtained from the quality control report provided to the researchers.

Figure B 23: CSAH 18 project map defined sections: Section B-C; Section D-E)

Figure B 24: CSAH 18 Sampled materials

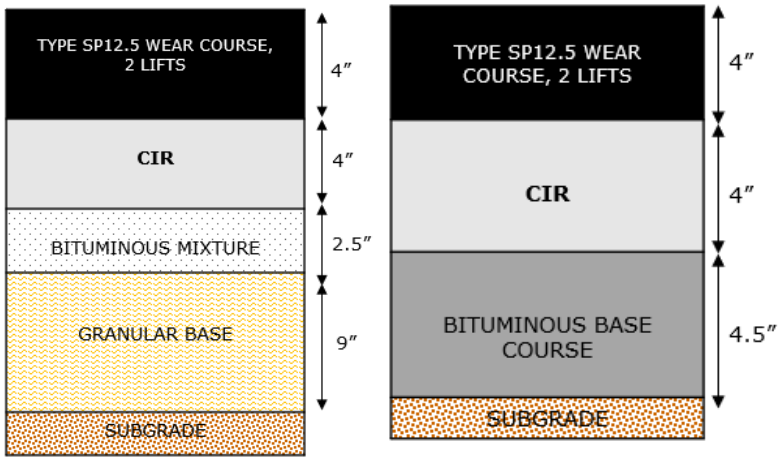

(a) (b)

Figure B 25: CSAH 18 final pavement cross section (a) Section A-D (d) Section D-F

Table B 5: CSAH 18 As-built job mix formula

Parameters	Attributes
Method of Binder Delivery	Engineered Emulsion (EE)
Grade of Emulsion	PG XX-28 Base Binder
Target Amount of Bituminous Material	3.3%
Type and Amount of Chemical Additive	N/A
Target Density	2068-kg/m^3 (129.1-pcf)

B.4 City of Maple Grove Public Works

B.4.1 CSAH 101 (From 73rd Avenue to 500' North of 83rd Avenue)

Test Section description and sampling: With two sections, one of which consisting of an SFDR layer while the other as a cement-treated layer, the designated areas for field testing were at lengths of 1000-ft (305 meters) along the northbound lane of the roadway. Figure B 26 shows the length and location of the defined sections. As a result of construction schedule and logistics constraints, SFDR loose mix were not obtained from this project though samples of RAP materials were retrieved alongside quality control report to aid replicating the as-built conditions in the laboratory. Figure B 27 shows the material sampled and stored for transportation to the laboratory for further investigations. The final pavement cross-section of both sections is depicted in Figure B 28. Table B 6 provides details on the as-built job mix obtained from the quality control report provided to the researchers.

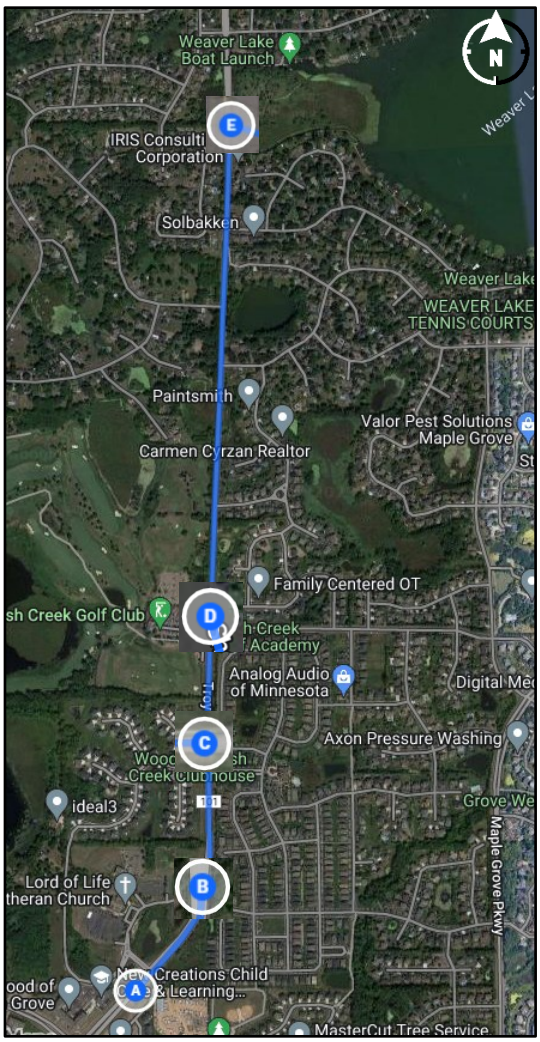

Figure B 26: CSAH 101 project map (SFDR section denoted by length B-C and D-E)

Figure B 27: CSAH 101 sampled materials

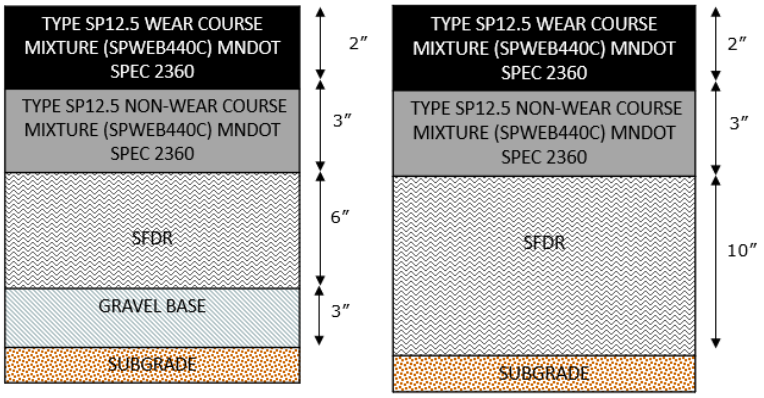

(a) (b)

Figure B 28: CSAH 101 Final Pavement structure (a) Section D-E (b) Section B-C

Table B 6: CSAH 101 As-built job formula

Parameters	Attributes	
	Section D-E (T1)	**Section B-C (T2)**
Method of Binder Delivery	Engineered Emulsion (EE)	NA
Amount of Bituminous Material	3.3%	NA
Type and Amount of Chemical Additive	Cement (0.5%)	Cement (4.2%)
Target Density	2134-kg/m^3 (133-pcf)	1936-kg/m^3 (121-pcf)

APPENDIX C
Quality Control Data

Report will be made available upon request.

APPENDIX D
Mohr Coloumb Envelope Data

Coefficient of determination (R^2) for all mixtures from the Mohr-Columb Envelope

Mixtures	R^2
BC11-X	1.00
BC11-A	0.92
BC11-B	0.90
BC11-C	1.00
BC11-D	0.92
BC20-X	0.88
BC20-A	0.94
BC20-B	0.99
BC24-X	0.99
BC24-A	0.99
BC24-B	0.93
BC24-C	0.99
BC24-D	0.98
CC18-X	0.99
CC18-A	0.99
CC18-B	0.96
CC18-C	0.93
CC18-D	0.91
DT30-X	0.99
DT95-X	1.00
DT75-X	1.00
BC08-X	1.00
BC11Z-X	1.00
BelC15-X	1.00
BelC15-A	0.87
BelC15-B	0.90
BelC15-C	0.99
BelC15-D	0.99
BelC15-E	0.97
BelC15-F	1.00
BelC15-G	0.99
BelC15-H	0.95
BelC15-I	0.99
BelC15-J	0.99
BelC15-K	0.99

BelC15-L	0.93
CMG101-C	0.88

APPENDIX E
Programmed Predictive Tool

The Excel Spreadsheet is provided as a supplementary material to this report.

See **https://hdl.handle.net/20.500.14153/mndot.18030.**